

HIGH RESOLUTION MICROSEISMICITY AND NEARLY-REPEATING
EVENTS IN THE MARMARA SEA

by

Nilay Başarır Baştürk

B.S., Geophysical Engineering, Çanakkale Onsekiz Mart University, 2007

M.S. Geophysics, Boğaziçi University, 2011

Submitted to the Kandilli Observatory and Earthquake Research
Institute in partial fulfillment of the requirements for the degree of

Doctor of Philosophy

Graduate Program in Geophysics

Boğaziçi University

2022

Dedicated to
my mother Nebahat Başarır & my daughter Kardelen
and my spouse Dođan.

ACKNOWLEDGEMENTS

I would like to express my deep and sincere gratitude to my thesis supervisor, Prof. Hayrullah Karabulut, for his invaluable supports, his great knowledge and patient throughout this research. I owe my deepest gratitude to my co-advisor Prof. Nurcan Meral Özel, who provided me precious assistance and guidance from the beginning to the end of the Phd.

With many thanks to Assoc. Prof. Ali Özgün Konca who is supportive, helpful, and sincere throughout my Phd days. I also would like to thank Prof. Semih Ergintav for his insights. I would like to thank Prof. Cemil Gürbüz for his sincerity.

Special thanks to my dearest friend Zeynep Yılmaz for her valuable friendship throughout my Phd Journey. I thank my friend Yasemin Korkusuz Öztürk for her meritorious supports and sincerity. Also, I would like to thank Gülten Polat for her precious friendship. I also thank to Fatih Turhan for his helps in some technical issues. I thank Uğur Mustafa Teoman for his friendship and kindness.

I would like to thank MARsite EU FP7 Project for the financial assistance during the thesis. I have been also supported financially by Turkish Directorate of Strategy and Budget under Telecommunications and Informatics Technologies Research Center (TETAM) Project number 2007K12-873 during the thesis.

I thank to all my colleagues and the faculty members in Geophysics Departments for their intimacy and encouragements throughout the Phd.

Last but not the least, I am grateful to my family; my mom Nebahat Başarır, my dad Ahmet Başarır, my husband Doğan Baştürk for their valuable encouragements and supports throughout this thesis and my life. I also thank to my lovely sister Çiğdem Başarır for her support.

ABSTRACT

HIGH RESOLUTION MICROSEISMICITY AND NEARLY-REPEATING EVENTS IN THE MARMARA SEA

The Main Marmara Fault beneath the Marmara Sea has a prominent seismic gap that can produce a devastating earthquake and a serious risk for the surroundings. It is important to scrutinize the seismic activity in region and relate this activity to the deformation of the fault zone. In this study, a new micro-earthquake database is created for the Marmara Sea between 2014-2016 using the data mostly from ocean-bottom seismometers. The detected and located seismicity indicate that Tekirdağ Basin hosts a diffuse activity from ~7 km to about 18 km depth. A high micro-earthquake activity rate predominates beneath the Central Basin, at depths from 3 km to 15 km. The abundance of earthquakes in the area can be attributed to a creeping zone, considering the conformity with the geodetic observations. On the other hand, Kumburgaz and the western part of Çınarcık Basins show sparse seismicity at depth ranges of 5-19 km and 3-18 km, respectively, signing to a locked fault compatible with the geodetic observations. In addition to micro-seismicity, the repeating events are detected using template matching method on the continuous waveforms from 2008-2021. The clusters of highly correlated detected earthquakes, which are closely spaced or partially overlapped, are attributed to the “near-repeating earthquakes”. The nine nearly-repeating earthquake clusters beneath the Central Basin are observed at 8-13 km depths, suggesting seismic creep behavior together with a high seismicity rate. The fault mechanisms of the near-repeater clusters have strike-slip mechanism consistent with Main Marmara Fault zone. The nearly-repeating events have two different patterns of repeating intervals, as long-term and short-term type events. The amount of slip rates from the near-repeater clusters shows varying slip rates but comparable to geodetic rate. The number of near-repeating events decreased significantly after the 2018 and no repeating event is observed during 2019 which Mw 5.8 Silivri earthquake occurred.

ÖZET

MARMARA DENİZİNDE YÜKSEK ÇÖZÜNÜRLÜKLÜ MİKROSİSMİSİTE VE YAKIN-TEKRARLAYAN DEPREMLER

Marmara Denizi'nden geçen Ana Marmara Fayı, yıkıcı bir deprem ve bölge için ciddi bir risk oluşturabilecek önemli bir sismik boşluğa sahiptir. Bölgedeki sismik aktiviteyi araştırmak ve bu aktiviteyi fay zonunun deformasyonu ile ilişkilendirmek önemlidir. Bu çalışmada, çoğunlukla deniz-dibi sismometrelerinden alınan veriler kullanılarak, 2014-2016 yılları arasında Marmara Denizi için yeni bir mikro-deprem veri tabanı oluşturulmuştur. Deprem belirleme ve lokasyonu tespitinden elde edilen depremsellik, Tekirdağ Havzası'nın ~7 km'den yaklaşık 18 km'ye kadar bir dağınık bir etkinliğe ev sahipliği yaptığını göstermektedir. Orta Havza'nın altında, 3 km ile 15 km arasında değişen yüksek bir mikro deprem etkinliği hakimdir. Bu alandaki depremlerin çok olması, jeodezik gözlemlerle olan uyumluluğu da göz önüne alındığında, akma (creep) özelliği olan bir zonla ilişkilendirilebilir. Kumburgaz Havzası ve Çınarcık Havzası'nın batısı ise sırasıyla, 5-19 km ve 3-18 km derinlik aralıklarında seyrek depremsellik göstermekte olup, jeodezik gözlemlerle uyumlu kilitli bir fay modeline işaret etmektedir. Mikrosismisiteye ek olarak, 2008-2021 yılları arasında sürekli dalga-formları üzerinde şablon-eşleştirme yöntemi uygulanarak tekrarlayan depremler tespit edilmiştir. Yakın aralıklı veya lokasyonları kısmen örtüşen, yüksek korelasyon oranına sahip olarak tespit edilen deprem kümeleri, yakın-tekrarlayan depremlere atfedilmektedir. Orta Havza'nın altında, 8 ila 13 km derinlik aralığında, 9 tane yakın-tekrarlayan deprem kümesi gözlenmekte olup, yüksek sismisite oranı ile birlikte bu bölge bir sismik krip davranışına işaret etmektedir. Yakın-tekrarlayan deprem kümelerinin fay mekanizmaları, Ana Marmara Fay zonu ile uyumlu doğrultu atımlı mekanizmaya sahiptir. Yakın-tekrarlayan depremler, uzun vadeli ve kısa vadeli tip depremler olarak, iki farklı tekrarlanma aralığı modeline sahiptir. Yakın-tekrarlayan deprem kümelerinin, kayma oranları, jeodezik hıza kıyasla düşük kayma oranları göstermektedir. Yakın-tekrarlayan depremler 2018 yılından sonra önemli ölçüde azalmıştır ve Mw=5.8 Silivri depreminin meydana geldiği 2019 yılında tekrarlayan deprem gözlenmemiştir.

TABLE OF CONTENTS

ACKNOWLEDGEMENTS.....	iv
ABSTRACT.....	v
ÖZET	vi
LIST OF FIGURES	ix
LIST OF TABLES.....	xvii
LIST OF SYMBOLS	xviii
LIST OF ACRONYMS/ABBREVIATIONS.....	xix
1. INTRODUCTION.....	1
2. SEISMOTECTONIC STRUCTURE AND HISTORICAL EARTHQUAKES IN THE MARMARA REGION.....	6
2.1. Tectonic Setting of the Marmara Region.....	6
2.2. Historical Earthquake Background of the Marmara Region	11
3. ANALYSIS AND PROCESS OF THE MICROSEISMICITY OF THE MARMARA SEA	14
3.1. Data.....	15
3.2. Earthquake Detection and Waveform Database	17
3.2.1 Application of STA/LTA Method on Continuous Seismic Data.....	18
3.3. The Velocity Model and Earthquake Location.....	19
3.4. Spatial Distribution of Microseismic Activity.....	24
3.4.1. Depth Distribution of Seismicity	26
3.4.2. A Comparative Analysis of Microearthquake Activity	29
4. REPEATING EARTHQUAKES	35
4.1. Introduction.....	35
4.2. The Physical Model of Repeating Earthquakes.....	40
4.2.1. Repeating Earthquakes and Fault Creep.....	41

4.3. Near Repeating Earthquakes.....	44
5. REPEATING EARTHQUAKES IN THE MARMARA SEA	46
5.1. Detection of the Repeating Earthquakes.....	46
5.2. Template Matching for Detecting Repeating Waveforms.....	48
5.2.1. Application of Template - Matching Method on Continuous Seismic Data	49
5.3. The Locations of the Repeating Earthquakes	53
5.4. Fault Mechanism Results for the Repeaters	54
5.5. Recurrence Time Intervals of the Repeating Events	60
5.5.1. Temporal Evolution of Detected Seismic Repeaters	62
5.6. Spectral Analysis of the Repeaters	63
5.6.1. Seismic Source Model	63
5.7. The Fault Slip Estimation Using Repeaters.....	65
5.7.1. Slip Rate Estimates from Nearly Repeating Events	71
5.8. Comparison of the Results with the other studies on Repeating Earthquakes in the Marmara Sea.....	80
6. DISCUSSION	84
6.1. Interpretation of Microseismicity in the Marmara Sea.....	85
6.2. Near-repeating Events in the Marmara Sea	88
7. CONCLUSIONS	94
REFERENCES	96

LIST OF FIGURES

Figure 2.1.	Tectonic motions around the Anatolian Plate. KTJ denotes Karlıova Triple Junction. The borders of the tectonic structures were indicated by the dashed lines. The lines including triangles depict the thrust faults. Main structures were taken from the McClusky et al. (2000). (Aktuğ et al. 2009).	6
Figure 2.2.	The GPS velocities with respect to Eurasia indicated by Reilinger et al. (2006).	7
Figure 2.3.	Bathymetry and active faults in the Marmara Sea (Filikçi et al., 2017).	10
Figure 2.4.	The estimated slip rate deficits and the total deficits accumulated since the last major earthquakes (Ergintav et al., 2014).....	11
Figure 2.5.	Important historical earthquakes with intensity IX-XI ($M_s \geq 7.0$) that occurred in the Marmara Region (Başarıır Baştürk et al., 2016b).	12
Figure 3.1.	Flow diagram showing the processes followed step by step from obtaining data to acquiring microseismicity database.....	14
Figure 3.2.	The locations of the OBS and land stations. The purple triangles indicate the first 15 OBS stations deployed in the scope of MARDIM project. The black solid triangles denote the OBS stations added later. The red triangles (SLVM, SLVT) show the land stations, also used for the detection of the nearly repeating events.....	15
Figure 3.3.	The parameters and the application of STA/LTA to data (Han et al., 2009).	18
Figure 3.4.	A SAC plot from the detected earthquake (2016-02-19 17:47:59) at MS02, MS07, MS08 station.....	19

Figure 3.5.	Example window of earthquake location using Zsac program. The event with origin time 20141008-1300 and magnitude ML=0.8.....	20
Figure 3.6.	1-D Initial velocity models for P and S waves (left), Final P(red) and S (green) velocity models (right) after inversion.	21
Figure 3.7.	Station corrections obtained from inversion for P (red) and S (green) waves.	22
Figure 3.8.	Statistics for the location accuracy of the seismicity catalog between 26.09.2014 and 31.12.2016. a) Latitude uncertainty b) Longitude uncertainty c) Depth uncertainty d) Magnitude-frequency distribution of the catalog and the b-value.....	23
Figure 3.9.	Error ellipses of the earthquakes computed from horizontal location uncertainties.	23
Figure 3.10.	Top: Map view of the seismicity in Marmara region between 2014-2016. The green circles show the locations of the nearly repeating events detected during the OBS deployments. Bottom: Depth view of seismicity. The green circles show the seismic repeaters. Fault lines were taken from Emre et al. (2013).	25
Figure 3.11.	Top: Map view of the seismicity in Marmara region between 2014-2016. Bottom: Depth view of seismicity for N-S section. The green circles show the seismic repeaters. Fault lines were taken from Emre et al. (2013).	26
Figure 3.12.	Depth distribution of earthquakes in the Tekirdağ Basin.....	27
Figure 3.13.	Depth distribution of earthquakes in the Central Basin.	28
Figure 3.14.	Depth distribution of earthquakes in the Kumburgaz and Çınarcık Basin..	28
Figure 3.15.	Seismicity activity between 2007-2016 (red) (after Schmittbuhl et al. (2015)) and this study (green). Top: Map view of the seismic activity. Bottom: Depth view of the seismic activity.....	30

- Figure 3.16. Seismicity activity between 2014.09-2015.07 (green) (after Yamamoto et al. (2017)) and this study (red). Top: Map view of the seismic activity. Bottom: Depth view of the seismic activity. 32
- Figure 3.17. Top: Seismicity distribution obtained using OBS data from this study. Bottom: P-wave seismic tomographic model crossing the center of Marmara Sea (Latitude 40.8N) in E-W direction. The pink area in the upper part of the model shows the water layer (Hayrullah Karabulut, pers.comm.). Red circles show the seismic events displayed on the top figure. 33
- Figure 4.1. 1922 and 1934 Parkfield events recorded at Berkeley, California. (<https://earthquake.usgs.gov/learn/parkfield/hist.php>)..... 37
- Figure 4.2. The repeating earthquakes in Parkfield region on the San Andreas Fault Zone, California(http://www.conservation.ca.gov/cgs/geologic_hazards/earthquakes/Pages/09282004_eq_info.aspx) 37
- Figure 4.3. The relation between creep and elastic strain (<http://funnel.sfsu.edu/creep/WhatsCreepPage.html>) 41
- Figure 4.4. The Schematic model demonstrating the types of asperities on a subduction zone (Behrmann et al., 2006). 43
- Figure 5.1. An example of three component template event from SLVM station (See Figure 3.2 for the location of the station)..... 51
- Figure 5.2. Template events for 9 repeating clusters from SLVM station used for the detection. E-W component (top) and N-S component (bottom). The numbers on the left of the traces (red labels) show the recording date of the event. The traces are normalized by their maximum values. 52

- Figure 5.3. Spatial distribution of the repeating event clusters. Each cluster is shown with different color. (a) Map view of the repeaters. (b) The depth distribution of the repeaters..... 53
- Figure 5.4. Composite focal mechanism solutions of the events within the detected Cluster 1 of seismic repeaters. Compression (C) and Dilatation (D) quadrants are shown for the lower- hemisphere projection of the focal sphere 55
- Figure 5.5. Composite focal mechanism solutions of the events within the detected Cluster 2 of seismic repeaters. Compression (C) and Dilatation (D) quadrants are shown for the lower- hemisphere projection of the focal sphere. 55
- Figure 5.6. Composite focal mechanism solutions of the events within the detected Cluster 3 of seismic repeaters. Compression (C) and Dilatation (D) quadrants are shown for the lower- hemisphere projection of the focal sphere. 56
- Figure 5.7. Composite focal mechanism solutions of the events within the detected Cluster 4 of seismic repeaters. Compression (C) and Dilatation (D) quadrants are shown for the lower- hemisphere projection of the focal sphere. 56
- Figure 5.8. Composite focal mechanism solutions of the events within the detected Cluster 5 of seismic repeaters. Compression (C) and Dilatation (D) quadrants are shown for the lower- hemisphere projection of the focal sphere. 57
- Figure 5.9. Composite focal mechanism solutions of the events within the detected Cluster 6 of seismic repeaters. Compression (C) and Dilatation (D) quadrants are shown for the lower- hemisphere projection of the focal sphere. 57

- Figure 5.10. Composite focal mechanism solutions of the events within the detected Cluster 7 of seismic repeaters. Compression (C) and Dilatation (D) quadrants are shown for the lower- hemisphere projection of the focal sphere. 58
- Figure 5.11. Composite focal mechanism solutions of the events within the detected Cluster 8 of seismic repeaters. Compression (C) and Dilatation (D) quadrants are shown for the lower- hemisphere projection of the focal sphere. 58
- Figure 5.12. Composite focal mechanism solutions of the events within the detected Cluster 9 of seismic repeaters. Compression (C) and Dilatation (D) quadrants are shown for the lower- hemisphere projection of the focal sphere. 59
- Figure 5.13. Seismicity distribution and composite focal mechanism solutions of the repeating event clusters in the Central Marmara. The green circles show the locations of the seismic repeaters. The mechanism of normal faulting of the Repeater Cluster 5 is shown by purple..... 59
- Figure 5.14. (a) The comparison for the relation between recurrence time (T_r) and seismic moment (M_0) for the repeating earthquakes occurred in different tectonic environments. (b) the number of repeating sequences, magnitude range, and coefficient of variation (COV) in recurrence intervals for different regions (after Chen et al., 2007) 61
- Figure 5.15. Demonstration of the recurrence time intervals of the near-repeaters acquired in this study from 2008-2021. 63
- Figure 5.16. The displacement spectrum of seismic source model (after Eaton et al., 2014) 64
- Figure 5.17. Left: the spectra of the E-W component waveforms detected in Cluster 1 at SLVM station. Each spectrum is normalized by its average value between 1-

- 5Hz. Right: Signal/Noise for the spectra of the signal and noise windows.
 65
- Figure 5.18. The relationship between the area (A), slip (d) with the seismic moment (M_0) in logarithmic scale. Left shows the relation of the area (A) versus moment (M_0). Right indicates relationship of slip (d) versus seismic moment (M_0) (Nadeau and Johnson, 1998)..... 66
- Figure 5.19. Magnitude and slip relationship between three slip models given by Equations (5.10), (5.11), (5.12) (after Uchida, 2019). 68
- Figure 5.20. The repeating waveforms detected in Cluster 1 from the SLVM station between 2008-2018: vertical (top), N-S (middle) and E-W (bottom) components. Traces are normalized by the maximum value of each trace. The numbers on the left of the traces (red labels) shows the recording date of the event. The numbers on the traces of the E-W components shows the moment magnitudes of each event. 72
- Figure 5.21. The analysis of E-W component of repeating events of Cluster 1 detected at SLVM stations shown in Figure 5.20. Top: Cumulative and daily seismic activity. Middle: The magnitudes of the repeating events in time. The data continuity of the SLVM station is shown on the top of the middle frame (blue). Bottom: Cumulative slip computed from the repeating events shown in the middle panel (blue) and the cumulative geodetic slip computed with a rate of 23 mm/year (red). 73
- Figure 5.22. The repeating waveforms detected in Cluster 1 from the SLVT station between 2008-2020: vertical (top), N-S (middle) and E-W (bottom) components. Traces are normalized by the maximum value of each trace. The numbers on the left of the traces (red labels) shows the recording date of the event. The numbers on the traces of the E-W components shows the moment magnitudes of each event. 74
- Figure 5.23. The analysis of E-W component of repeating events of Cluster 1 detected at SLVT stations shown in Figure 5.22. Top: Cumulative and daily seismic

activity. Middle: The magnitudes of the repeating events in time. The data continuity of the SLVT station is shown on the top of the middle frame (blue). Bottom: Cumulative slip computed from the repeating events shown in the middle panel (blue) and the cumulative geodetic slip computed with a rate of 23 mm/year (red). 75

Figure 5.24. The repeating waveforms detected in Cluster 3 from the SLVM station between 2008-2018: vertical (top), N-S (middle) and E-W (bottom) components. Traces are normalized by the maximum value of each trace. The numbers on the left of the traces (red labels) shows the recording date of the event. The numbers on the traces of the E-W components shows the moment magnitudes of each event. 76

Figure 5.25. The analysis of E-W component of repeating events of Cluster 3 detected at SLVM stations shown in Figure 5.24. Top: Cumulative and daily seismic activity. Middle: The magnitudes of the repeating events in time. The data continuity of the SLVM station is shown on the top of the middle frame (blue). Bottom: Cumulative slip computed from the repeating events shown in the middle panel (blue) and the cumulative geodetic slip computed with a rate of 23 mm/year (red). 77

Figure 5.26. The repeating waveforms detected in Cluster 3 from the SLVT station between 2008-2020: vertical (top), N-S (middle) and E-W (bottom) components. Traces are normalized by the maximum value of each trace. The numbers on the left of the traces (red labels) shows the recording date of the event. The numbers on the traces of the E-W components shows the moment magnitudes of each event. 78

Figure 5.27. The analysis of E-W component of repeating events of Cluster 3 detected at SLVT stations shown in Figure 5.26. Top: Cumulative and daily seismic activity. Middle: The magnitudes of the repeating events in time. The data continuity of the SLVT station is shown on the top of the middle frame (blue). Bottom: Cumulative slip computed from the repeating events shown

- in the middle panel (blue) and the cumulative geodetic slip computed with a rate of 23 mm/year (red). 79
- Figure 5.28. The comparison of the microearthquake locations of the current study and Yamamoto et al. (2017). The red circles denote the locations from the present study. The black circles indicate the results of Yamamoto et al. (2017). Green circles show the repeaters obtained in this study. Orange dots denote the repeater found in Uchida et al. (2019). The black line denotes the locking depth given by Schmittbuhl et al. (2015). Top: The horizontal distribution of the earthquake locations. Middle: The depth section obtained in the thesis. Bottom: The depth section depicting the depth results from Yamamoto et al. (2017) with the hypocentral locations of the repeaters from Uchida et al. (2019)..... 82
- Figure 6.1. The seismicity map (top) and depth (bottom) sections from this study (red circles). The yellow circles show the aftershock locations of 2019 Mw5.8 Silivri earthquake (Karabulut et al., 2020)..... 87
- Figure 6.2. The repeater activity between 21.11.2014 and 23.11.2014. Each cluster is shown circles by different color and their cluster numbers are given. Stars denote the regular events occurred in the area. (a) Map view of the locations of the near-repeating clusters. (b) The depth distribution of near-repeater clusters..... 91
- Figure 6.3. The temporal change of the repeater activity between 21.11.2014 and 23.11.2014. Orange, pink, light brown and yellow denote Cluster 5, 4, 8 ,9, respectively. Stars denote the regular events occurred in the area..... 92
- Figure 6.4. Schematic demonstration of the interaction of the asperities in a creeping fault zone. The ruptured asperities in interaction are denoted by blue strips. The arrows represent creeping motions. The red area shows stress increase due to the rupture of the asperity..... 92

LIST OF TABLES

Table 3.1.	The recording time period of the OBS and land stations.....	16
Table 3.2.	The 1-D velocity model obtained in this study using VELEST inversion code (Kissling, 1994).....	22
Table 5.1.	The locations of the repeating earthquake clusters and the uncertainties of the calculation for dip, strike and rake calculations.....	60
Table 5.2.	The methods for the slip estimations of recent studies in the Marmara Region.....	83

LIST OF SYMBOLS

C	Free Surface Correction
C	Strain Hardening Coefficient
d	Slip
f_c	Corner frequency
$G(r)$	Geometrical Spreading
M_0	Seismic Moment
R	Source Radius
T_r	Recurrence Time Interval
$\overline{T_r}$	Mean interevent time of the T_r
T_r^{nor}	Normalized Recurrence Interval
v	Wave velocity
V_s	Shear wave
V_r	Rupture velocity
α	Crack Radius
μ	Rigidity
ΔU	Slip
$\Delta \delta$	Stress Drop
ρ	Density
Ω_0	Low frequency Level
$R_{\theta\phi}$	Radiation Pattern

LIST OF ACRONYMS/ABBREVIATIONS

COV	Coefficient of Variations
CB	Çınarcık Basin
CC	Cross Correlation
CeB	Central Basin
Hz	Hertz
KOERI	Kandilli Observatory and Earthquake Research Institute
KB	Kumburgaz Basin
MMF	Main Marmara Fault
MMFZ	Main Marmara Fault Zone
MAM	Marmara Araştırma Merkezi
NAF	North Anatolian Fault
NAFZ	North Anatolian Fault Zone
OBS	Ocean Bottom Seismometer
RMS	Root Mean Square
S/N	Signal/Noise
Sec	Second
TUBITAK	Scientific and Technological Research Council of Turkey
TB	Tekirdağ Basin
USA	United State of America

1. INTRODUCTION

Over the years, The Marmara Region has witnessed many devastating earthquakes. The seismotectonic and geodynamic role on this earthquake potential of the region has been questioned by many studies (Mihailovich, 1927; Ambraseys and Jackson, 2000; Ambraseys, 2002). Although the surveys address some questions, the evidence is still not enough to solve the mysteries of this unique and special fault structure and earthquake behavior of the region. However, it is certain that The North Anatolian fault (NAF) plays a significant role on the deformation and led to destructive earthquakes along the Main Marmara Fault zone throughout the years. The earthquakes along the NAF have been migrating since 1939 Erzincan earthquake from east to west. The last of the migrated events in the west of the NAF is the 1999 İzmit earthquake. Together with the 1999 Bolu-Düzce Earthquake, there has been a surface break of about 160 km in the region. In 1912, Ganos-Mürefte Earthquake $M=7.4$ occurred in the west and it broke a segment approximately 80 km long (Armijo et al., 2005). The North Anatolian fault continues under the Main Marmara fault (MMF) with about a 160 km unruptured segment, which is also defined as a seismic gap (Armijo et al., 2005, Parsons et al., 2000). Also, a Poisson probability of İstanbul hit by a $M > 7.3$ event at İstanbul in 30 years has been estimated as %35. This value shows an increment to %35 regarding transfer of stress and time dependency (Murru et al., 2016). Considering the recurrence interval of the historical large earthquakes about 250-400 years for the area, including creeping zone, from paleoseismic data combined with the geodetic data reveals that the region has a potential to produce a large event about $M_w=7.4 - 7.5$ with a moment rate deficit $M_d = 6.4 \times 10^{17}$ (Meghraoui et al., 2021). This seismic gap in the Marmara Sea threatens the lives living in the metropol İstanbul and its surrounding (Parsons et al., 2000; Hubert and Ferrari et al., 2000; Ozel et al., 2011; Parsons, 2004; Hancılar, 2012); therefore, faults segments in silence are critical issues that should be understood in terms of the seismological action.

Defining the behavior of this fault segment called as a “seismic gap” in terms of its strain accumulation is crucial to evaluate the seismic hazard assessment of the region. The question of which fault segments are creeping and locked segments is waiting an answer to

make an interpretation for the possible location of the next forthcoming devastating earthquake in the region (Schmittbuhl et al., 2015; Ergintav et al., 2014).

One method to figure out this behavior can be the observations based on the geodetic measurements on the area. Recent land GPS data pointed out that the fault segments have a variable locking behavior on the central part of MMF (Ergintav et al., 2014; Klein et al., 2017). According to Ergintav et al. (2014), Central, Kumburgaz and Tekirdağ Basins do not exhibit a coupling behavior. On the other hand, Prince Island fault segment may have accumulated strain.

The studies on micro-seismicity can also provide us a comprehend knowledge about the coupling behavior of the fault over large area, which necessities reliable earthquake location procedures (Yamamoto et al., 2019). Especially, the observations from the Sea of Marmara is vital for a realistic seismotectonic interpretation. Generally, the high seismicity is associated to the seismogenic zone and viewed as the sign of the creeping areas resulted from the heterogeneities that is also called as “asperities” on the fault zone (Yamamoto et al., 2015; Schmittbuhl et al., 2015; Schmittbuhl et al., 2016). Recently, the study of microseismicity of the region implemented by Schmittbuhl et al. (2015), the micro-earthquake activity of the region between 2007-2015 was investigated in order to indicate the behavior of the fault segments of the MMF, and the study reported that Tekirdağ and Central Basins are creeping zones indicating high seismicity rate distributed from surface to 17 km, while the Kumburgaz and Çınarcık Basins are locked segments. The micro-earthquake observations demonstrate that the seismicity is very sparse in the Çınarcık Basin area, and the depth range is between 8 and 14 km except at both ends of this basin. The study reported that the lower limit of seismogenic zone along the MMF is about 16 km depth and the Çınarcık segment has been defined to be locked to 10 km (Schmittbuhl et al., 2015; Karabulut et al., 2020). Yamamoto et al. (2017) and (2019) have also found plentiful micro-earthquakes in the Western High, Central Basin and scarce seismicity in Kumburgaz and Çınarcık segments by using the ocean bottom seismometers deployed in the Marmara Sea.

Recent studies carried out in order to characterize the creeping zones in Marmara segment of the NAF agrees with each other in existence of creep in the Central part of the fault. Sakic et al. (2016) demonstrated a surface locking in the Central High and a creep rate smaller than 0.6 cm/yr in 6 months. That work strengthened the idea that Western High has a deep creep component while the Central Basin shows a shallow creeping patch along the Main Marmara Fault. Yamamoto et al. (2019) reported a surface creep of 1.1 cm/yr in the Western High using sea bottom acoustic range at two points along the Marmara Segment and that the fault is locked partially in the 0-8 km, full locked in the 8-11 km depth range, and completely decoupled below 11 km depth. Recently, 3-D elastic model carried out by Yılmaz et al. (2022) for understanding of the interseismic behavior showed that the locking depth for the Çınarcık Basin is 5 km. Also, Ganos and İzmit segments seem to be locked down to 7.5 km. The results obtained from these studies for the creeping areas are also almost consistent with the high seismicity and reported repeating events.

Although the studies based on the GPS measurements (Ergintav et al., 2014) and extensometer observations at one point in long term (Yamamoto et al., 2019) can provide reliable results, they are insufficient to confirm the situation of creep in the area; and they need to be supported by the studies related to the search of the repeating earthquakes (Schmittbuhl et al., 2016). Besides these geodetic observations, detection of the repeating earthquakes which are identical in magnitudes, locations and waveform shapes, is a useful indicator for the definition of the distribution of aseismically slipping(creeping) areas to a wide extent along the fault beneath the Marmara Sea since the locations of geodetic observations made by Sakic et al. (2016) and Yamamoto et al. (2019) are confined with two points on the fault zones (Uchida et al., 2019).

The repeating earthquakes, which are good indicators for the slow fault slip on a fault plane, can be investigated to indicate the creeping behavior on a fault zone (Kato et al., 2012; Bouchon et al., 2011, Uchida et al., 2019). The observations of the repeating events will also give a unique chance to estimate the slip on a fault zone (Uchida et al., 2019). However, the search of the repeaters in a region is not a straightforward process, and it necessitates a meticulous work of process of a mass of seismic data. Hence, a robust analysis of detection of the waveform similarity and an accurate assessment of the

seismological properties, such as locations, magnitudes and the characteristic behavior like recurrence intervals, for these events are of great importance to acknowledge them as repeaters (Nadeau et al., 1994; Uchida et al., 2005, Schmittbuhl et al., 2016, Uchida et al., 2019).

As the researchers investigate the repeating events, special features of these events are also indicated. The repeating earthquakes, having different magnitudes that are very close to each other with highly correlated waveforms are called as “near-repeating events” by Shaddock et al. (2021). These events are also marks of aseismic slip in a region and can be utilized for the estimation of slip.

Recently, studies carried out in the Marmara Sea region showed the presence of the repeating events especially in the Central Basin (Uchida et al., 2019, Schmittbuhl et al., 2016, Bonnhoff et al., 2017) which agrees with the results demonstrating that the area is creeping that were reported by the studies based on GPS measurements such as (Ergintav et al., 2014).

This thesis aims at defining the microseismic activity of the Marmara Region and assessing the seismic hazard of the region by investigating the repeating earthquakes to indicate the creeping and the locked zones along the western part of the NAFZ. In the scope of this thesis, the microseismic earthquakes of the Marmara Region are focused and the seismograms from the OBS stations deployed in the Marmara Sea region are analyzed.

The process of this study is started by obtaining the OBS data recorded in the Marmara Sea and followed by different earthquake detection techniques used for both microseismicity and the search for repeating earthquakes. In the scope of this thesis, first the relocation process for the earthquakes is performed for the period between September 2014 and July 2015 in the catalog reported by Yamamoto et al. (2017). STA/LTA method is used for identification of earthquakes of the data obtained for the time period of July, 2015 and April, 2016. P and S phases are picked manually using Zsac software and relocated by HYPOCENTER code (Lienert et al., 1986; Lienert and Havskov, 1995). Using the velocity models of Becel et al. (2010) and Bayrakçı et al. (2013) for the shallow sections and Karabulut et al. (2011) for the deeper section, a new initial model has been

produced. A 1-D velocity model is estimated using VELEST code (Kissling, 1994) inversion code. The deviations from 1-D velocity model are accounted in the station corrections.

Analyses of the microseismicity of the region gives a general picture of the behavior of the fault segments beneath the Marmara Sea. The approach of the thesis to analyze the repeaters of the region is the search the template events within the continuous seismograms using template matching method. For this purpose, the template events recorded at SLVM station used in the study of Schmittbuhl et al. (2016) were used for the repeater search from 2008-2018 at SLVM station. The search of the repeating earthquakes was also extended to 2021 at SLVT station. Then, the properties of the repeating events have been scrutinized, such as their locations, fault mechanisms and recurrence time intervals.

The thesis is formed by 7 chapters. After presenting the introduction part, Chapter 2 concentrates on the seismotectonic structure and historical earthquake background for the Marmara Region.

Chapter 3 shows the analyses for the microseismicity in the Marmara Sea region. The chapter includes the processes of the STA/LTA detection and location of the detected events.

Chapter 4 synthesizes the repeating earthquakes in theory and the difficulties that are faced with in practical by presenting the studies on this subject. The definition and the physical model behind the repeating earthquakes are also presented. The nearly repeating events are also described in this chapter.

Chapter 5 describes the process of the search for the repeater using template matching method. Also, this chapter focuses on the characterization for the repeaters by estimating locations and the fault mechanisms and the using OBS data. The recurrence intervals of the near-repeating events were also viewed. The spectral analyses and the fault slip estimations for the repeaters are also indicated in this chapter.

Chapter 6 and Chapter 7 include “Discussion” and “Conclusion” parts, respectively.

2. SEISMOTECTONIC STRUCTURE AND HISTORICAL EARTHQUAKES IN THE MARMARA REGION

2.1. Tectonic Setting of the Marmara Region

The Anatolian Plate is a seismically active area, which leads to devastating earthquakes throughout the history. Undoubtedly, it is inevitable to describe this activeness as the cause of the collision between the Arabian Plate in the south and Eurasian Plate in the north, which leads Anatolian Plate to move westward. In addition to this, African plate subducts northward beneath western Turkey and the Aegean region (Figure 2.1). These movements are controlled mostly by The North Anatolian Fault Zone (NAFZ) which is a right-lateral strike-slip fault, running from East to West of the country, about 1200 kilometers (McClusky et al., 2000) with a westward motion of 20-25 mm/yr (Figure 2.2) (Reilinger et al., 2006; Meade et al., 2002).

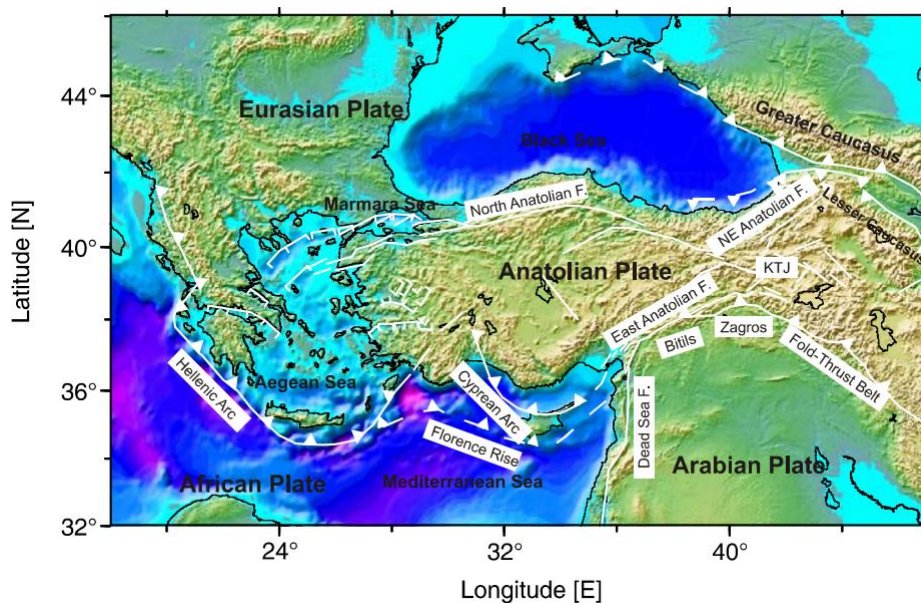


Figure 2.1. Tectonic motions around the Anatolian Plate. KTJ denotes Karlova Triple Junction. The borders of the tectonic structures were indicated by the dashed lines. The lines including triangles depict the thrust faults. Main structures were taken from the McClusky et al. (2000). (Aktuğ et al. 2009).

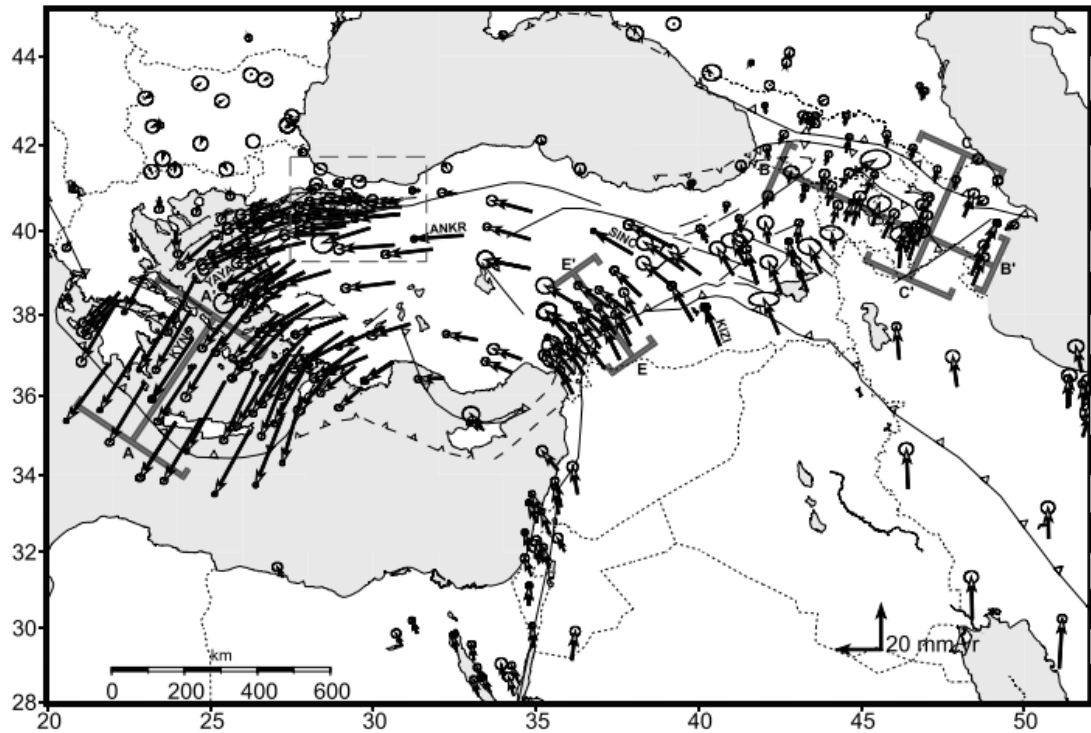


Figure 2.2. The GPS velocities with respect to Eurasia indicated by Reilinger et al. (2006).

The NAF system was responsible for many destructive earthquakes in the past, which caused the seismic activity to propagate westward by a sequence of earthquakes since 1939 as suggested by Barka (1996); Akyüz et al. (2002); Hubert-Ferrari et al. (2000); Parsons et al. (2000); Stein et al. (1997); Toksöz et al. (1979); Reilinger et al. (2000). Undoubtedly, The Marmara Region is one of the most affected areas by these events (Ambraseys and Jackson, 2000) since NAF divides into two branches in the north and south in the Sea of Marmara starting from Gulf of Izmit.

1912, Şarköy-Mürefte event, occurred on the Ganos Fault Zone, was one of the largest earthquakes in the western Marmara Sea and it was reported that it caused tsunami (Mihailovich, 1927; Ambraseys and Finkel, 1987, 1991). Its magnitude was assigned as $M_s=7.3$ using macroseismic data by Ambraseys (1988). Recently, this earthquake has been investigated using modern seismological methods applying on analog records by Başarır (2011). The study found the magnitude $M_w=7.13$, radius of the source zone $R=41.6$ km and stress drop $\Delta\sigma=26.09$ bar. Aksoy et al. (2010) indicated that the 1912 Earthquake has

strike-slip fault mechanism using the P wave first motion polarities of some analog records. The length of rupture of this event and at which point it terminated in the east is a critical question. The fault rupture calculated for this event was reported as approximately 80 km by Başarır (2011) and 100 km by Armijo et al. (2005). On the other hand, Parsons (2004) suggested that the rupture terminated at the Tekirdağ Basin based on the macroseismic observations.

Another significant earthquake was the 1999 İzmit Earthquake, one of the most devastating events occurred on the eastern part of the area because of the earthquake migration of NAFZ (Reilinger et al., 2000, 2002; Gürbüz et al., 2000) and it was followed by the 1999 Bolu-Düzce event. The fault break of the 1999 İzmit earthquake was given as 120 km with observed surface offsets ranged from 1.5 to 5 m by Barka (1999) and 145 km based on the morphological analyses by Uçarkuş et al. (2011). Although the western termination of the rupture of the 1999 earthquake is debatable, it may have reached to Çınarcık Basin (Çakır et al., 2003). The two devastating earthquakes together have led to surface breaks approximately 160 km (Armijo et al., 2005). Also, looking for the historical records (Ambraseys, 2009; Başarır Baştürk et al., 2017), 1766 earthquake is indicated to be the last devastating earthquake occurred on the western part of NAF (Parsons, 2000), which resulted in creation of a seismic gap with about 150 km long segment (Le Pichon et al. 2001; Oglesby et al 2008; Schmittbuhl et al., 2015; Armijo et al., 2002).

In near history, the location of the 1963 earthquake is also significant since the rupture of this event and the termination of the 1999 earthquake rupture in the west remain debatable. The faulting mechanisms of the 1963 earthquake showed the normal faulting that located close to the Princes Island Fault (PIF) by Başarır Baştürk et al. (2016a), implying that the Çınarcık Basin has normal components of compressional and strike-slip motions together with the confirming studies such as Taymaz et al. (1991), Korkusuz Öztürk et al. (2015). Looking for the locations and faulting mechanisms of the 1935 Marmara Island earthquakes, occurred at 14:41 and 16:20 at the same day, demonstrating the normal faults at 4 km and 10 km, respectively (Başarır Baştürk et al., 2016a). The locations of these events which are on the north and south of the Marmara Island are backed up by the presence of the faults displayed by Hergert et al. (2011). In addition, the normal faulting mechanisms of the earthquakes that may form the deep basins in the area

coincides with the pull-apart model suggested by Armijo et al. (2005). As stated in Taymaz et al. (1991), the normal faults in the area may be responsible for the uplift of the Marmara and Princes Island.

There are basically two remarkable fault models proposed for the Main Marmara Fault based on bathymetry and seismic reflection studies. One of them is the single strike-slip model which has been proposed by Le Pichon et al. (2001, 2003) and the other one is the pull apart model, which is thought to be a graben consisting of right-lateral faults showing normal movements (Barka and Kadinsky-Cade, 1988), suggested by Armijo et al. (2002, 2005). These two models agree with each other in terms of the location of the MMF although they suggest different fault models. Yet, it is needed to achieve more research in the Marmara Sea to indicate its complex fault network and geometry, especially using multichannel seismic surveys (Yamamoto et al., 2020).

In literature, The Main Marmara Fault is defined by four basins which can be considered as the fault segments in the region. These are Çınarcık Basin, Kumburgaz Basin, Central Basin and Tekirdağ Basin (Figure 2.3). Firstly, it has been suggested the Marmara Sea Basin seems as a graben or consists of right-lateral faults indicating an overall normal motion (Barka and Kadinsky-Cade, 1988). The Sea of Marmara is marine basin, consisting of shallow shelf to the south, about 230 km long and 70 km wide. The active faults located on the land is comparatively understood. However, the faults lying in the basins in the sea is not well understood (Ambraseys, 2002). In the west, Tekirdağ Basin and in the east, Çınarcık Basin show high local seismicity from the depth and steep bathymetric gradients (Smith et al., 1995; Wong et al., 1995; Parke et al., 2000; Okay et al., 2000).

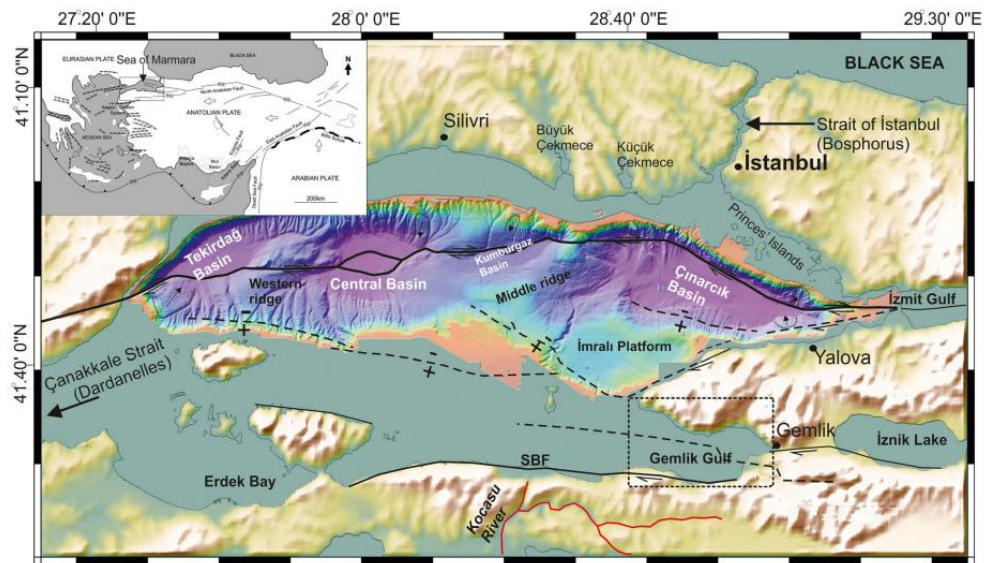


Figure 2.3. Bathymetry and active faults in the Marmara Sea (Filikçi et al., 2017).

To understand the behavior of the fault segments, one commonly used criterion is whether they are creeping or locked. Definition of these segments in terms of their creeping or locked situation and how much strain they accumulate are important to assess the seismic hazard in the region (Schmittbuhl et al., 2015, 2016; Klein et al., 2017, Sakic et al., 2016; Ergintav et al., 2014). In the study of Ergintav et al. (2014), the slip deficit estimations on the fault segments of MMF based on GPS measurements indicated that Central Basin is suggested as the creeping segment with a slip deficit smaller than 2 m, which means that it shows a slow and a constant slip. On the other hand, the Çınarcık Basin has a slip deficit rate of 10-15 mm/yr and a slip deficit about 2.5 m-3.7 m (Figure 2.4), which means that the fault does not slip since the 1766 earthquake and accumulates strain which will be released during a large earthquake (Ergintav et al., 2014).

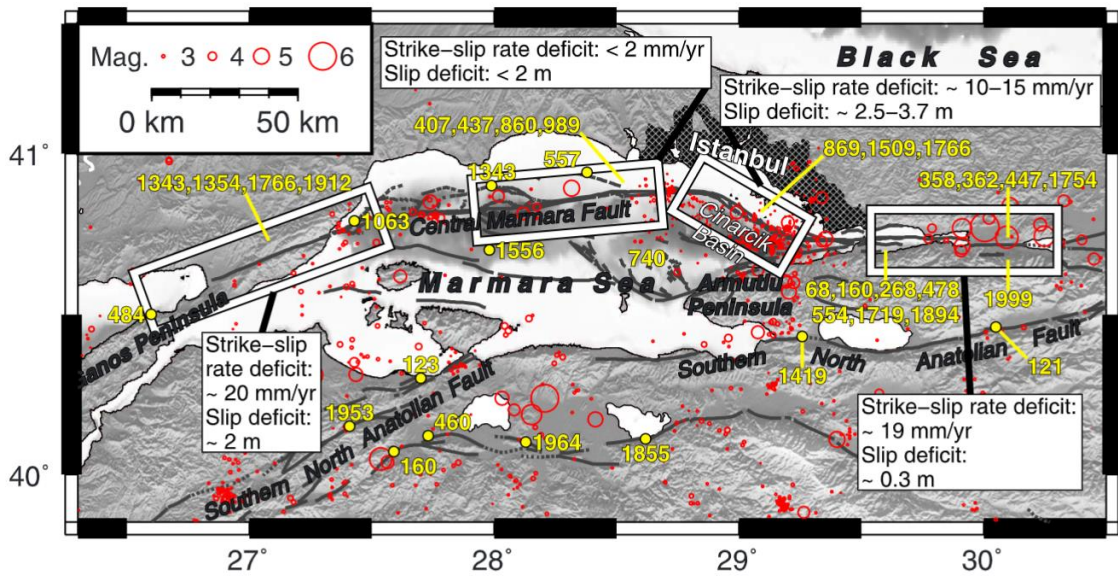


Figure 2.4. The estimated slip rate deficits and the total deficits accumulated since the last major earthquakes (Ergintav et al., 2014).

Also, the presence of the sediment layer beneath the Marmara Sea has been depicted by Becel et al. (2010) to 7 km using the of reflection and refraction gathered during the SEISMARMARA. Although the geodetic observations provide good results to comprehend the locking state of the fault segment, it is limited to monitor the behavior of the fault segments since the MMF is beneath Marmara Sea (Schmittbuhl et al., 2015; Klein et al., 2017; Yamamoto et al., 2019; Yamamoto et al., 2020).

2.2. Historical Earthquake Background of the Marmara Region

To assess the seismotectonic of the Marmara Region, it is essential to research the earthquakes occurred on the North Anatolian Fault Zone, in both historical and instrumental period. Particularly, the historical earthquakes, prior the instrumental era, necessitates a meticulous work since the documents regarding the historical earthquakes are limited. There are limited catalogues concerning the historical earthquakes occurred in Anatolia and surrounding regions such as Ambraseys and Jackson (1998); Tan et al. (2008); Ambraseys (2009); Soysal et al. (1981); Güçlü et al. (1986); Pınar and Lahn (1952); Ergin et al. (1967, 1971) (Başarı Baştürk et al., 2017).

Recently, Başarır Baştürk et al. (2017) reported 576 earthquakes for Marmara Region between the dates of 2000 B.C. and 1900 A.D., compiling over 20 historical sources including Ambraseys (2009), Soysal et al. (1981), Guidoboni et al. (1994), Altınok et al. (2011), Ambraseys (1989), Ambraseys (2002), Ambraseys and Finkel (1995), Ambraseys and Jackson (1998, 2000), Berberian and Arshadi (1976), Ergin et al. (1967, 1971), Guidoboni and Comastri (2005), Papazachos et al. (1997, 2003), Shebalin et al. (1974), Sbeinati et al. (2005), Shebalin and Tatevossian (1997), Soysal et al. (1981), Suleiman et al. (2004), Stucchi et al. (2013). The map given in Figure 2.5 shows the devastating historical earthquakes with intensity IX-XI ($M_s \geq 7.0$) that occurred in the Marmara Region from 2000 B.C. to 1900 A.D.

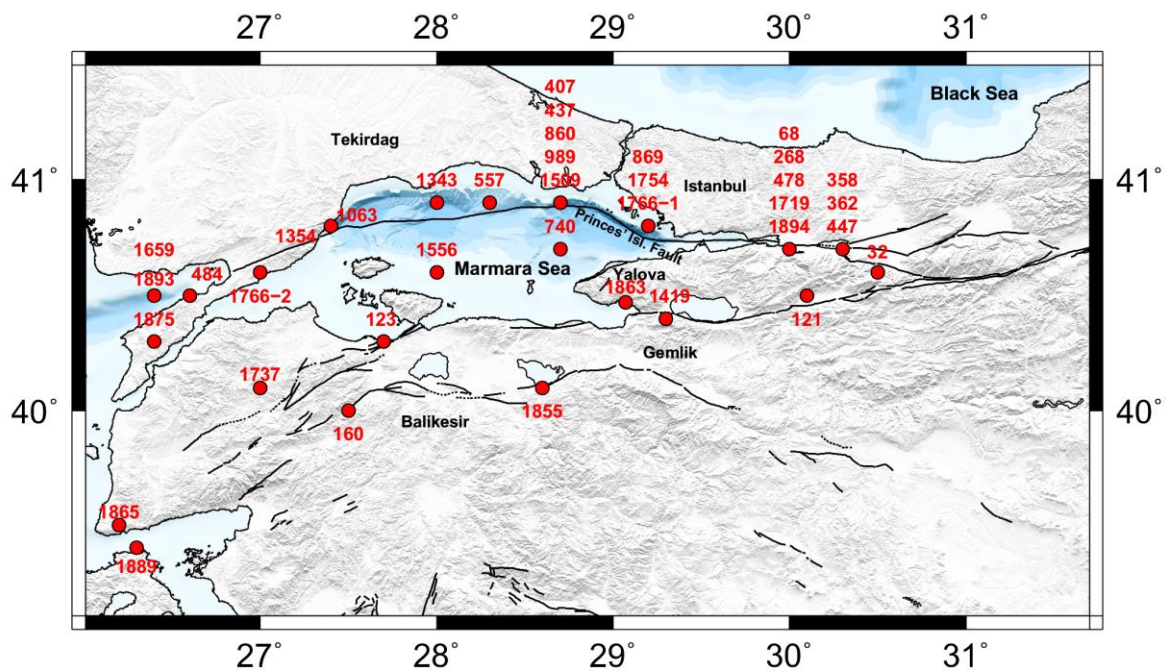


Figure 2.5. Important historical earthquakes with intensity IX-XI ($M_s \geq 7.0$) that occurred in the Marmara Region (Başarır Baştürk et al., 2016b).

One of the most devastating historical earthquakes is the 1509 Earthquake which has been occurred in the northeast in the Marmara Sea. It was felt in a very large area, from Bolu to Edirne. The earthquake destroyed over 1000 houses, killing 4000-5000 people and injured 10.000 people. Another important event is the 1766 Earthquake. The location of this event has been reported in the Sea of Marmara and the damage was severe as it

extended from İzmit to Tekirdağ. Although location of the 1766 earthquake is unclear, it seems to be the most recent $M > 7$ earthquake occurred in the east of the Marmara Segment beneath the Marmara Sea (Ambraseys, 2009; Parsons et al., 2004; Pondard et al., 2007; Başarır Baştürk et al., 2017). The 1894 earthquake, on the other hand, seems to be related to the faults in the Gulf of İzmit on the NAFZ (Ambraseys, 2001; 2009). Also, the 1719 earthquake led to damage in Yalova, Pazarköy, Karamürsel, Kazıklı and İzmit and the villages around the İzmit Gulf extending from Sapanca to Düzce. It has been told that more than 6000 people have died as a result of this earthquake. The earthquake caused damage in 40 mosque and 17 tower. Also, there has been damage in the houses and city walls in İstanbul. It has been reported that the damage extended to the Thrace (Ambraseys, 2009; Başarır Baştürk et al., 2017). Looking for the macroseismic information, the damage caused by 1999 İzmit Earthquake seems to be likeness to the damage reported for the 1719. Moreover, two earthquakes occurred in 1766 and 1754 earthquake have been reported to be possibly resulted from fault ruptures closer to İstanbul (Başarır, 2011; Ambraseys and Jackson, 2000; Ambraseys, 2002). Thus, the fault segments beneath the Marmara Sea have a silence in terms of producing a large event ($M > 7$), which increases the possibility of the forthcoming event to occur in the eastern segment since it did not rupture for more than 250 years (Ergintav et al., 2014; Yamamoto et al., 2020).

3. ANALYSIS AND PROCESS OF THE MICROSEISMICITY OF THE MARMARA SEA

In this study, the first target has been to create a database of the micro-earthquakes in the study area. As a first stage, the micro-earthquake catalogue of Yamamoto et al. (2017) has been used for the time period between 26.09.2014 – 25.07.2015. In addition to stations used by Yamamoto et al. (2017), six OBS from IFREMER, four OBS stations from GFZ in the frame of the MARSITE Project and two land stations (SLVM, MARM) are added to the database. This resulted in more precise hypocenters determination of the microseismicity of under the eastern part of the Central Basin to the Kumburgaz Basin. For the time period between July 2015 and April 2016, we used STA/LTA for the detection of events. After applying STA/LTA detection on the seismic data, the event database has been created and the location process has been performed. After all, this analysis enabled to reach the micro-earthquake catalogue, which is one of the main goals of this thesis. Step by step progress of working process is summarized in Figure 3.1.

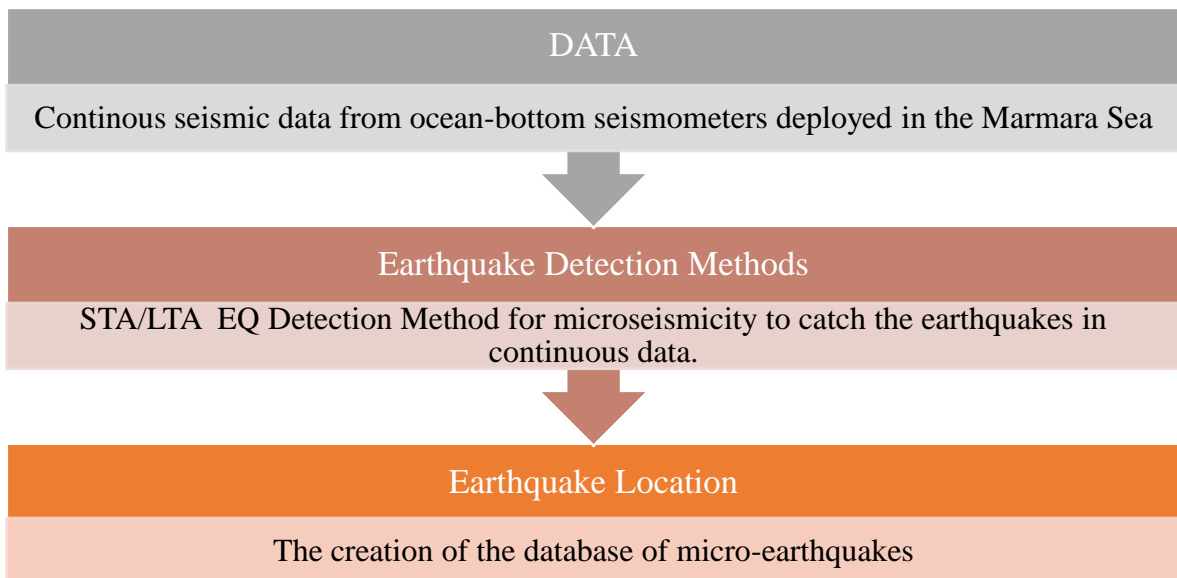


Figure 3.1. Flow diagram showing the processes followed step by step from obtaining data to acquiring microseismicity database

3.1. Data

In the scope of this study, the continuous data recorded at ocean bottom seismometers have been obtained to determine microseismic activity near the fault zone of the Marmara Sea. A total of 21 OBS stations are operated between 04.02.2014 and 05.12.2016 in the Marmara Sea (Figure 3.2). The OBS stations contain 4 component high frequency geophones (4Hz), 2 horizontal, one vertical, one pressure sensors. The data were sampled and recorded with 100 sps. 15 of these stations were deployed within the MARDIM Project (Yamamoto et al., 2017). The average spacing of about 10 km, enables to catch the small events as possible. The time calibration of the stations has been performed with the clock accuracy better than 0.05 s through the OBS clock with Global Navigation Satellite System (Yamamoto et al., 2017). In addition, 6 OBS stations were included, that were deployed by Ifremer between 19.09.2014 – 14.11.2014 and 5 stations by GFZ between 25.04.2015 – 13.04.2016 in the frame of MARSITE Project. Two land-based stations nearest to the OBS deployments are also included (SLVM, MARM) to this database. Figure 3.2 shows the locations and operation periods of the stations displayed in Table 3.1.

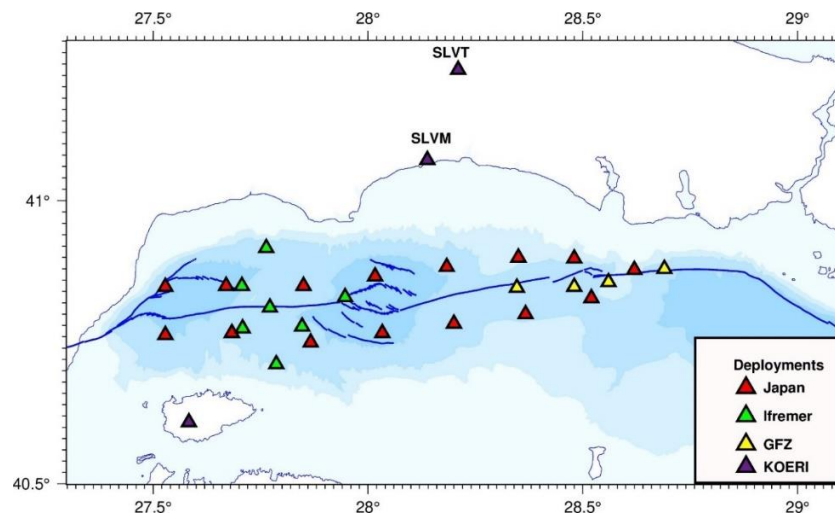


Figure 3.2. The locations of the OBS and land stations. The purple triangles indicate the first 15 OBS stations deployed in the scope of MARDIM project. The black solid triangles denote the OBS stations added later. The red triangles (SLVM, SLVT) show the land stations, also used for the detection of the nearly repeating events.

Table 3.1. The recording time period of the OBS and land stations

Station Code	Start	End	Start	End
MS01A	26.09.2014	20.07.2015	01.01.2016	25.07.2016
MS02A	26.09.2014	20.07.2015	25.07.2015	20.06.2016
MS03A	26.09.2014	20.07.2015	25.07.2015	20.06.2016
MS04A	26.09.2014	20.07.2015	25.07.2015	20.06.2016
MS05A	26.09.2014	20.07.2015	25.07.2015	20.06.2016
MS06A	26.09.2014	20.07.2015	25.07.2015	21.06.2016
MS07A	26.09.2014	20.07.2015	25.07.2015	21.06.2016
MS08A	26.09.2014	20.07.2015	25.07.2015	21.06.2016
MS09A	26.09.2014	20.07.2015	25.07.2015	20.06.2016
MS10A	26.09.2014	20.07.2015	25.07.2015	20.06.2016
MS11A	17.03.2015	20.07.2015	25.07.2015	20.06.2016
MS12A	18.03.2015	20.07.2015	25.07.2015	20.06.2016
MS13A	18.03.2015	22.07.2015	25.07.2015	20.06.2016
MS14A	18.03.2015	21.07.2015	25.07.2015	21.06.2016
MS15A	18.03.2015	21.07.2015	01.01.2016	25.07.2016
OB01	19.09.2014	14.11.2014	19.09.2014	14.11.2014
OB02	19.09.2014	14.11.2014	19.09.2014	14.11.2014
OB03	19.09.2014	14.11.2014	19.09.2014	14.11.2014
OB04	19.09.2014	14.11.2014	19.09.2014	14.11.2014
OB05	19.09.2014	14.11.2014	19.09.2014	14.11.2014
OB06	19.09.2014	14.11.2014	19.09.2014	14.11.2014
OBN1	25.04.2015	13.04.2016	25.04.2015	13.04.2016
OBN2	25.04.2015	13.04.2016	25.04.2015	13.04.2016
OBN3	25.04.2015	13.04.2016	25.04.2015	13.04.2016

OBN4	25.04.2015	13.04.2016	25.04.2015	13.04.2016
OBN5	25.04.2015	13.04.2016	25.04.2015	13.04.2016
MADM	27.09.2014	24.09.2015	27.09.2014	24.09.2016
SLVM	27.09.2014	27.09.2016	27.09.2014	27.09.2016
SLVT	27.09.2014	14.08.2015	27.09.2014	14.08.2015

3.2. Earthquake Detection and Waveform Database

Identification of the seismic events with high signal-to-noise ratio can be successfully carried out using STA/LTA detection method (Yoon et al., 2015). Also, the usage of this method has an advantage of detecting earthquakes without a prior knowledge of the event waveform, which enables a general applicability (Perol et al., 2018; Yoon et al., 2015). The STA/LTA method relies basically on detection of an earthquake which has been recorded continuously by multiple stations, seeking for signals that exceeds the threshold for the ratio of short-term average in a short time window to long-term average in a longer time window, as the windows move in the continuous data (Figure 3.3).

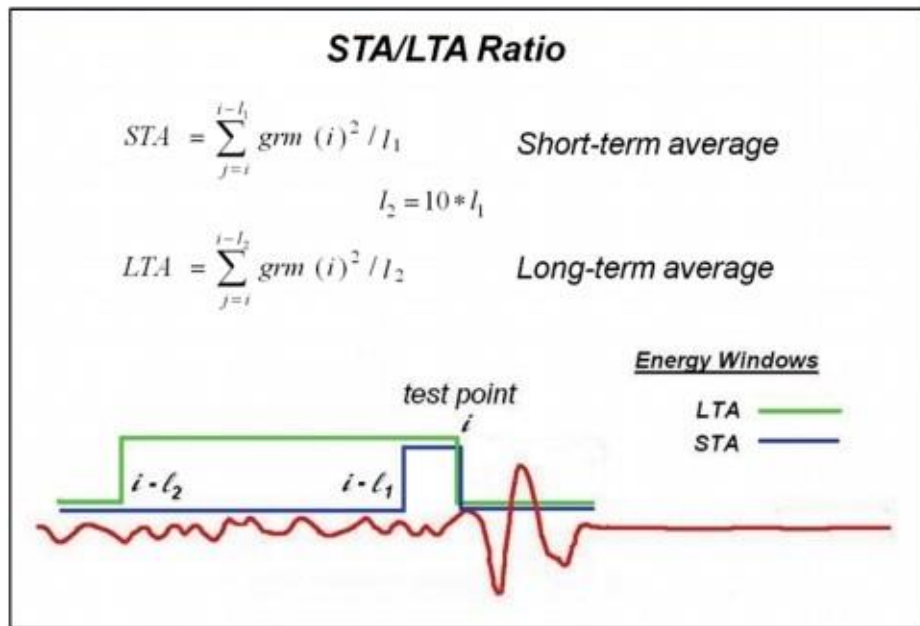


Figure 3.3. The parameters and the application of STA/LTA to data (Han et al., 2009).

In this method, when P wave arrives at the station, the difference occurred in the amplitude and frequency of the signal is defined as a characteristic function. When two consecutive windows, the STA and LTA, move in the continuous seismograms, the ratio of the average absolute amplitude value is estimated. The LTA (Long Term Average) expresses the change of the seismic noise depending on time. The STA (Short Term Average) related to the seismological events (Öztürk and Örgülü, 2018).

3.2.1 Application of STA/LTA Method on Continuous Seismic Data

The STA/LTA method was applied for the detection of seismic events on the continuously recorded seismogram data obtained from OBS stations. A ratio of 2 is used for the LTA/STA and 10 sec delay is applied for the next detection. The detection is applied to horizontal components of the OBS stations with the highest S/N and several stations individually searched for the events. The detected events from several stations are manually revised and an event catalog is formed. Figure 3.4 shows the waveforms of a detected earthquake.

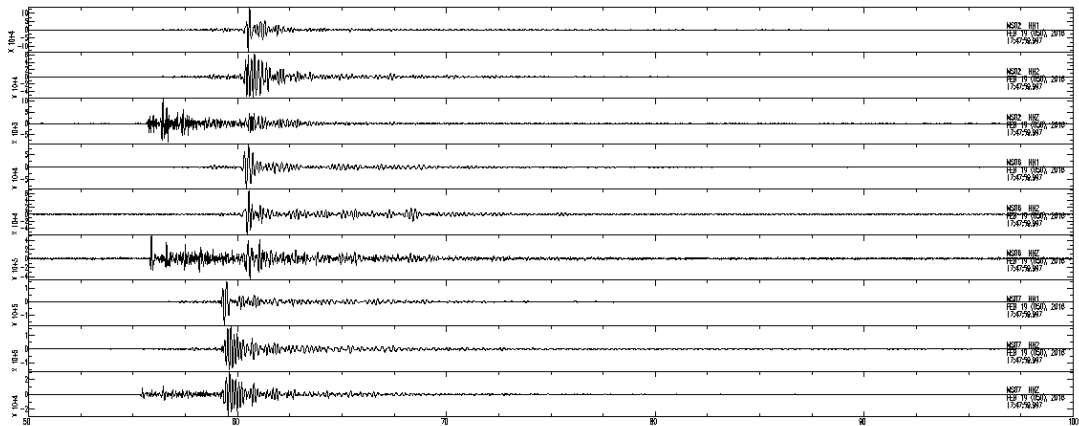


Figure 3.4. A SAC plot from the detected earthquake (2016-02-19 17:47:59) at MS02, MS07, MS08 station.

At this stage, one important criterion to include the seismic waveforms as a candidate event is to catch them at least by 4 stations. Using this method, a total of 1419 events are considered as candidate events and created a seismic waveform database using 21 OBS stations and 2 land stations (SLVT, MRMT).

3.3. The Velocity Model and Earthquake Location

The waveform database has been obtained by merging the events from the catalogue of Yamamoto et al. (2017) and detected earthquakes by this study between September 2014 and July 2016. Manual picking of P and S phases for the events has been carried out using Zsac program for both catalog events and detected events in the scope of this thesis. The example of the window from zSac software is shown in Figure 3.5.

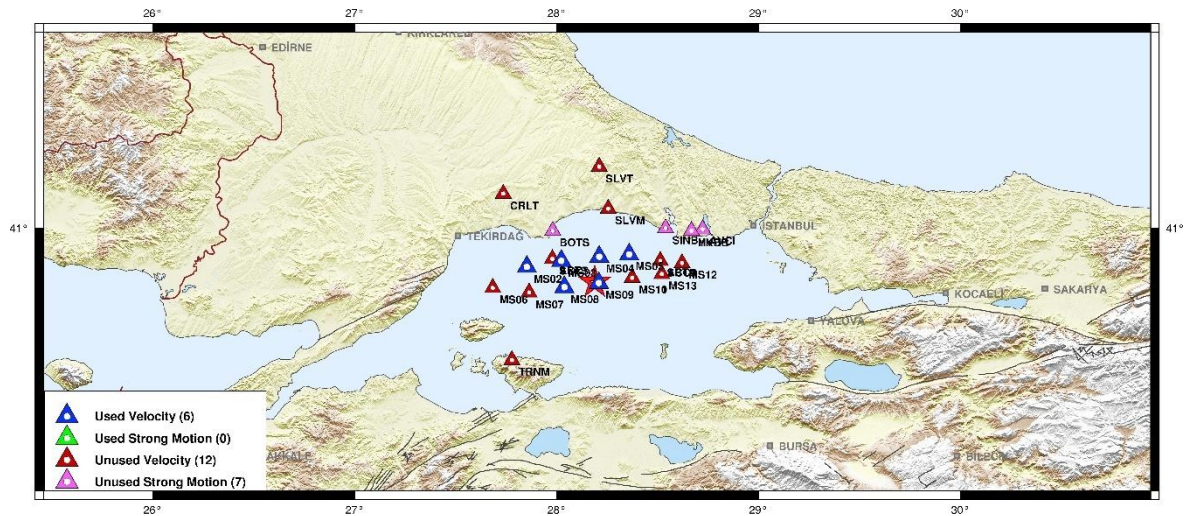


Figure 3.5. Example window of earthquake location using Zsac program. The event with origin time 20141008-1300 and magnitude $M_L=0.8$.

In total, 1454 earthquakes have been relocated using HYPOCENTER (Lienert et al., 1986; Lienert and Havskov, 1995). The initial velocity model of Karabulut et al. (2011) was used to locate earthquakes. The initial RMS error of 1454 events was 0.330 sec. A new crustal model was obtained to improve the location of the events recorded by only OBS stations. The reference of the velocity model of Karabulut et al. (2011) was the land seismic stations, therefore not appropriate for the OBS stations located on the top of the deep Marmara basins. The new initial velocity model is created based on refraction and tomographic models of Becel et al. (2010) and Bayrakci et al. (2013) for the shallow part (<5 km) and Karabulut et al. (2011) for the deeper part. A 1-D velocity model is computed from the sub-catalog using VELEST (Kissling, 1994) inversion code. A sub-catalog 200 events are selected from the initial catalog with at least 10 phase readings and less than 150 degrees of azimuthal coverage for the inversion.

The layer velocities of the initial 1-D earth model are randomly perturbed and 100 new initial models are created as input for VELEST (Figure 3.6a). The results of the 100 inversion runs are displayed in Figure 3.6b. The deviations from 1-D velocity model are accounted in the station corrections (Figure 3.7) which improved the performance of the velocity model.

Reference station is located at the north-east of Central Basin with the smallest station corrections, as also demonstrated in Figure 3.7. The station corrections are larger at the stations located in the deep basins. The layer velocities converge similar values between 5 and 20km depths but show deviations for shallower (<5km) and deeper layers (>20km). For shallow layers, this is due to subvertically travelling waves and lack of rays for the deeper layers as a result of small epicentral distances.

After the relocation using the new velocity model and station corrections, the mean RMS of the initial catalog is reduced from 0.330 s to 0.105 sec. The local magnitudes are computed from the horizontal components of waveforms.

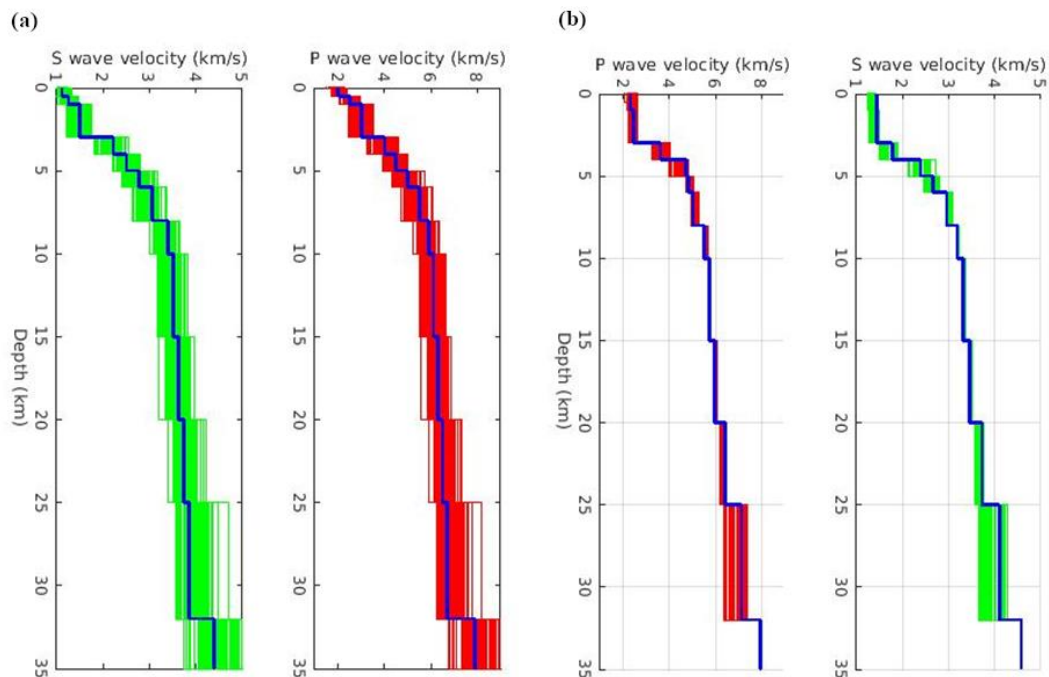


Figure 3.6. 1-D Initial velocity models for P and S waves (left), Final P (red) and S (green) velocity models (right) after inversion.

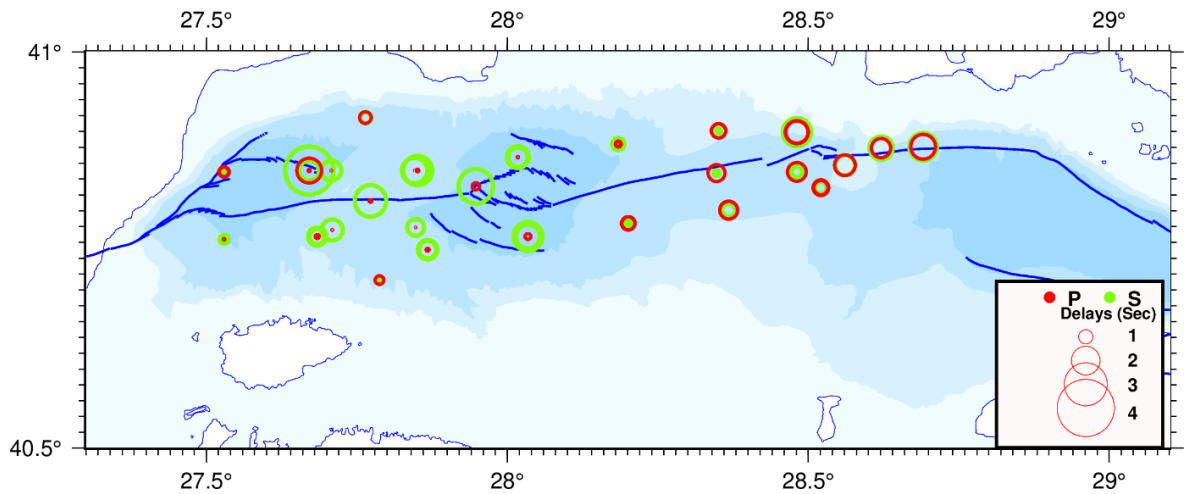


Figure 3.7. Station corrections obtained from inversion for P (red) and S (green) waves.

Table 3.2. The 1-D velocity model obtained in this study using VELEST inversion code (Kissling, 1994).

Vp(km/s)	Depth(km)	Vs(Km/s)
2.50	0.0	1.29
2.50	0.5	1.29
2.50	1.0	1.41
3.52	3.0	1.77
4.64	4.0	2.50
5.02	5.0	2.67
5.05	6.0	3.01
5.58	8.0	3.19
5.71	10.0	3.31
5.93	15.0	3.42
6.31	20.0	3.63
6.73	25.0	3.87
7.95	30.0	4.57
8.00	35.0	4.60

Figure 3.8 shows the statistics of the final catalog. The magnitude completeness of the catalog is observed as ~ 1.0 . The mean horizontal location uncertainty is ~ 1.0 km and 0.5 km for latitude and longitude, respectively. The mean of the depth uncertainty is ~ 1.5 km, varying between 0.5 and 6 km.

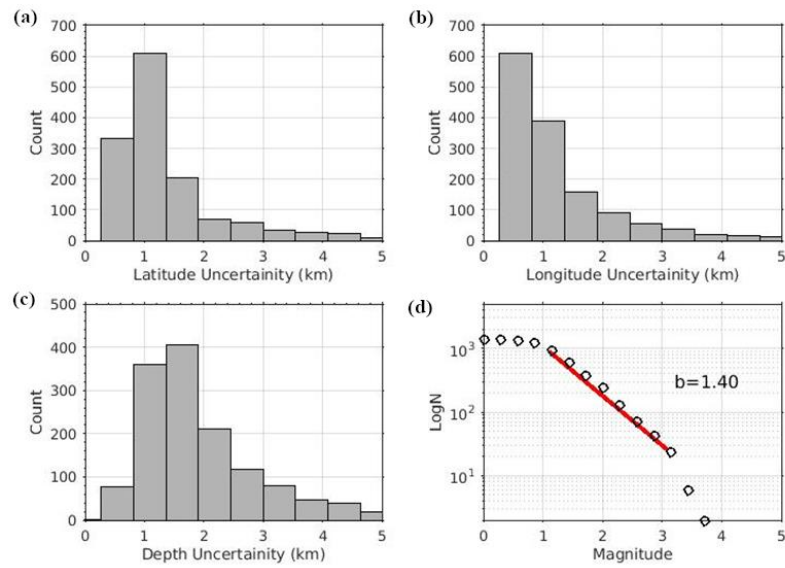


Figure 3.8. Statistics for the location accuracy of the seismicity catalog between 26.09.2014 and 31.12.2016. a) Latitude uncertainty b) Longitude uncertainty c) Depth uncertainty d) Magnitude-frequency distribution of the catalog and the b-value.

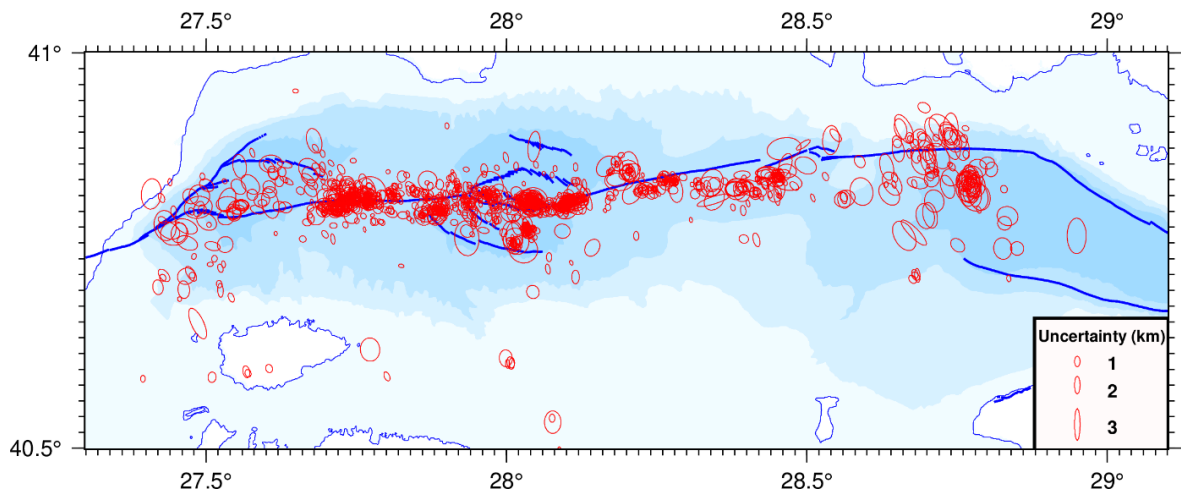


Figure 3.9. Error ellipses of the earthquakes computed from horizontal location uncertainties.

Figure 3.9 shows the error ellipses for the locations of micro-earthquakes estimated in this study. The uncertainties are large at both ends, in Tekirdağ Basin and Çınarcık Basin as the azimuthal gaps increase.

3.4. Spatial Distribution of Microseismic Activity

Adding new OBS and land stations in addition to stations used by Yamamoto et al. (2017) improved locations. The performance of 1-D velocity model also contributed to the accuracy of the locations. Figure 3.10 shows the seismicity in map view and E-W vertical cross section. The depth sections along 7 N-S profiles are shown in Figure 3.11. Below, the locations of the micro events can be interpreted as in 4 sections. These regions are Tekirdağ, Central, Kumburgaz and Çınarcık Basins.

The general trend of the located events closely follows the surface trace of the Main Marmara Fault with smaller location uncertainties between 27.7°E and 28.5°E (see the error ellipses in Figure 3.9). Between 27.7°E-27.9°E of the Central High, seismicity on the map view takes place within ± 3 km of the surface fault trace of the MMF. In the Central Basin, the seismicity is diffuse at the western end of the basin where the junction of the bounding faults of the basin. Between 27.9°E-28.15°E, most of the seismic activity crosses the center of the basin within ± 2 km the surface fault trace. However, two seismic clusters also appear on the southern part of the Central Basin. At the eastern end of the CeB, the seismicity deviates from the surface trace of the MMF to the north and continues within a narrow zone of the Kumburgaz segment. The seismicity takes place on the south of the surface trace of the MMF along the Kumburgaz segment up to 28.4°E. Between 28.3°E and 28.8°E, the seismicity is partly diffuse due to the larger uncertainties of the located events but also its transitional character from pure strike slip to extensional tectonics.

The nearly repeating events forming 9 clusters occurred during the observation period of the OBS deployments are displayed in Figure 3.10 (green circles). They take place closely in the Central Basin and located on the surface trace of the MMF, between 8-10 km depths.

The striking feature of the E-W depth section is the absence of seismic event at depth shallower than 4 km. This is even deeper for the Central Basin (between 27.85°E - 28.20°E). The maximum depth of the seismogenic zone reaches to ~18 km from Tekirdağ Basin to the middle of the Central Basin. To the east of 28.0°E, the seismicity is sparse, and

it appears that the seismogenic depth reduces to ~11 km. The overall seismicity rate is low along Kumburgaz segment, but reaches to a depth of ~16 km.

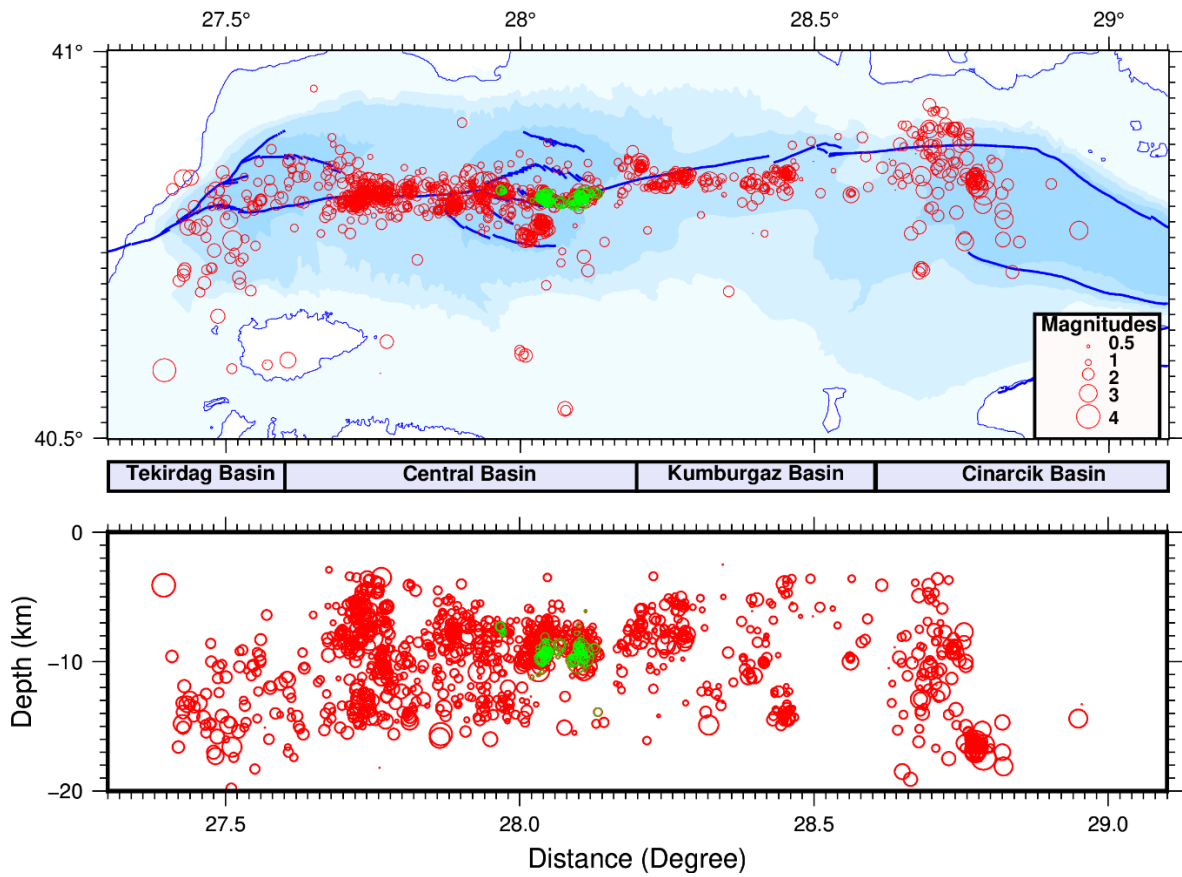


Figure 3.10. Top: Map view of the seismicity in Marmara region between 2014-2016. The green circles show the locations of the nearly repeating events detected during the OBS deployments. Bottom: Depth view of seismicity. The green circles show the seismic repeaters. Fault lines were taken from Emre et al. (2013).

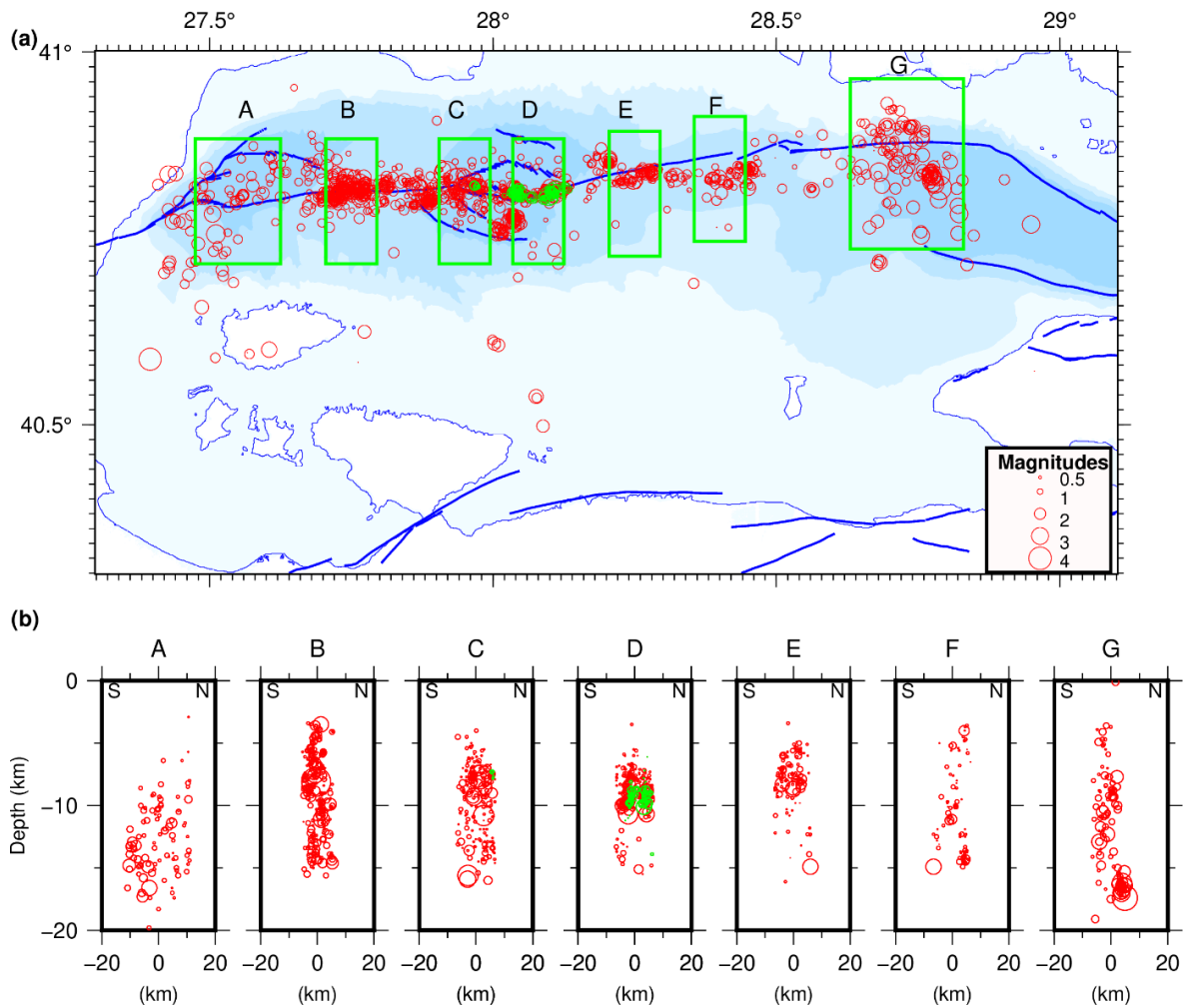


Figure 3.11. Top: Map view of the seismicity in Marmara region between 2014-2016. Bottom: Depth view of seismicity for N-S section. The green circles show the seismic repeaters. Fault lines were taken from Emre et al. (2013).

3.4.1. Depth Distribution of Seismicity

Figure 3.11b displays N-S depth cross sections of the seismicity within ± 20 km of the surface fault trace. The cross section in Tekirdağ Basin (A) shows no localized seismicity with ± 10 km of the fault trace. Localization of seismicity starts at the central High, Profile B, the dip of the seismic activity is almost vertical and spread over ± 4 km of the fault trace. The seismicity extends from 3 km to 15 km depth. In the west of the Central Basin (Profile C), the dip of the seismicity is close to vertical and spread over ± 8 km of the fault trace from 5 km to 16 km depths. In the west of the Central Basin (Profile D), an

apparent change occurs on the depth limits of the seismicity, between 7 and 12 km. On the Profile E in the first profile of the Kumburgaz Basin, the seismicity localizes between 5 and 9 km depths. On the Profile F, the depth of the seismicity takes place between 3 and 15 km. It appears that the seismicity slightly dips to south although the low seismicity rate limits the precise determination of the dip. The largest magnitude events (>3.5) occur in the Central High and Central Basin while decreasing sharply along the Kumburgaz Basin.

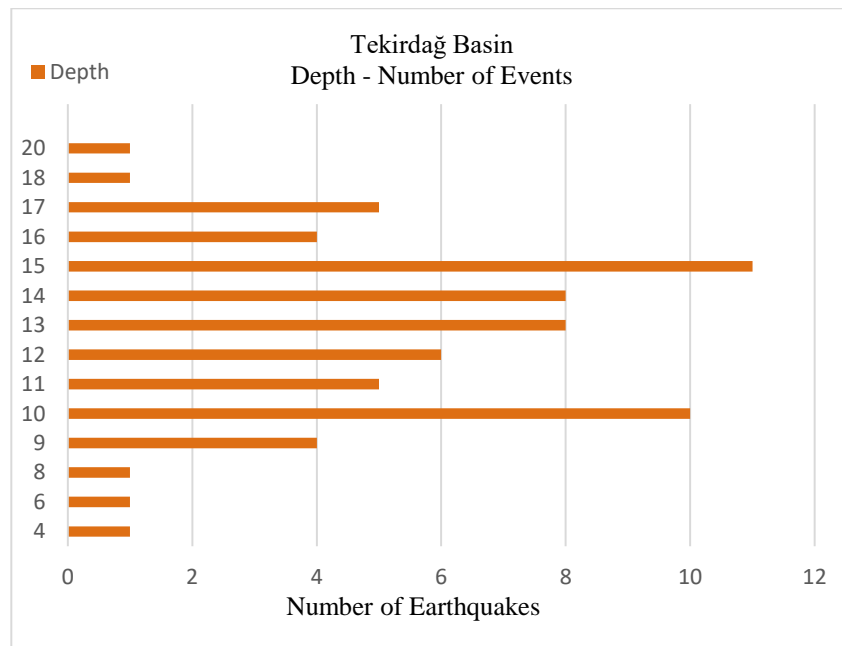


Figure 3.12. Depth distribution of earthquakes in the Tekirdağ Basin.

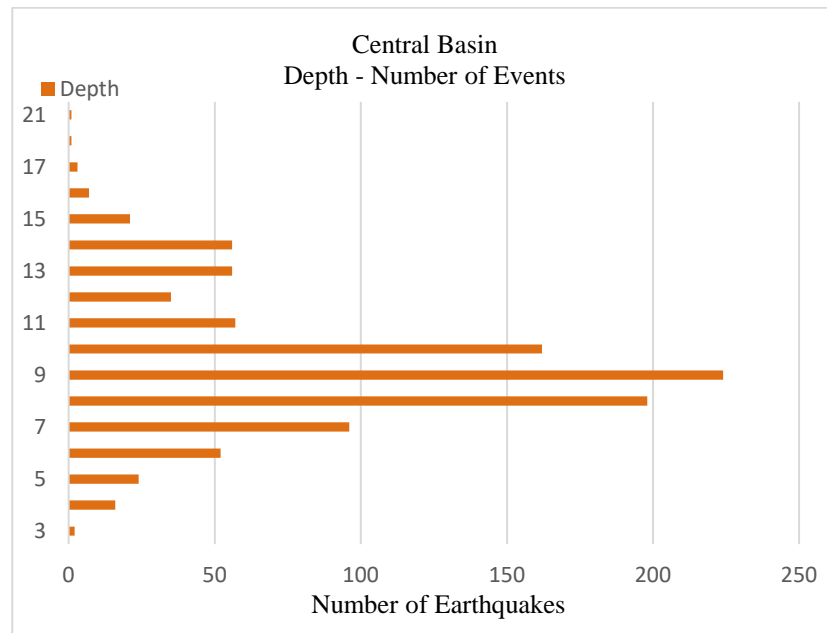


Figure 3.13. Depth distribution of earthquakes in the Central Basin.

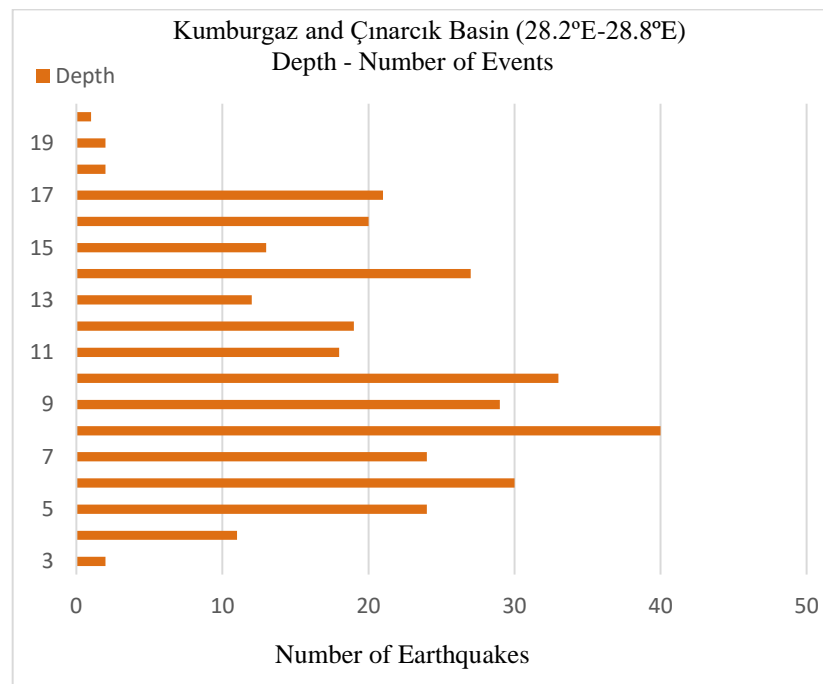


Figure 3.14. Depth distribution of earthquakes in the Kumburgaz and Çınarcık Basin.

The demonstration of the depth distribution of the seismicity of the fault segments can contribute to the characterization of the seismogenic zone of the MMF. In this study, the depth distributions were computed for Tekirdağ, Central, Kumburgaz and Çınarcık Basins as shown in Figure 3.12, Figure 3.13 and Figure 3.14, respectively. As stated in Schmittbuhl et al. (2015), the seismicity in a region is related to the locking depth since the seismic activity is happening above the locking depth where the brittle and velocity weakening mechanism come up. Below the locking depth, the crust is expected to respond to the plate driving force ductility following velocity strengthening processes with no seismicity.

3.4.2. A Comparative Analysis of Microearthquake Activity

The spatial and temporal monitoring of the microearthquake activity in the Marmara region is critical for the present state of the Main Marmara Fault and the hazard assessment for the surrounding cities. Various monitoring activities, including microseismicity are carried out at different scales and precisions. The studies are based on the land stations, OBS stations, or both. They used different velocity models and location tools. Therefore, a comparative analysis of the locations is relevant in order to understand the similarities and differences.

One of these studies carried out by Schmittbuhl et al. (2015) investigated the seismicity along the MMF beneath the Marmara Sea for the time period of 2007-2016 using the data from the broadband stations around the Marmara Sea (Figure 3.2). According to their results, the Tekirdağ and Central Basins have micro events in abundance. The depth range of the earthquakes is about 17 km from surface. The depth values vary in a wide range for the transition zone between Tekirdağ and Central Basin. In this study, for TB, the depth extension starts at about 5 km and in general it extends 20 km, which is similar to the results of Schmittbuhl et al. (2015). As for the eastern part of the TB, which can be defined as a transition zone and named as Western high Cluster, the results are revealing that the depth values vary from about 3 km to 18 km at longitude around 27.7°E. It is also apparent that the depth extension is slightly narrower than the result of Schmittbuhl et al. (2015) for this section.

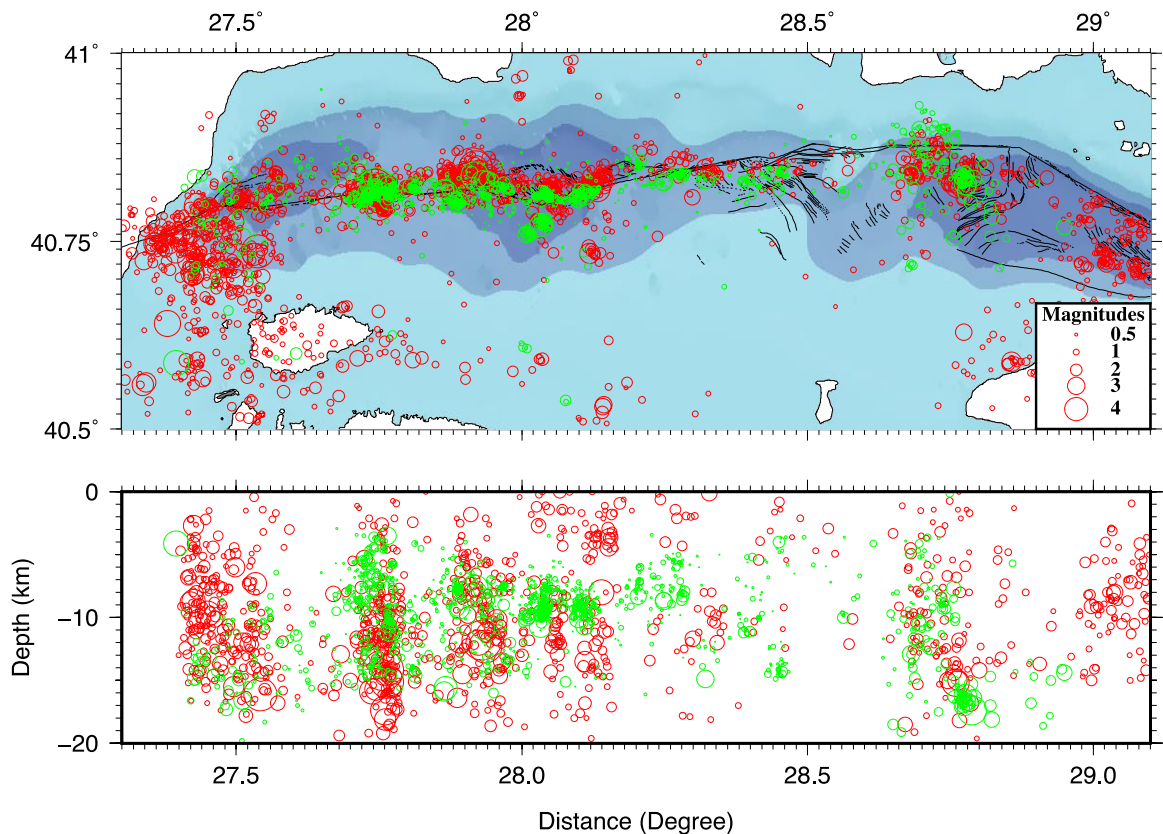


Figure 3.15. Seismicity activity between 2007-2016 (red) (after Schmittbuhl et al., (2015)) and this study (green). Top: Map view of the seismic activity. Bottom: Depth view of the seismic activity.

Between the longitudes at 27.8°E-28.2°E, which can be described as Central Basin, results obtained in this thesis indicated that the depths vary from 5 km to 15 km, while the depth results of Schmittbuhl et al. (2015) changes in a very extended depth cluster (between 2-20 km). In this study, the depth values at western end of the Kumburgaz Basin (at 28.2°) start about 7 km and the depth extends to 18 km. In this area, a sparse seismicity can be seen as in the study of Schmittbuhl et al. (2015). Also, the results of this thesis and Schmittbuhl et al. (2015) agrees for Çınarcık Basin in terms of the depth range. Both studies show that the seismicity starts deeper for this part revealing a narrower depth range. For the west of the Çınarcık Basin, the seismicity is starting at about 5 km and extending 20 km. However, the seismicity decreases to the east of the Çınarcık Basin. In Schmittbuhl et al. (2015), for the Çınarcık and Kumburgaz Basins, the study found that the depth range is between 8 and 14 km.

A recent study carried out by Yamamoto et al. (2020) analyzed the continuous seismic data obtained from 15 off-shore stations for in the years between 2014-2016 using the STA/LTA method to create the microseismic event database along the MMF fault segment from 27.4°E to 28.8°E. They identified 820 micro events beneath the MMF. The study defined two inactive areas of microseismicity located in the western segment which corresponds the 1912 earthquake rupture area. The hypocentral locations from Yamamoto et al. (2017) are displayed with the result of this study in the same time period (Figure 3.16). Another seismically inactive area is in the eastern segment, which is considered as a fully locked segment that has the potential for a large earthquake. Yamamoto et al. (2020) also stated that the epicentral locations of the mainshock and aftershocks of the September 26, 2019, M 5.7 earthquake are located much closer to the MMF than locations reported from only land-based results, given in KOERI catalog, which are located on the northern of MMF. Also, the earthquake location results of Yamamoto et al. (2020) indicated that the micro-earthquake activity is between 8 and 22 depth range for the Western High Cluster. Batsi et al. (2018) claimed that these results found by Yamamoto et al. (2017) are too deep and most of the micro events occurred much shallower than 7 km in the Western High section. The RMS values are given as 0.2-0.3 and 0.4 for common earthquakes in the studies of Yamamoto et al. (2017) and Batsi et al. (2018), respectively (Yamamoto et al., 2020). As for the boundary between the Western High Cluster and the Central Basin (at about the longitude 27.74°E), Yamamoto et al. (2020) reported that the earthquakes seem to be extending to 22 km, but to the east, we see that their results become shallower. However, the results of Yamamoto et al. (2020) are deeper compared to the current study for this section. For Central Basin, it can be clearly seen that the results for the depths are changing between the 8-20 km at longitude between 27.9°E - 28.2°E in Yamamoto et al. (2020), which is a wider depth extension compared to this study. At longitude 28.05°, the sudden change of depths to a shallower value at about 12 km has been reported in that study. Between the longitudes at 28.2°E-28.4°E, in the western part of the KB, we see that the depth results of Yamamoto et al. (2020) are consistent with the results acquired in the thesis (starting at 5 km to 18 km) varying between 5-15 km. To the east, between the longitudes at 28.4°E - 28.6°E, results of the current study are deeper than theirs'. In the eastern part of the Kumburgaz Basin, at longitude around 28.7°E, the seismicity happens at the depths of 8-13 km according to the results of Yamamoto et al. (2020). Their depth extension findings are narrower than calculated in this study presenting the depths changes

at between 3 km to 20 km at longitudes between 28.7°E- 28.8°E. Figure 3.16 shows the comparison between the location results obtained in this study and Yamamoto et al. (2017).

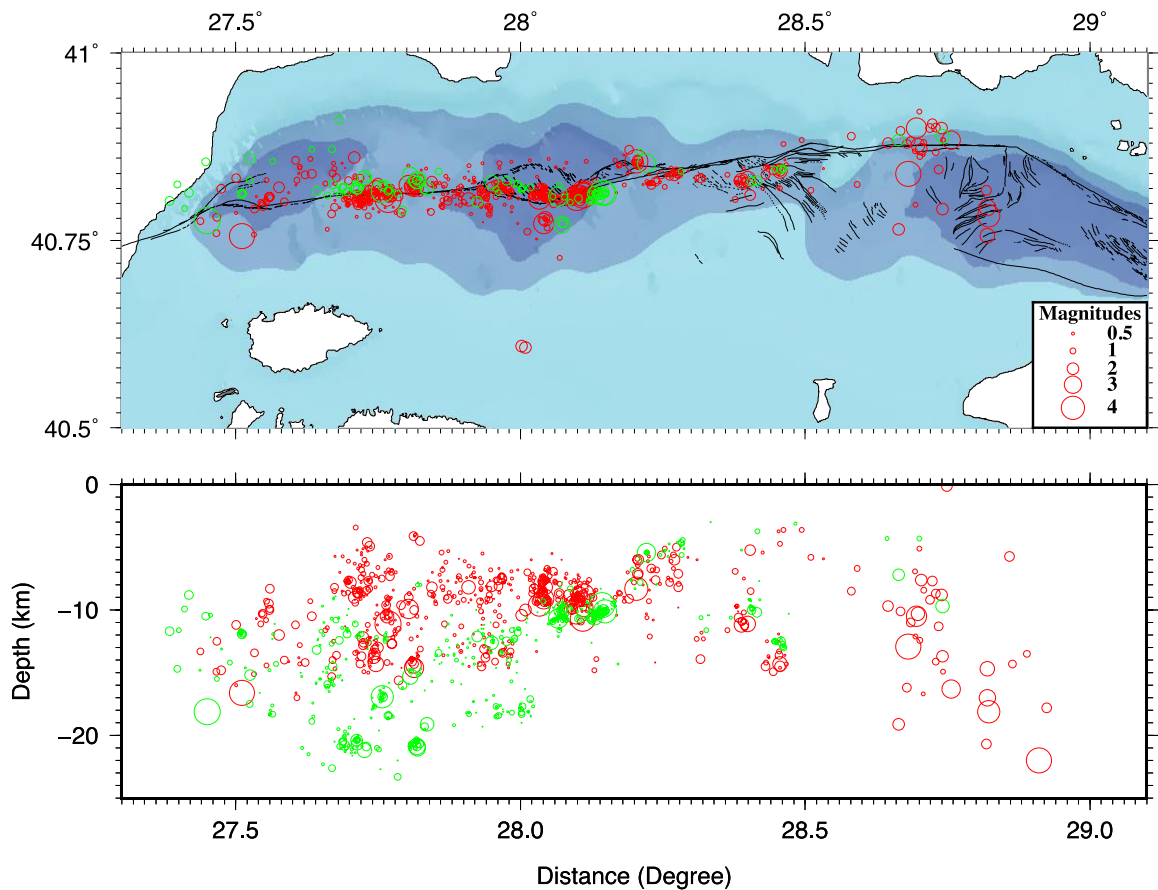


Figure 3.16. Seismicity activity between 2014.09-2015.07 (green) (after Yamamoto et al. (2017)) and this study (red). Top: Map view of the seismic activity. Bottom: Depth view of the seismic activity.

The microseismic activity monitored by permanent seismic networks and OBS studies display similar epicentral distributions (Schmittbuhl et al., 2015), but also show differences in hypocentral depths. It is important to understand such observations as the absence of the earthquake activity at shallow depths also indicate upper bound of the seismogenic zone, reducing the seismogenic thickness. A more accurate estimate of the seismogenic thickness provide more reliable earth models for rupture scenarios. Figure 3.17 shows P-wave seismic tomographic model crossing the center of Marmara Sea

(Latitude 40.8° N) in E-W direction (Hayrullah Karabulut, personnel communication). The model computed from the seismic reflection data collected during 2001 SEISMARMARA experiment (Laigle et al., 2008).

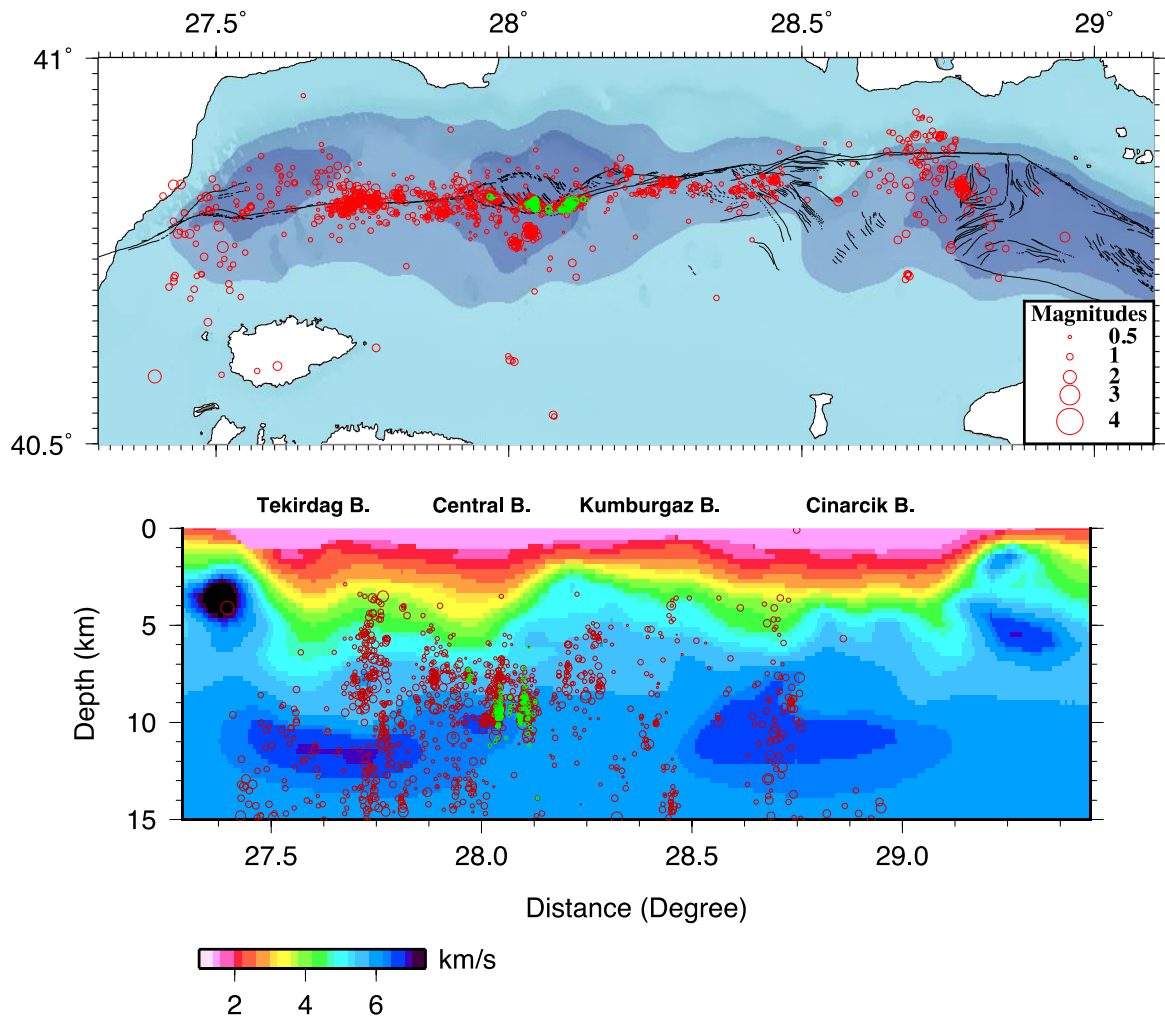


Figure 3.17. Top: Seismicity distribution obtained using OBS data from this study. Bottom: P-wave seismic tomographic model crossing the center of Marmara Sea (Latitude 40.8° N) in E-W direction. The pink area in the upper part of the model shows the water layer (Hayrullah Karabulut, pers.comm.). Red circles show the seismic events displayed on the top figure.

The microseismic activity displayed on the P-wave tomographic model indicates that no seismic events are located in the low sedimentary basin structures. Overall, the microearthquake locations follows the depths with P-wave velocities $> \sim 3.5 \text{ km/s}$.

It is apparent from Figure 3.17 the location results of the earthquakes are under the sedimentary basement which is represented by low-velocity zone beneath the Central Basin. The ratio of overlap between the sediment layer and micro-earthquakes seems more realistic in this study than Yamamoto et al. (2017)'s results that starts at deeper beneath the sediment part. The study defined some active and inactive areas along the segments underneath MMF. Additionally, Yamamoto et al. (2020) acquired micro earthquake locations from OBS data and the comparison with Yamamoto et al. (2017) shows nearly the same results. The extensometer data from Yamamoto et al. (2019) revealed that there is a slip rate of $10.7 \pm 4.7 \text{ mm/year}$ around WH cluster which contains 8-km thick sediment layer indicated by Bayrakci et al. (2013).

4. REPEATING EARTHQUAKES

4.1. Introduction

Earthquakes occurring close to each other have similarities in their waveform shapes (Omori, 1905; McEvilly and Casaday 1967; Hamaguchi and Hasegawa, 1975; Poupinet et al., 1984; Geller and Mueller, 1980). The neighboring earthquakes that are very close to each other in location and having the same slip area are the similar earthquakes (Uchida and Bürgmann, 2019). These events have a wide range of implications. Both very close and co-located events can provide the slip history of a point on the fault zone.

Seismic repeaters have been observed all around the world including USA, Taiwan, Japan, Turkey, Indonesia. The repeating earthquakes provide evidence for slow slip, precursors, and seismic creep (e.g., Kato et al., 2012; Bouchon et al., 2011; Nadeau and McEvilly 1999; Igarashi et al., 2003; Uchida et al., 2019). Various features of the slow slip related to different physical processes can be estimated through the assessment of the repeating events, e.g., postseismic slip (e.g., Uchida et al., 2004; Hayward and Bostock, 2017), spontaneous slow episodic slip (e.g., Nadeau and McEvilly 2004; Uchida et al., 2016), preseismic slip (Kato et al., 2012).

Repeating Earthquakes can be defined as the families of two or more events of the same locations on a fault zone with nearly same magnitudes. One clue helping to search the repeating events is that they have nearly identical waveforms recorded at the same stations (Templeton et al., 2007; Chalumeau et al., 2021; Chen et al., 2007). The other criterion is that they rupture similar fault locations (Chalumeau et al., 2021; Chen et al., 2007). It has been observed that the earthquakes tend to have a repetition for a fault rupture of fixed patch along the San Andreas Fault for the Parkfield section, which can also be explained by the stick-slip mechanisms, by the Nadeau and Johnson (1998), Nadeau et al. (1994), Cole and Ellsworth (1995). They were interpreted as the characteristically repeated rupture of asperities within slipping regions on the fault through the time. Similarly, Uchida et al. (2003), found the distribution of repeating earthquakes on the plate boundary in Japan, concluded that these events are mostly concentrated within freely slipping

portions of the plate boundary. In addition, Uchida et al. (2015) examined postseismic response of repeating earthquakes around 2011 Tohoko-oki earthquake(M=9) in the Japan subduction zone for the time period from 1984 to 2011, by investigating the temporal variations of the size of the earthquakes related to 2011 Tohoko-oki earthquake(M=9) and the slip area.

The case of Parkfield earthquake sequence, on San Andreas Fault Zone, is one of the first and the striking example for the repeating earthquakes. The earthquakes of magnitude about 6 have occurred on the Parkfield region in the same area with a regular recurrence time intervals in the years of 1857, 1881, 1901, 1922, 1934 and 1966 (Figure 4.2) (Bakun et al., 1986). Since they are historical earthquakes and belong an era with little seismic instrument, there is not so much information about the first three events, 1857, 1881 and 1901 earthquakes. However, available data indicate that these 6 events occurred with a repetition of about 22 year and represented repeated ruptures on the same area of the fault zone, which may be interpreted as characteristics of them. Looking on the historical records of 1934 and 1966, it can be seen that these events initiated at the same spot of the fault (Bakun and Lindh, 1985 ; Bakun and McEvelly, 1979). Figure 4.1 shows the historical seismograms of the east-west component recorded by Galitzin instruments at De Bilt, the Netherlands. It is remarkable that the 1934 and 1966 events are similar in terms of their waveform shapes.

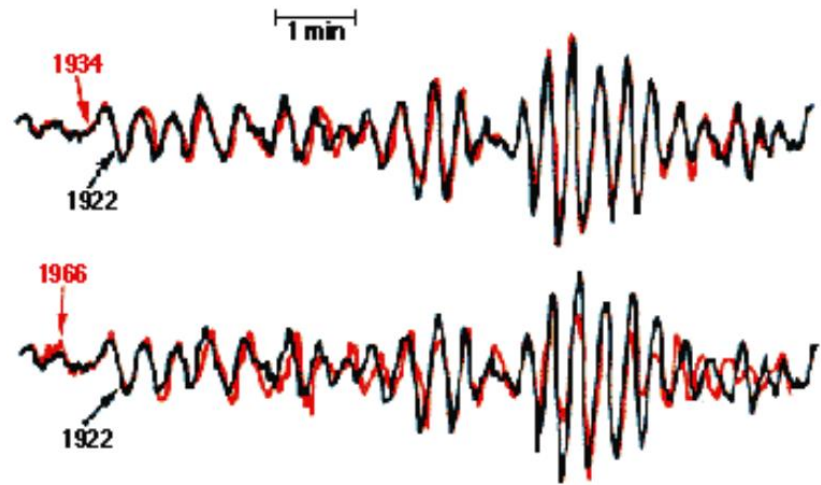


Figure 4.1. 1922 and 1934 Parkfield events recorded at Berkeley, California.
(<https://earthquake.usgs.gov/learn/parkfield/hist.php>)

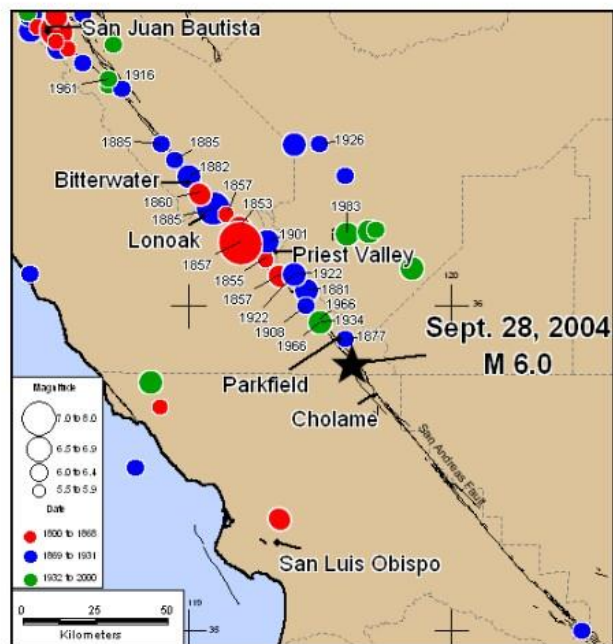


Figure 4. 2. The repeating earthquakes in Parkfield region on the San Andreas Fault Zone, California(http://www.conservation.ca.gov/cgs/geologic_hazards/earthquakes/Pages/09282004_eq_info.aspx)

The important point that should be considered for the evaluation of the repeaters is to distinguish the neighboring events. The waveforms of these events may show a high coherency and their locations may be very close to each other. Therefore, the exclusion of the non-repeating events that are both neighboring and triggered events is one of the major processes that must be achieved (Uchida, 2019). The triggered events are affected by the stress change occurred by a previous event. The repeaters, on the other hand, may be triggered by slow slip or afterslip. They were observed in the borders of afterslip release where large aftershocks occurred. The occurrence of aftershocks diminishes with time after the main event according to Omori law (Zerbst, 2020; Chalumeau et al., 2021). The study of Chen et al. (2013) on repeaters with a small number of nearby events behave more periodically and have a coefficient of variation (COV) smaller than 0.3. The neighbor events that occurred in the vicinity of the repeaters affected the temporal properties of the repeating events. The recurrence intervals of these events have been affected moderately by the uneven stress variation. The study reported that the repeaters that emerged in a shorter time than 1 day essentially have faced with high stress change and this has given rise to a triggering situation that shortened the recurrence interval (Chen et al., 2013). The recurrence times of repeater are reduced by a preceding event, showing an increment in events that follows Omori law (Chalumeau et al., 2021).

We take benefit from the appraisal of the recurrence interval of these events because triggered events are also distinguishable with their temporal properties from the repeater candidates (Uchida, 2019). As an example, study carried out by Lengline and Marsan (2009) aimed at lightened the properties of the triggering events from the repeaters that they found by using the similarity of the waveforms and location results (Uchida et al., 2019). They focused on the earthquakes between 1984-2007 in Parkfield region and had chance to observe if any perturbation happened by 2004 Mw=6.0 Parkfield Earthquake. The assessment of the repeating earthquake sequences has indicated that many of the repeater sequences displayed increment after the Parkfield event. On the other hand, some of them halted their activity during the main shock. The reasons behind this periodicity perturbation are the change of the distribution of coseismic stress and the characteristic timing behavior of the afterslip on the fault plane (Lengline and Marsan, 2009).

Lengline and Marsan (2009) also reviewed the repeating events regarding their temporal evolution. The repeating earthquake sequences before the mainshock were investigated by describing the \bar{T}_r value which is the mean interevent time of the T_r (recurrence interval time) values. A probability density function for the normalized recurrence times, T_r/\bar{T}_r , has been acquired to look for the cases of short-term and long-term recurrence times for a repeater sequence. The cases for short-term and long-term repeating events have been expressed as $T_r < 0.1 \times \bar{T}_r$ and $T_r > 0.1 \times \bar{T}_r$, respectively. The recurrence interval of the repeating earthquakes shorter than 10 percent of the mean recurrence time interval, which has been considered to be the short-term events, displayed a power law decay rate concordant with the Omori law. So, the rate of the change is an indication of a triggering process representing short-term earthquakes that were likely caused by the slip of a nearby asperity. Their locations are not so tightly clustered in the fault zone of the repeater sequence. On the other hand, recurrence interval of the repeater longer than 10 percent of the mean recurrence interval indicated a good correlation in their locations and a periodicity (Lengline and Marsan, 2009; Uchida, 2019). This observation indeed agrees with the idea that a fault patch is hard to be reloaded in a very short recurrence time interval, except for the cases of the post-seismic behavior after a large event. At this point, the evaluation for the short-term repeater requires more caution, as stated in Uchida (2019).

Two possible explanations for the short-term earthquakes have been made by Lengline and Marsan (2009). When a priori event has not ruptured the whole asperity, remaining stress on the same asperity may have caused the short-term events. The second supposition for the short-term events is that they are the results of a close but separate asperity (Lengline and Marsan, 2009).

Although the mechanism behind both short- and long-term earthquakes arise from the asperities reloading and rupturing over and over again, the main reasons causing the accumulation of strain around the asperities are the different mechanisms. For adequately large events, the mechanism behind the long-term repeaters is assigned to the tectonic loading mechanism (Lengline and Marsan, 2009). Another assumption is the slip occurring slowly and aseismically around asperity on the fault zone (Igarashi et al., 2003; Bourouis and Bernard, 2007). As shown in Bouchon et al. (2011), Kato et al. (2012), repeating

events with much more shorter recurrence intervals, are more presumably related to a fast nucleation process. (Bentz, 2020).

As shown in the studies of (e.g., Lengliné and Marsan, 2009; Igarashi et al., 2003; Bourouis and Bernard, 2007), tectonic loading process or usually slow-slip of the fault zone around the asperity set stages for the long-lasting repeaters. On the other hand, the repeating earthquakes with shorter recurrence intervals of time seems to be related to the nucleation of acceleration process, observed by Kato et al. (2012). These types of events were also observed in the process of the reloading of asperities caused by afterslip of large events, suggested by Peng and Zhao (2009).

It should be noted that the recurrence interval or slip scaling remains inconsistent particularly for the repeating events. Observed repeating sequences follow the relation that scales recurrence interval T_r with $M_o^{0.17}$ as suggested by Chen et al. (2007), Lengline and Marsan (2009), Nadeau and Johnson (1998). Yet, as observed in Allmann and Shearer (2007), the slip or the recurrence interval follow a scaling with $M_o^{1/3}$ if the events were supposed to have stress drops with magnitude dependent (Williams et al, 2019).

4.2. The Physical Model of Repeating Earthquakes

The studies over the last 25 years indicated that repeating events have been observed within a variety of tectonic regimes, e.g., the strike-slip faults (Nadeau and Johnson; 1998), normal faults (Duverger et al., 2018) and reverse faults (Chen et al., 2008). Dominguez et al. (2016) and Uchida et al. (2003) also found that the megathrust faults produced repeaters. These studies pointed out that the aseismic slip, creep, afterslip or slow slip events (SSEs) are actually related to the generation of repeaters in a fault zone (Chalumeau et al., 2021).

In a fault zone, the slip can be observed in various types. It can occur as an aseismic creep which is caused by sliding stable, not produced by a notable earthquake, or can be observed after a sudden release of accumulated seismic energy by an earthquake. The relationship between seismic and aseismic slip is crucial since it can give us an insight about the rupture size of an expected earthquake. Also, aseismic slip transients may initiate

the big events or may lead to nucleation for the devastating earthquakes (Shaddox et al., 2021).

4.2.1. Repeating Earthquakes and Fault Creep

Many studies have investigated the physical mechanisms of creep on faults. Proposed mechanisms include, as Harris (2017) summarized, frictional properties on the fault zone (Jolivet et al., 2013), the increment in pore fluid pressure (Hreinsdóttir and Bennett, 2009; Anderlini et al., 2016, Savage and Lisowski, 1993) increased temperatures (Blanpied et al., 1995), fault geometry (Funning et al., 2007) and chemical reactions (Moore and Lockner, 2013).

The low frictional strength on the fault may cause a decrease in effective normal stress on a fault, which has impacts on the fault behavior by leading to low normal stress acting on the fault in the shallow crust. The degree of elastic strain in the lower crust and the locking behavior of the fault depending on the depth are related to the creeping rate defined at the surface of the earth (Savage and Lisowski, 1993). In Figure 4.3, a model for a fault zone representing the creeping, locked sections and the relation between elastic strain and creep can be seen.

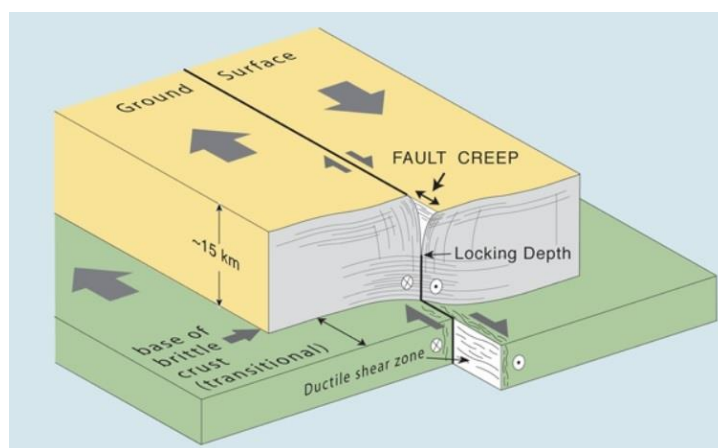


Figure 4. 3. The relation between creep and elastic strain
(<http://funnel.sfsu.edu/creep/WhatsCreepPage.html>)

Harris (2017) pointed out that creep also seems to be associated with the rock type since the frictional strength of a fault is increased by particular rock types. Moore and Rymer (2007) observed that the samples of serpentinite from Parkfield on the San Andreas Fault zone, which is known to be a creeping portion, decreased the fault shear strength of the fault and led fault to be stable-sliding and behave aseismically. The study also revealed that the frictional properties of talc are present at depths more than 10 km rather than earth's surface (Harris, 2017). The part of the fault which is composed of these ingredients (e.g., serpentinite, talc, salt and clay) may withstand slipping faster and it shows obstacles to the spreading earthquake ruptures (Chen and Bürgmann, 2017).

The conditions of pressure have been supposed as a cause for creeping on a fault as reviewed in Scholz (1998). Wei et al. (2009) assumed that increased pore pressure in the sedimentary layers of the fault could be responsible for the creep in Superstition fault, California. However, the experiments in the laboratory at room temperature using samples of porous sandstone showing a failure by brittle deformation indicated that pore pressure led rocks to fail at a lower shear strength even though they are still in brittle deformation (Harris, 2017).

The creep on a fault zone has also been attributed to the permanent effects of previous events. At this point, aseismic slip has been viewed as a process of seismic cycle for the fault zone creeping, for North Anatolian Fault Zone in Çakır et al. (2012). The idea is that the regions exhibiting both interseismic creeping faulting and large events may indicate the impacts following large earthquakes. Namely, creep on a fault zone is actually an elongation of postseismic slip on the fault zone. Çakır et al. (2012) indicated that İzmit section creeps since the last large earthquake on the North Anatolian Fault. They suggested that the creep on the fault zone is, in fact, the afterslip of the large event and pointed out the similar behavior of the Hayward fault (Harris, 2017). Herein, the creep rate on the fault zone has also been discussed by Harris (2017). According to Perfettini and Avouac (2004) and Langbein et al. (2006), the relationship between the creep rate on a fault zone and time since the last event should display an inverse proportion for a model of afterslip (Harris, 2017).

The importance of the repeating earthquakes comes from the fact that they can be unique measurements for the calculation of the creep on the fault zone (Uchida et al., 2019). The weak parts of the fault plane that rupture afterslip produce a large number of small repeating events (Templeton et al., 2007). So, these events are caused by the heterogeneities on the creeping areas, which are called as call asperities on the fault zone (Figure 4.4). A seismic asperity is being regularly loaded by aseismic slip and they rupture the same location of the fault at regular recurrence intervals (Chen and Lapusta, 2009; Chalumeau et al., 2021). So, in interseismic period, the creep on the fault zone can be estimated using the repeating earthquakes (Uchida et al., 2019).

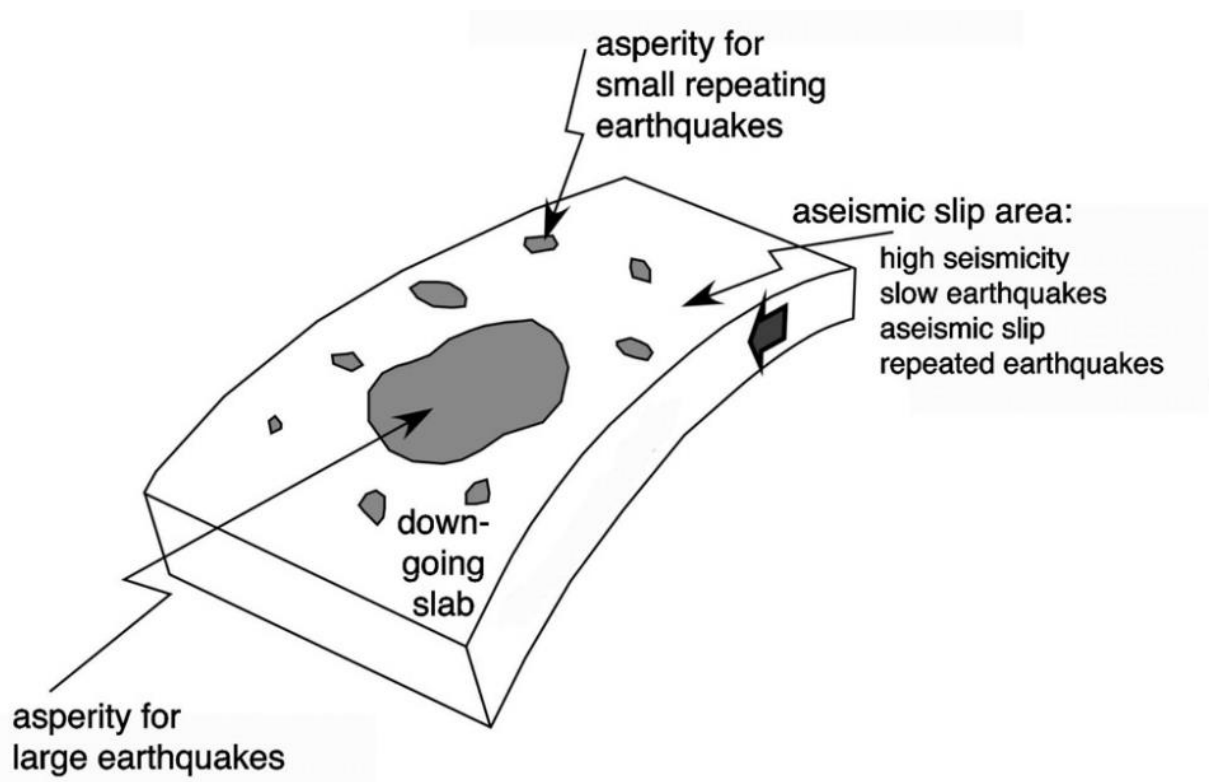


Figure 4.4. The Schematic model demonstrating the types of asperities on a subduction zone (Behrmann et al., 2006).

The repeating earthquakes have also been suggested to be related to velocity strengthening friction of the fault in terms of their physical process (Dieterich, 1978; Perfettini et al., 2001, 2003). The logarithmic relationship between shear stress and fault slip rate, which is caused by the physical mechanisms of these events, results in

nonlinearity at the time intervals of the recurrence of the repeaters as seen in Perfettini et al. (2003) for the reaction of a fault to a perturbed stress (Schmittbuhl et al., 2016).

Schaff et al. (1998) demonstrated that creeping rheology is related to the repeating earthquakes in terms of physical meaning for the aftershock sequence and postseismic slip. An abrupt change in the stress will lead to an increase as $1/t$ in the recurrence time T_r with the postseismic time t . This relation appears to suggest that the number of repeating earthquakes increase during the foreshock sequences, which is related to the growth in mechanism of the nucleation, which can be seen in the studies of Bouchon et al. (2011); Kato et al. (2012); Bouchon et al. (2013); Meng et al. (2015) (Schmittbuhl et al., 2016).

Repeating earthquakes developing over time, which are related to the induced seismicity, are suggested to be associated with the creep (Bourouis and Bernard, 2007; Lengliné et al., 2014). Conversely, the recurrence time T_r is likely to be constant. Therefore, the repeating earthquake observations are actually in agreement with the creep structure on the fault zone (Nadeau and Johnson, 1998; Chen et al., 2007; Chen and Lapusta, 2009; Lengliné and Marsan, 2009).

4.3. Near Repeating Earthquakes

Understanding which mechanism behind the timing of the earthquakes is key to comprehend the behavior of the cycle of the earthquakes. It is a well-known fact that knowledge of the controlling factors related to recurrence times behind the earthquakes will enable to indicate the seismic hazard assessment. Nonetheless, the nature of the earthquakes and the uncertainty of the recurrences of earthquakes remains controversial (Chen et al., 2013).

At this point, the Parkfield case, which demonstrates small characteristic repeating events, actually gives an opportunity to the seismologists to build the relations between earthquakes and their effects to each other in terms of the recurrence features (Chen et al., 2013). Although the repeaters observed on the San Andreas Fault zone indicate characteristic behavior, Nadeau et al. (1995) found that the earthquake clusters near the repeaters in this area revealed aperiodic recurrence time intervals, changing between

minutes to days. These events, showing a short-term recurrence interval, were clustered within 100-200 m apart to each other. These types of short-term repeating events near Parkfield have also been noticed by Lengline and Marsan (2009). They noticed that the behavior of these events in terms of their locations does not present a typical repeating earthquake characteristic. Their interpretation for these events is that they ruptured partially from the same asperity or they are caused by the distinct asperities very close to each other (Shaddock et al., 2020).

Shaddock et al. (2020) proposed that these types of events showing highly correlated waveforms and spaced closely to each other within 200 m with variable magnitudes and aperiodic repeat intervals can be named as “near-repeating events”. The asperities overlapped partially or spaced adjacent to each other may trigger to rupture the short-term repeating events. Therefore, these events actually differ from the characteristic repeating events with their source. Many studies on slow-slip events such as Igarashi (2010), Yao et al. (2017), Igarashi et al. (2003), Li et al. (2013), Templeton et al. (2008), related these events to the transient aseismic slip, as well as afterslip rather than creep on a fault zone. Kato et al. (2012) and Meng et al. (2015) suggested these events are in relation with precursory slow-slip activity that precedes the main rupture. Recently, Shaddock and Schwartz (2019) proposed that these events have been associated with the aseismic slip caused by the pressure of moving fluid (Shaddock et al., 2020).

Konca et al. (2021) has also defined near-repeating earthquake sequences occurred in long-term in the East Anatolian Fault (EAF) zone. The study proposed that the repeating events have been triggered by the nearby events loaded by the creeping section of the fault that is also demonstrating coupling parts. Detected waveforms with CC larger than 0.95 from 10 years observation at ELZG broadband station were specified as 4 repeating earthquake sequences. In addition to these earthquakes, the repeater clusters with short-term recurrences and having large correlation coefficients within the mutual source zone about 5 km were thought as short-term clusters. These events were referred as “near-repeating earthquakes”, which has been suggested as a new term by Shaddock et al. (2021) to define the repeaters that have irregular pattern concerning their variable recurrence times and magnitudes (Konca et al., 2021). As also specified in Shaddock et al. (2021), the crucial point is whether these events are coming from the same sources or not.

5. REPEATING EARTHQUAKES IN THE MARMARA SEA

5.1. Detection of the Repeating Earthquakes

There are two general ways to search for the repeating events. One of them is based on the calculation of hypocenters which display overlapping areas of source to identify the repeaters. Here, the usage of the waveform-based differential time to get the exact relative earthquake locations (Ellsworth, 1995; Waldhauser and Schaff 2008; Yu, 2013) is a suitable way for repeating events since they have similar waveforms and performing waveform cross-correlation give their time differentials accurately. This method gives the uncertainty of locations with just a few meters. However, it has some limitations since it requires adequate number of stations with a good station coverage (Uchida, 2019).

The more common method to detect the repeating earthquakes is to use waveform similarity. As mentioned before, the repeating earthquakes exhibit the similar waveforms since they rupture the same source if the medium properties and the instrumentation remains same (Uchida 2019; Chalumeau et al., 2021). This method shows more robust results if the parameters necessary for the analysis are selected properly as suggested in Uchida (2019). The searching for repeaters based on the waveform similarity also entails less data, that is, one station is mostly enough to proceed the analysis although various seismic stations enable more powerful detection (Uchida, 2019).

The cross-correlation method is a fundamental method for assessing the waveform similarity. The degree of the similarity of the waveforms is assessed by the cross-correlation coefficient given below.

$$C(\tau) = \frac{1}{N} \sum_{t=1}^N f_x(t) f_y(t + \tau) \quad (5.1)$$

where f_x and f_y are the time series representing the waveforms of the x and y earthquakes. N indicates the discrete samples. τ is the delay time (Uchida, 2019).

Other major method to assess the waveform similarity is cross spectra method, the coherency of the waveforms is defined as;

$$\text{coh}(\omega) = \sqrt{\frac{|S_{xy}(\omega)|^2}{S_{xx}(\omega)S_{yy}(\omega)}} \quad (5.2)$$

where the cross spectrum, $S_{xy}(\omega)$ for the events x and y is estimated from the Fourier transform.

In cross-correlation method, the frequency range is defined before performing cross-correlation process for the assessment of the waveform coherency. The cross-correlation value for a waveform pair recorded at the same station is used to assess the overlapping sources having the same locations (Uchida, 2019). When two waveforms highly correlate, the CC value close to 1. Usually, CC value is chosen as 0.95, which is sufficient for the waveforms that nearly matches as identical (Can, 2019).

The process of detection of repeating events based on the similarity of the waveforms requires optimization of some parameters as stated in Uchida (2019). These parameters are the selection of the time windows and bandwidth of the signal (Gao et al., 2021; Uchida, 2019). During the analysis of detection of the repeaters, selection of long-time window may result in a high cross-correlation value, but, on the other hand, this may result in low signal to noise ratio. Also, many studies prefer to use a fixed window length which is long enough and can capture the target events (e.g. Taira et al., 2014; Meng et al., 2015).

Uchida et al. (2019) has mentioned a quantitative measure for the analysis of repeating earthquake detection. Taking “quarter wavelength rule” proposed by (Geller and Muller, 1980) into account for the similarity of the waveforms, he stated that the frequency condition for the overlapping events coming from equivalent source size is;

$$f \geq \frac{V_s}{4r} \quad (5.3)$$

where V_s is shear speed and r is the radius of source.

For the repeaters in different slip area, the upper limit of the proper frequency is regarded to be associated with the heterogeneous structure of the source for the waveforms having high frequencies. This may result changes in the rupture process for the slip area of the repeaters sharing the same source area. It has been argued that the frequency range lower than the corner frequency may be insufficient to eliminate the earthquakes showing the different patterns of rupture. Therefore, the optimal choice for the frequency range will be actually dependent on the earthquake size. Igarashi et al. (2010), Taira et al. (2014) and Meng et al. (2015) selected the repeating events using the frequency ranges considering their magnitudes (Uchida et al., 2019).

Identification of repeaters based on waveform similarity is a popular method. In a more general way, the events with waveforms with cross-correlation coefficient above a threshold (changing between 0.70 – 0.98) are defined as the candidate repeaters. Gao et al. (2021) investigated the performance of the cross-correlation in detection of repeaters. The waveforms of non-repeating events can also show similarity. Also, the waveforms from repeating events may demonstrate small differences related to the highly low level of noise at a station, which is the result of the variability in rupture properties. Here, the basic aspect that should be keep in mind is the proximity of the source zones of the repeating earthquakes (Gao et al., 2021; Shaddox et al., 2021; Konca et al., 2021). As Gao et al. (2021) stated, the filtering, particularly applied band-pass filter on waveforms, may lead to the removal of the high frequencies with low similar waveforms and thus may seem similar waveforms of non-repeaters. But it also presents a solution to the inconsistency of the waveform similarity of the true repeaters. Here, the filtering process for the selection of the repeaters using just the waveform similarity by cross-correlation may be misleading. Therefore, it is extremely important to consider physical criterion such as overlapped source zones of the repeaters.

5.2. Template Matching for Detecting Repeating Waveforms

The template matching method is used for the detection of repeating events in this study. The method relies on the search of pre-detected seismic events (template events) in continuous seismic data recorded by a seismic station using cross correlation method. The implementation of the method is easy and fast and can work with single station/channel

data. The method has an advantage in terms of sensitivity of detection since the cross correlation can identify low S/N events and it does not need to be carried out with high computational efficiency since a search of small set of template waveforms is confronted in the continuous data (Yoon et al., 2015). On the other hand, the performance of the CC depends on several factors, e.g., window length, bandwidth. The selection of these parameters becomes critical with low Signal/Noise data and in the presence of long wavelength background signal. The method is widely used to catch the repeating events as indicated by many studies such as Schmittbuhl et al. (2016), Yoon et al. (2015), Chalumeau et al. (2021).

The template matching is, undoubtedly, one of the strongest approaches to search the repeating events since it manages to tweeze the signal in noisy data. Cross-correlation of the waveforms uses the resemblance of the waveforms as a sensitive detector for the earthquake search. So, the template matching method, which is also called as matched-filter, scores high on the sensitivity in detection even in the noisy dataset. One major drawback of this method is the necessity of the prior event signal (Yoon et al., 2015, Bentz et al., 2020). Luckily, a bunch of template events for the repeating earthquake search was available and used in the current study. This enabled to perform a comprehensive search in terms of the finding repeaters. As Yoon et al. (2015) pointed out, many studies take advantage of the sophisticated property of the template matching by detecting new events such as foreshocks (Kato and Nakawaga, 2014), aftershocks (Peng and Zhao, 2009), earthquake swarms (Shelly et al., 2013), triggered events (Meng et al., 2013), low-frequency events (Shelly et al., 2007).

5.2.1. Application of Template-Matching Method on Continuous Seismic Data

The seismic repeaters along the Main Marmara Fault (MMF) are searched through the continuous data from the broadband stations to detect the possible creeping segments of the fault. The search for the repeaters is performed at several steps. Initially, search is performed manually on the continuous recordings of the permanent OBS stations deployed by KOERI and operated between 2011-2013 (Schmittbuhl et al., 2016). The main reason to start the search with the OBS station is that they are the closest stations to the fault therefore small magnitude events have better S/N compared to the land stations located at

distances $> 25\text{km}$. Then the manually detected events from the OBSs are used as templates and performed a more extensive search by cross correlation using the same OBS recordings. This allowed to detect lower magnitude events. This process was repeated for the 4 OBS sites of KOERI, located in Tekirdağ Basin, Central Marmara Basin, Kumburgaz Basin and Çınarcık Basin, operated between 2011-2013. The detected events are analyzed and classified for their long-term repeating behaviors. As a result of the search based on 4 OBS sites, that repeating earthquakes are detected in the Tekirdağ Basin and the Central Marmara Basin but none in the Kumburgaz Basin or the Çınarcık Basin.

Based on the initial analysis of the sites from 4 OBS, a catalog of template events is built for a more extensive search using the land stations operated longer time periods in the region. The origin times of the events detected from the OBS recordings are used to extract waveforms from the recordings of land stations. The waveforms with high S/N are used as templates to detect the events between 2008 and 2020. A low threshold is used for cross correlation coefficient (>0.6) initially to detect low S/N ratio events or events with less similarity. This allowed to create a large, detected waveform database to construct more extensive repeating event waveform catalog. Then, cross correlation is again used to find highly similar events with $CC > 0.9$ from the detected waveform database and form waveform clusters. Finally, the repeaters are selected as waveforms with $CC > 0.95$ and with several occurrences from 2008 to 2020. The waveform clusters repeating fewer than 4 during this observation period are not considered for the analysis.

This part of the study is a continuation of the work done by Schmittbuhl et al. (2016) in the time period of 2008-2015 at SLVM station. The distance of SLVM station is $\sim 30\text{km}$ from the Main Marmara Fault, closest to the detected events. The SLVM station was operated by TUBITAK-MAM between 2008-2018 and not available since 2019. The other stations operated in the Marmara region by TUBITAK-MAM and KOERI are also used in the detection and analysis, but the SLVM station has the best data continuity and quality. In order to monitor the evolution and continuity of the repeating events, the SLVT station operated by KOERI since 2008 is also used. The SLVT station is $\sim 46\text{km}$ far from the detected activity but is in the similar azimuth as SLVM. As the station SLVT is farther the magnitude detection limit is higher and S/N is lower. However, some of the repeating clusters with magnitudes > 2.5 has been successfully recovered.

The template preparation step contains a routine that cuts waveforms around picks to use as templates for earthquake detection by using cross-correlation. The whole process for the template matching was performed by the MATLAB code used in Schmittbuhl et al. (2016). As a result of this process, the search for the repeating events is extended to the end of 2020. Consequently, more earthquakes that repeat themselves in the same cluster have been found. Figure 5.1 shows the example of a template event used for the search the repeater in this study. Figure 5.2 shows the E-W and N-S components of the 9 template events from SLVM station used for the detection.

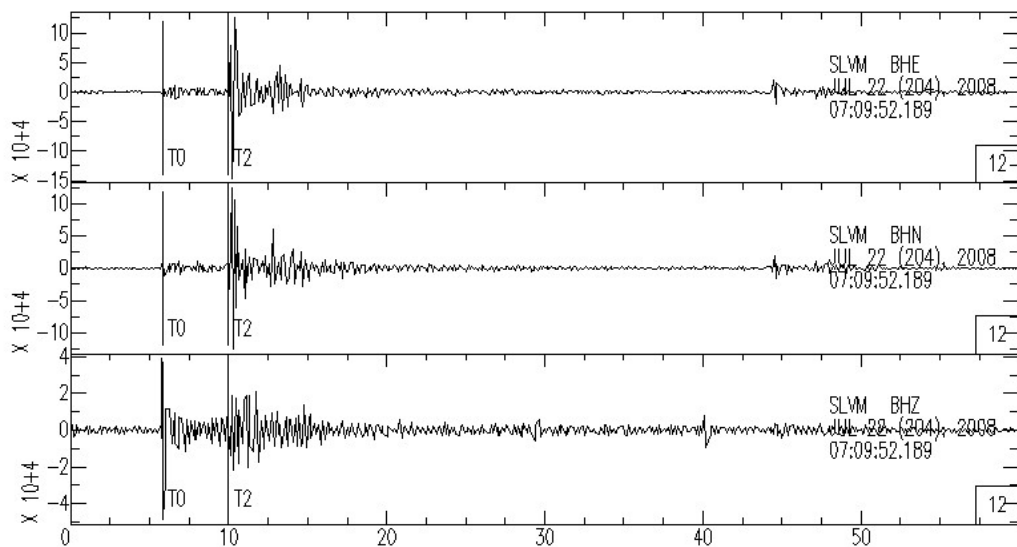


Figure 5.1. An example of three component template event from SLVM station (See Figure 3.2 for the location of the station).

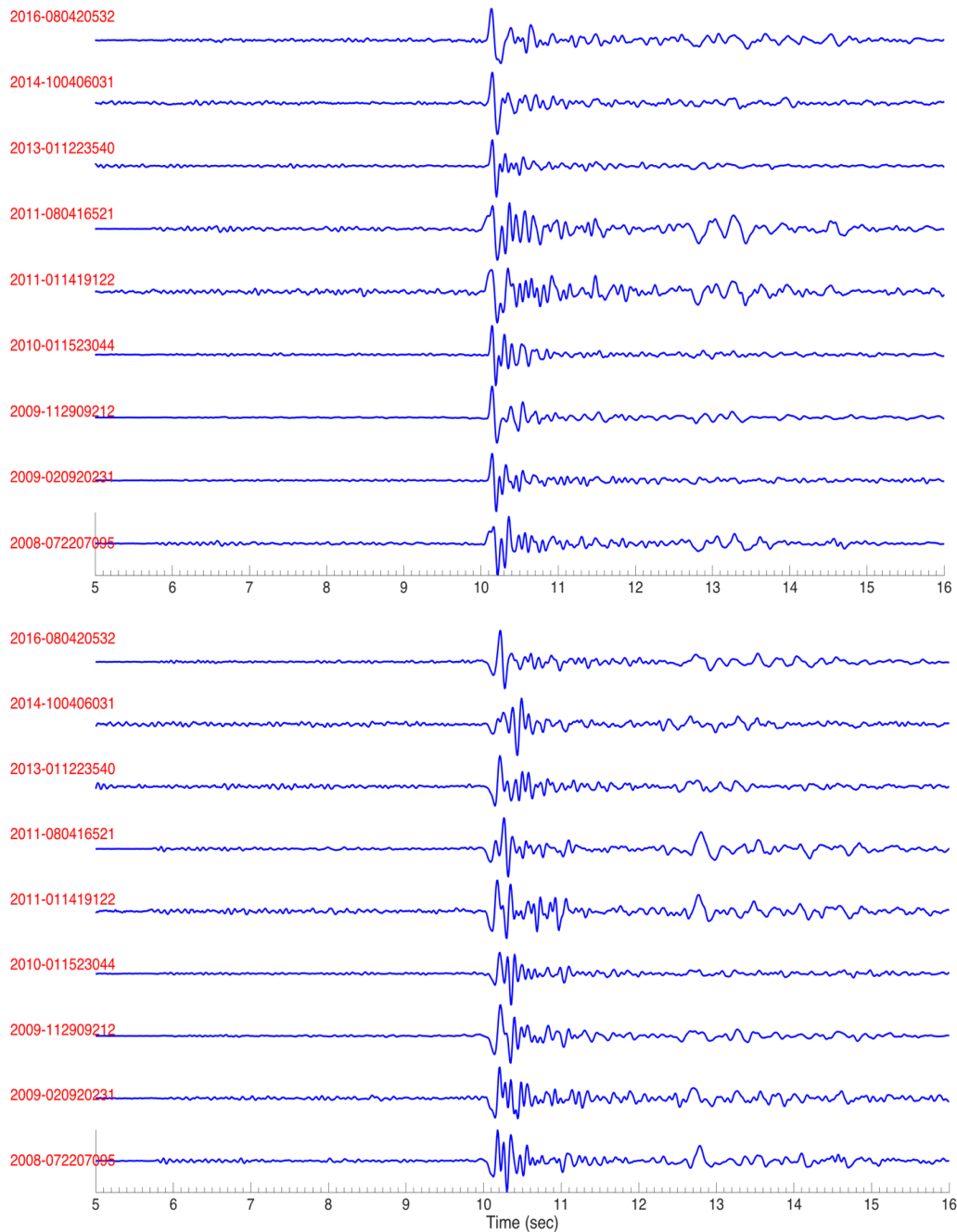


Figure 5.2. Template events for 9 repeating clusters from SLVM station used for the detection. E-W component (top) and N-S component (bottom). The numbers on the left of the traces (red labels) show the recording date of the event. The traces are normalized by their maximum values.

The detected 9 template events are search through the continuous data of SLVM and SLVT stations. The detected events from each template are manually visualized for the data quality and the event clusters of waveforms having $CC > 0.9$ are formed.

5.3. The Locations of the Repeating Earthquakes

In this study, 9 repeater clusters in the Central Basin were detected and analyzed based on the template events of Schmittbuhl et al. (2016). The majority of the repeating events has low magnitudes and recorded only by few land stations. Therefore, the location uncertainties of the individual events were initially large. However, several OBS campaigns with long observations periods recorded some episodes of the repeating events in each cluster. The locations of the repeating events within each cluster have been improved using the OBS stations and by applying cross correlation to the waveforms for more accurate estimates of P and S arrival times.

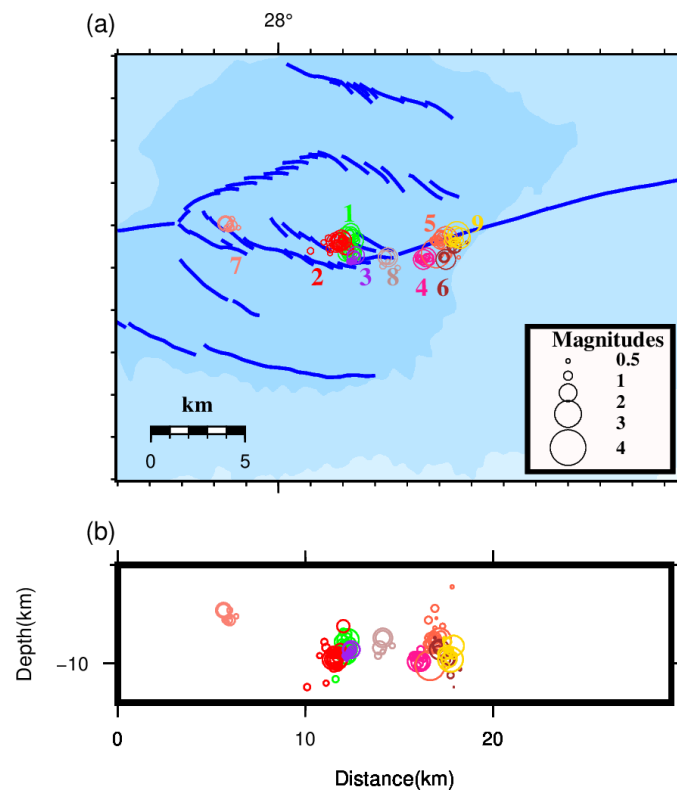


Figure 5.3. Spatial distribution of the repeating event clusters. Each cluster is shown with different color. (a) Map view of the repeaters. (b) The depth distribution of the repeaters.

Figures 3.10 and 3.11 show the located repeating events detected during the OBS campaigns used in this study (See also Table 5.1 for locations). Figure 5.3 shows the spatial distribution of each repeating cluster with different color. The clusters of the repeating earthquakes are located at depths between 8-13 km.

5.4. Fault Mechanism Results for the Repeaters

The focal mechanism solutions of the detected clusters provide important kinematic constraints on the mechanics of the creeping segment of the fault. The locations of the repeating event clusters are aligned with the surface trace of the southern branch of the Main Marmara Fault. Based on the waveform similarities and with the same first motion polarities, the events in the same cluster can be considered having the same source mechanism solutions. Therefore, composite source mechanism solutions are obtained using the first motions of the events within the same repeater cluster. The fault mechanism solutions are obtained from the first motion polarities of P wave for the earthquakes for the detected 9 repeater clusters by using the SEISAN algorithm FOCMEC. Figure 5.4, 5.5, 5.6, 5.7, 5.8, 5.9, 5.10, 5.11 and 5.12 show the composite focal mechanism solutions of repeating cluster 1, 2, 3, 4, 5, 6, 7, 8 and 9, respectively. The uncertainties are large as the magnitudes of the events are small and the epicentral distances to the receivers provide only a limited constraint. The composite solutions of 8 clusters of 9 indicate dominant strike-slip mechanisms in accordance with the fault kinematics, which is demonstrated in Figure 5.13. The cluster 5, denoted by purple shows almost pure normal fault solution and the solution for the cluster 1 does not have unique solution showing both normal and strike-slip mechanisms.

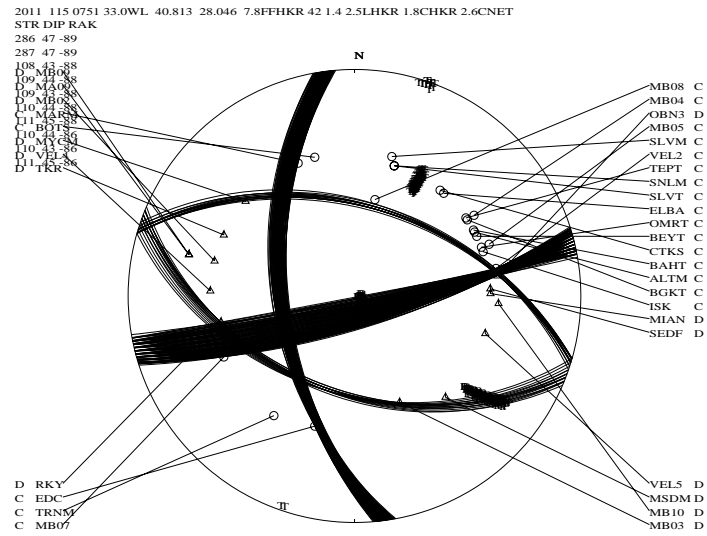


Figure 5.4. Composite focal mechanism solutions of the events within the detected Cluster 1 of seismic repeaters. Compression (C) and Dilatation (D) quadrants are shown for the lower- hemisphere projection of the focal sphere.

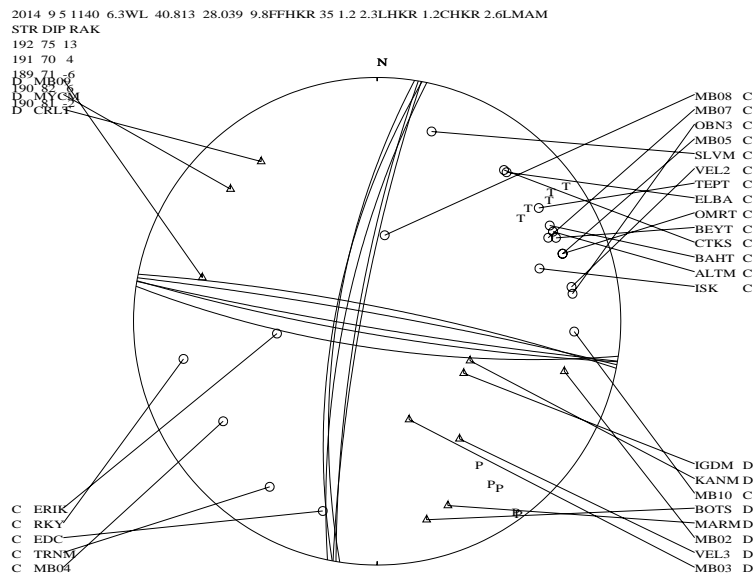


Figure 5.5. Composite focal mechanism solutions of the events within the detected Cluster 2 of seismic repeaters. Compression (C) and Dilatation (D) quadrants are shown for the lower- hemisphere projection of the focal sphere.

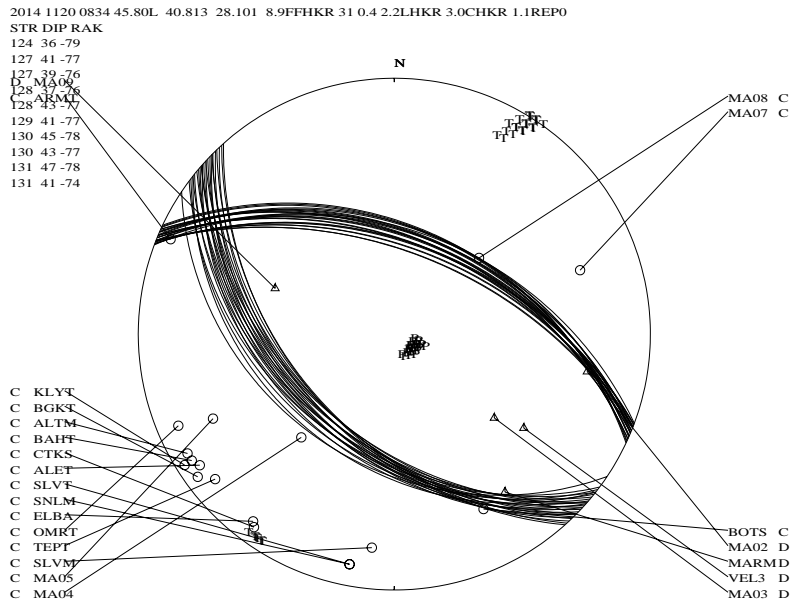


Figure 5.8. Composite focal mechanism solutions of the events within the detected Cluster 5 of seismic repeaters. Compression (C) and Dilatation (D) quadrants are shown for the lower- hemisphere projection of the focal sphere.

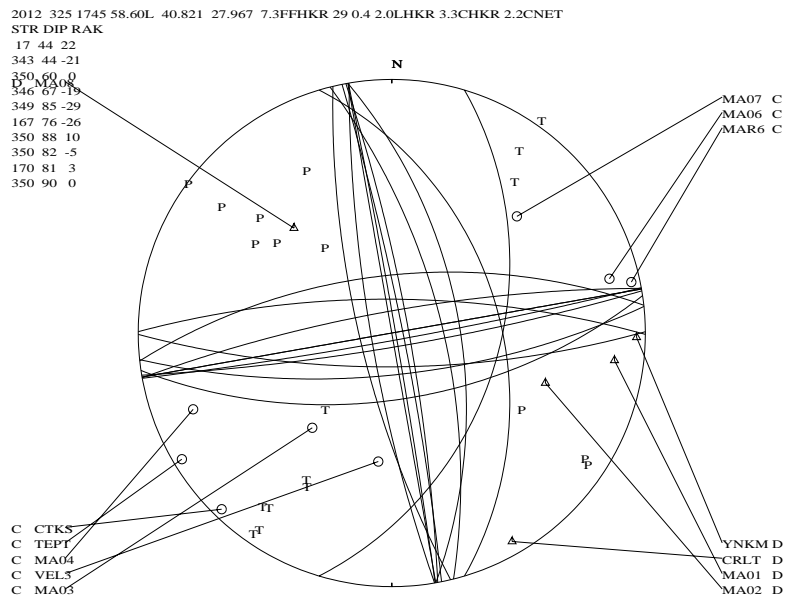


Figure 5.9. Composite focal mechanism solutions of the events within the detected Cluster 6 of seismic repeaters. Compression (C) and Dilatation (D) quadrants are shown for the lower- hemisphere projection of the focal sphere.

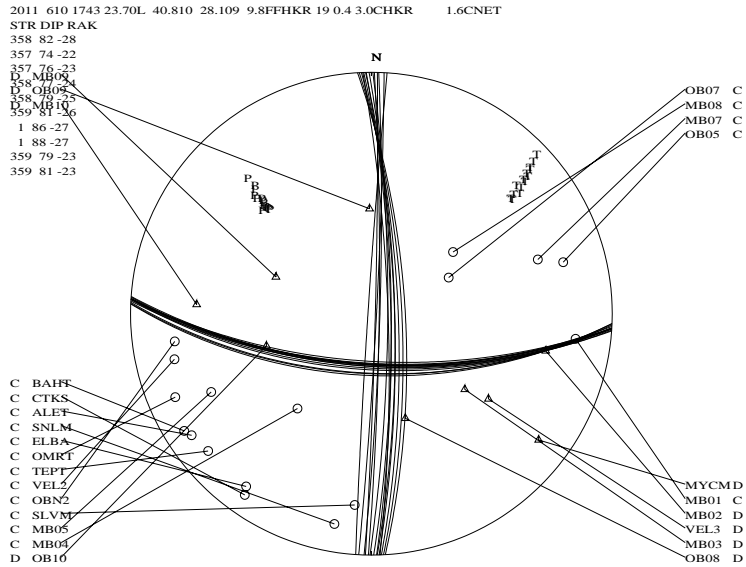


Figure 5.10. Composite focal mechanism solutions of the events within the detected Cluster 7 of seismic repeaters. Compression (C) and Dilatation (D) quadrants are shown for the lower- hemisphere projection of the focal sphere.

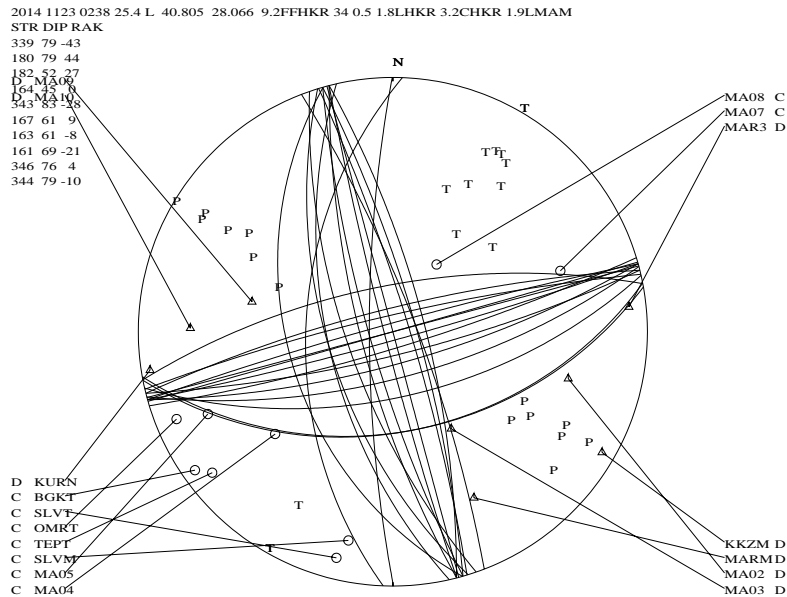


Figure 5.11. Composite focal mechanism solutions of the events within the detected Cluster 8 of seismic repeaters. Compression (C) and Dilatation (D) quadrants are shown for the lower- hemisphere projection of the focal sphere.

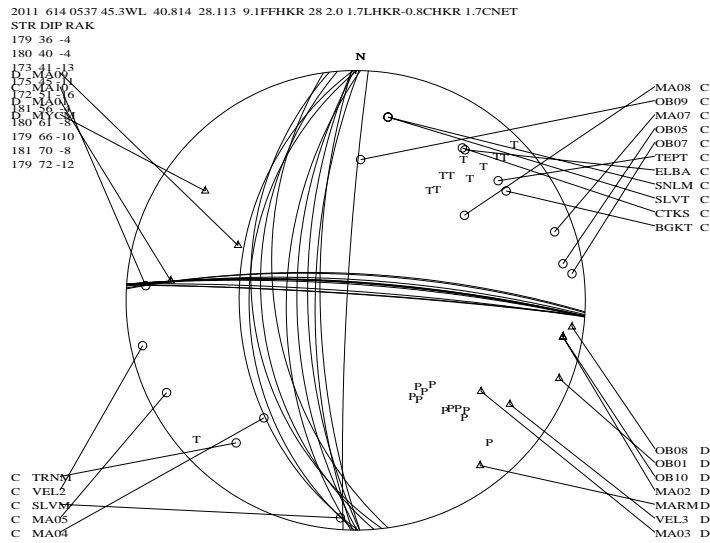


Figure 5.12. Composite focal mechanism solutions of the events within the detected Cluster 9 of seismic repeaters. Compression (C) and Dilatation (D) quadrants are shown for the lower- hemisphere projection of the focal sphere.

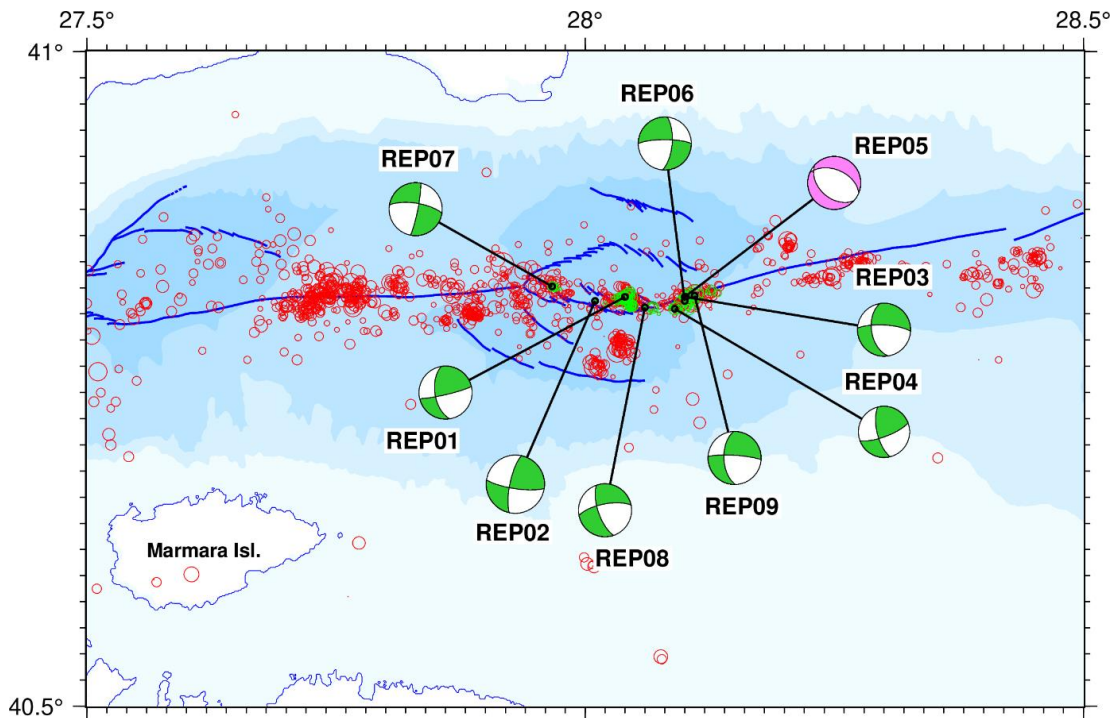


Figure 5.13. Seismicity distribution and composite focal mechanism solutions of the repeating event clusters in the Central Marmara. The green circles show the locations of the seismic repeaters. The mechanism of normal faulting of the Repeater Cluster 5 is shown by purple.

Table 5.1. The locations of the repeating earthquake clusters and the uncertainties of the calculation for dip, strike and rake calculations.

	Lat.	Lon.	Depth (km)	Dip	Strike	Rake	Num. of Pol.	Dip Uncertainty	Strike Uncertainty	Rake Uncertainty
Rep. Clus. 1	40.8	28.04	9	57.68	171.1	7.56	35	2.69	0.39	5.24
Rep. Clus. 2	40.81	28.04	9.6	78.07	189.7	-1.36	31	5.97	0.8	7.02
Rep. Clus. 3	40.803	28.04	9.5	51.44	171.2	-19.64	19	16.13	9.69	14.4
Rep. Clus. 4	40.8	28.08	9.7	68.17	166.3	16.46	41	12.64	4.25	4.18
Rep. Clus. 5	40.81	28.1	8.4	43.1	132	-75.54	23	3.26	3.66	2.4
Rep. Clus. 6	40.8	28.1	9.6	78.52	358.1	-25.27	26	2.75	0.9	1.87
Rep. Clus. 7	40.81	27.97	7.7	65.49	346	-24.05	13	6.51	2.67	4.91
Rep. Clus. 8	40.8	28.06	9.3	78.04	270.2	-23.37	17	5.07	26.29	3.73
Rep. Clus. 9	40.81	28.1	9.3	56.92	178.5	-10.07	27	4.73	3.44	3.94

Table 5.1 shows the uncertainty results for the calculated dip, strike and rake estimations. In general, the repeater clusters show acceptable uncertainty for the estimation of fault mechanism.

5.5. Recurrence Time Intervals of the Repeating Events

The recurrence interval is an important criterion that should be taken into account while making the assessment for the repeating earthquakes (Chen et al., 2007; Chen et al., 2013; Uchida, 2019). Nadeau and Johnson (1998) have observed a scaling relationship for repeating earthquakes in California as;

$$T_r \sim M_0^{1/6} \quad (5.4)$$

where T_r denotes the recurrence interval and M_0 is seismic moment.

Here, the loading rate controls recurrence time (T_r) and it is possible to mention about a particular statistic that $\log(T_r)$ proportional to $\log(M_0^{1/6})$. This observation is also

supported for the repeaters in Taiwan (Chen et al., 2007), which indicates the repeaters are associated with the rates of tectonic loading. This makes repeaters a useful tool for measuring slip directly on the fault.

In Figure 5.14, the comparison for the relation between recurrence time (T_r) and seismic moment (M_0) for the repeating earthquakes occurred in different countries including Taiwan, USA (San Andreas Fault) and Japan can be seen.

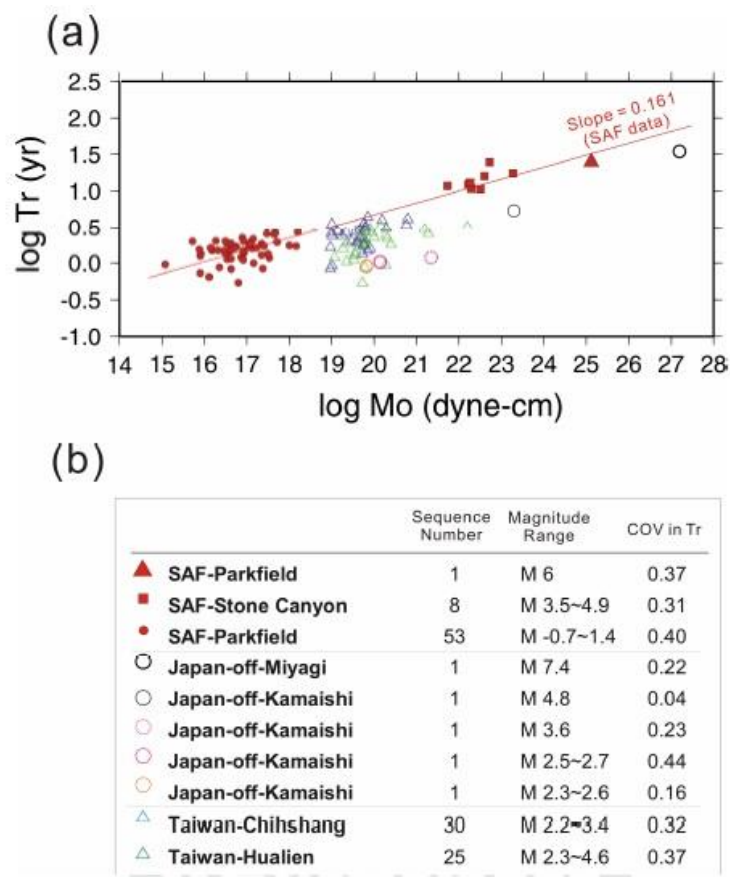


Figure 5.14. (a) The comparison for the relation between recurrence time (T_r) and seismic moment (M_0) for the repeating earthquakes occurred in different tectonic environments. (b) the number of repeating sequences, magnitude range, and coefficient of variation (COV) in recurrence intervals for different regions (after Chen et al., 2007).

Chen et al. (2013) questioned how triggered earthquakes affected the process of the selection of repeaters. For this reason, they assessed the relationship between the recurrence interval change of the events and the nearby seismic activity. Below, Equation

(5.5) gives the coefficient of variations (COV) for an earthquake sequence. Here, this equation calculates the standard deviation of the recurrence intervals divided by their mean.

$$\text{COV} = \frac{\sqrt{\sum_{i=1}^N (T_{ri} - \bar{T}_r)^2 / N}}{\bar{T}_r} \quad (5.5)$$

In Equation (5.5) given above, \bar{T}_r indicates the mean duration. N denotes the recurrence intervals of a sequence. Here, a COV value means perfect periodicity if it is 0. If COV value is near to 1, it is consistent with Poissonian distribution. If it is larger than 1 then it reflects temporal clustering. The COV value of 0.5 has been found for the repeating natural earthquakes (Ellsworth et al., 1995). On the other hand, the regular events have generally COV value of ~1, complying with Poisson distribution which usually indicates the random earthquake sequences (Chen et al., 2013).

Generally, the repeating events can be categorized into two types relative to their pattern of the recurrence interval. Those having short repeat times can be classified as “transient repeaters” as also pointed out by Schmittbuhl et al. (2016). Transient repeaters may include the earthquake swarms and series of foreshocks, aftershocks and mainshocks. The other type of the repeaters is the long-lasting repeaters occurring in a time intervals of months and years.

5.5.1. Temporal Evolution of Detected Seismic Repeaters

The recurrence time intervals for 9 near-repeating earthquake clusters detected from SLVM and SLVT stations between 2008 - 2021 can be seen in Figure 5.15. Each cluster is represented by different color. The event interval times within the same cluster are varying significantly from 5 minutes to 9 months.

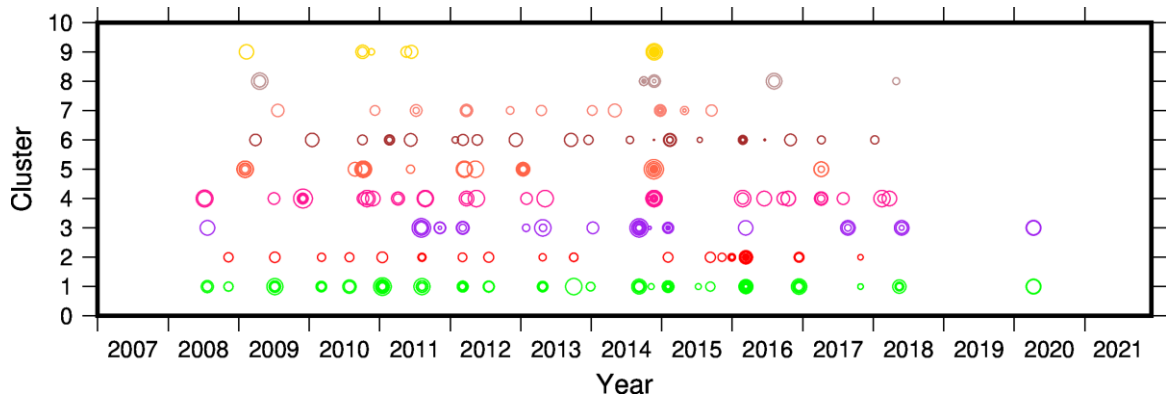


Figure 5.15. Demonstration of the recurrence time intervals of the near-repeaters acquired in this study from 2008-2021.

Here, the short-term repeaters can be considered as the aftershocks or the foreshocks of the largest events and obey the similar laws as regular earthquakes, e.g., Gutenberg-Richter and Omori law.

5.6. Spectral Analysis of the Repeaters

5.6.1. Seismic Source Model

The rupture parameters of the repeating events, such as magnitude, rupture dimensions, stress drop, can be estimated using various formulations of earthquake source (e.g. Brune, 1970; Abercrombie, 1995; Talebi and Boone, 1998; Stabile et al., 2012; Zollo et al., 2014). It is possible to calculate these parameters by utilizing displacement spectrum of P and S waves (Godana et al., 2015).

The seismic source model defined by Brune (1970) is commonly used for the earthquakes for the regions having different tectonic settings. The displacement spectrum given in Figure 5.16 represents a seismic source model which has been based to this study to calculate the seismic source parameters of the repeating events (Schmittbuhl et al., 2016).

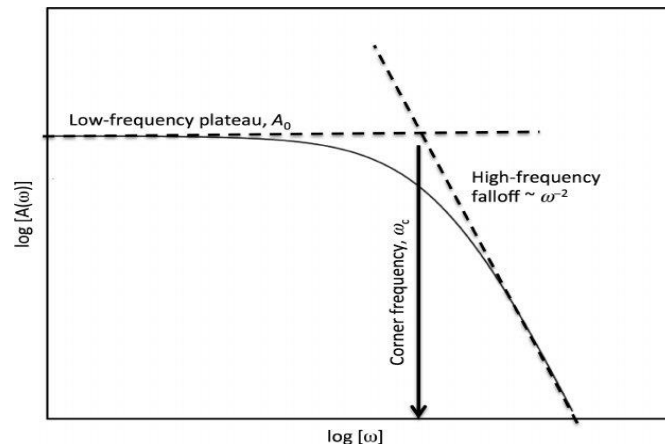


Figure 5.16. The displacement spectrum of seismic source model (after Eaton et al., 2014)

The seismic source spectrum is defined by Brune (1970),

$$S(f) = \frac{(2\pi f)^2}{1 + \left(\frac{f}{f_c}\right)^2} \quad (5.6)$$

where f_c is the corner frequency of seismic source.

In this study, the spectra of the repeaters were obtained using the S wave of the waveforms for the time window of 0.7 sec. Figure 5.17 shows the calculated spectra for the repeaters. The spectra give a corner frequency of about 13 Hz as seen in Figure 5.17.

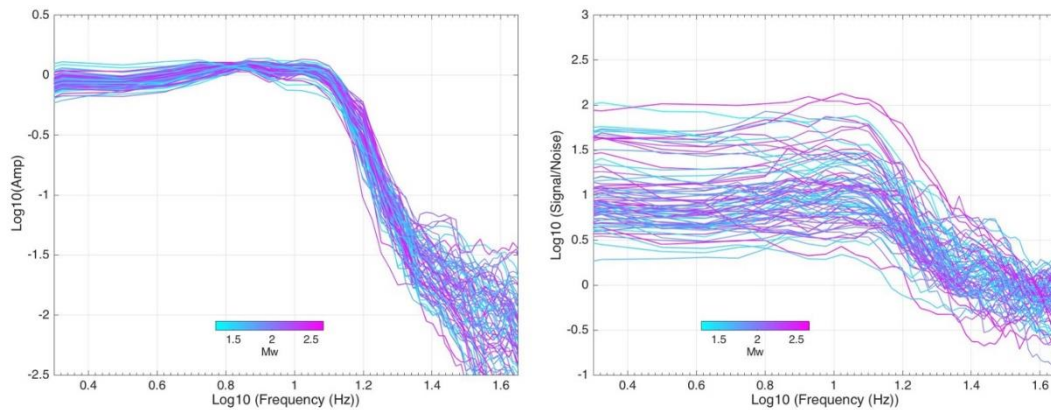


Figure 5.17. Left: the spectra of the E-W component waveforms detected in Cluster 1 at SLVM station. Each spectrum is normalized by its average value between 1-5Hz. Right: Signal/Noise for the spectra of the signal and noise windows.

Here, it should be noted that the distance between the micro-events and the SLVM station, which is about 30 km, and station site attenuation led to loss of high frequencies (>15 Hz) of waveforms. Therefore, no additional filtering was needed.

5.7. The Fault Slip Estimation Using Repeaters

The relationship between area and the moment of the source, independent from the location and depth, has been given in Nadeau and Johnson (1998). This relationship shows that the earthquakes have a linear relationship between their area and moment in logarithmic scale, which has been inferred from the observations from the earthquakes. Furthermore, the slip values (d) of the repeating events display a linear relationship with the moment (M_0) (Figure 5.18).

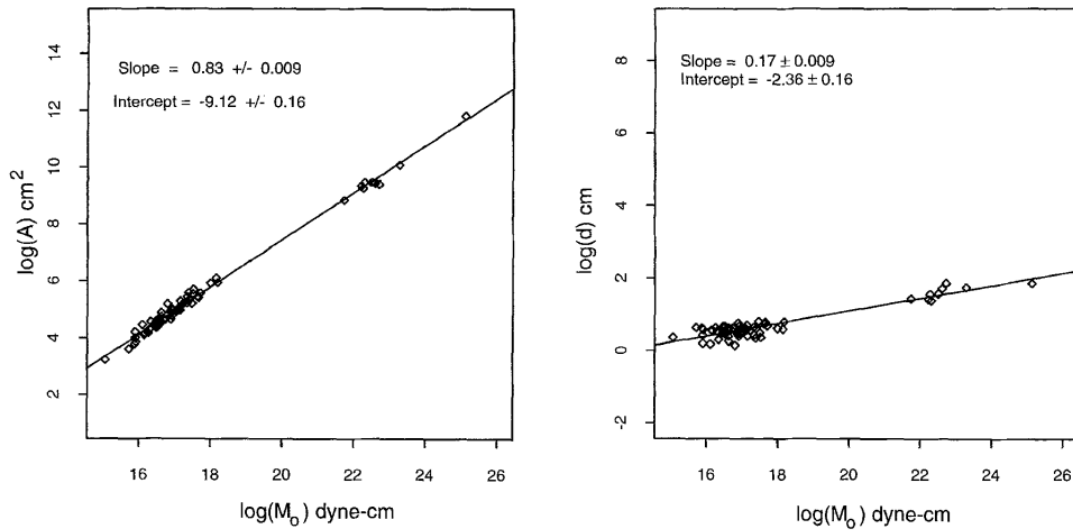


Figure 5.18. The relationship between the area (A), slip (d) with the seismic moment (M_0) in logarithmic scale. Left shows the relation of the area (A) versus moment (M_0). Right indicates relationship of slip (d) versus seismic moment (M_0) (Nadeau and Johnson, 1998)

The empirical relationship suggested by Nadeau and Johnson (1998), has been built using geodetic creep rates and the moment release rates of the repeaters in Parkfield and Stone Canyon.

$$d = 10^{-2.36} M_0^{0.17} \quad (5.7)$$

where d is slip (cm) and M_0 is seismic moment (dyne.cm).

On the basis of Equation (5.7), the scaling between recurrence interval and seismic moment, $T_r \sim M_0^{1/6}$ has been inferred. It is important to realize this relation differentiates from the relationship of $T_r \sim M_0^{1/3}$ derived from the accepting constant stress drop for regular earthquakes (Nadeau and Johnson, 1998). In other words, the recurrence intervals T_r for the repeating sequences, especially for small ones, display a scaling with $M_0^{1/6}$, as observed in Chen et al. (2007), Lengline and Marsan (2009); Nadeau and Johnson (1998). However, the recurrence interval or the slip of the events have a scaling relationship as $T_r \sim M_0^{1/3}$ when assuming a constant stress drop which is magnitude-independent (e.g.,

Allmann and Shearer, 2007, 2009). In this case, the ratio of slip of each event to the long-term slip rate is equal to the recurrence interval of the events if the earthquakes give the sum of all the slip on the fault zone (Williams et al., 2019). This has been expressed as in Equation (5.8) in Chen et al. (2007) for the Parkfield case.

$$T_r^{\text{nor}} = \frac{T_r \times V_f}{V_{\text{Parkfield}}} \quad (5.8)$$

where T_r^{nor} is normalized recurrence interval, T_r denotes the recurrence time interval of the events, V_f long-term average slip rates derived geodetically and $V_{\text{Parkfield}} = 2.3 \text{ cm/y}$ is the loading rate assumed as a reference value (Chen et al., 2007, Uchida, 2019).

Besides the relationship of Nadeau and Johnson (1998), Beeler et al. (2001) has put forward the equation for the total slip amount estimation of repeating earthquakes, by taking effect of the aseismic slip in an earthquake cycle into account. The expression that calculates the aseismic slip for each earthquake cycle proposed by Beeler et al. (2001) is;

$$d = \Delta\delta \left[\frac{1}{1.81\mu} \left(\frac{M_0}{\Delta\delta} \right)^{\frac{1}{3}} + \frac{1}{C} \right] \quad (5.9)$$

where μ is rigidity, $\Delta\delta$ is the stress drop and C denotes the strain hardening coefficient.

An alternative way, similar to regular earthquakes, is to use the standard crack model for the estimation of slip by assuming constant stress drop. This standard calculation has been used to compute slip of the nearly repeating events with irregular recurrence intervals (Schmittbuhl et al., 2015; Yao et al., 2017).

$$d = \frac{M_0}{\pi\mu\alpha^2} \quad (5.10)$$

where α is the crack radius.

Here, the crack radius can be obtained from the equation by assuming a constant stress drop, as in Eshelby (1957), on the basis of the relationship between seismic moment (M_0) and source radius (r) (Uchida, 2019).

$$r = \left[\left(\frac{7}{16} \right) \left(\frac{M_0}{\Delta \delta} \right) \right]^{1/3} \quad (5.11)$$

The seismic moment can be estimated using the relationship suggested by Hanks and Kanamori (1979).

$$\log M_0 = 1.5M + 9.1 \quad (5.12)$$

Figure 5.19 demonstrates the moment magnitude and slip relation for the three models that are commonly used.

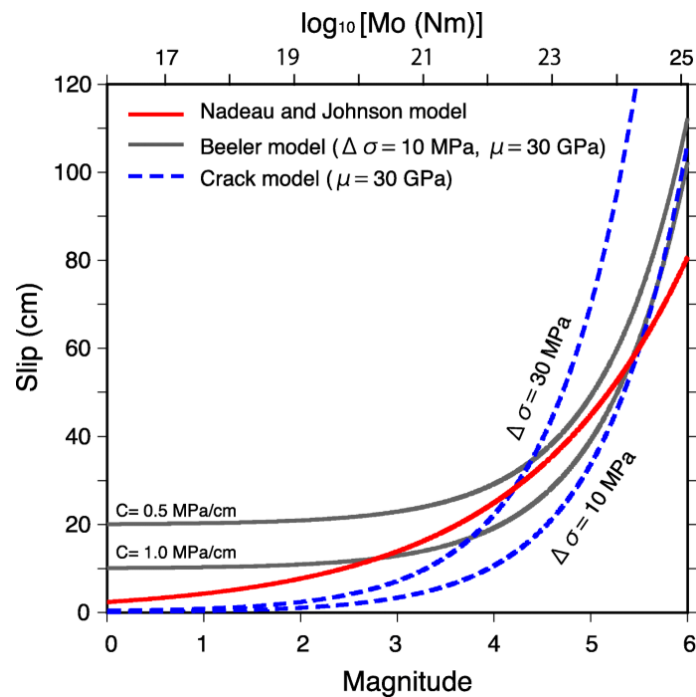


Figure 5.19. Magnitude and slip relationship between three slip models given by Equations (5.10), (5.11), (5.12) (after Uchida, 2019).

Depending on the selection of which model is used, there may be differences for estimation of slip from the repeaters, which will actually result in discrepancy of magnitude more than an order despite their dependency on the constants and magnitudes. In the study of Igarashi et al. (2001), Nadeau and Johnson's relation, which is shown by red in Figure 5.19, resembles each other for the magnitude ranges between 2.5 and 5.0 for Tohoku Earthquakes for the suitable C values changing between 0.5 – 1.0 MPa/cm. Based

on the assumption of a constant stress drop, Beeler's model seems to be close to the standard crack model. However, this model gives larger slip values for especially small events depending on the C values. On the other hand, the crack model may yield smaller slip values for the events $M < 3$. Yet, these relationships show similar spatio-temporal behavior if the repeaters' magnitude-ranges are not large (Uchida, 2019).

Here, the calculations were made on the basis of the connection between the seismic moment (M_0) by Keilis-Borok (1960), with given in Nm, moment magnitude (M_w) by Hanks and Kanamori (1979) and the source radius (R), which are given in Equation (5.13), Equation (5.15), and Equation (5.16), respectively.

$$M_0 = \frac{4\pi\rho v^3 \Omega_0}{G(r) R_{\theta\phi} C} \quad (5.13)$$

where ρ is the density, v is wave velocity, Ω_0 is low frequency level, $G(r)$ is geometrical spreading, $R_{\theta\phi}$ is radiation pattern and C is free surface correction.

Geometrical spreading, which is denoted as $G(r)$, is also an important function that changes depending on the distance and the depth. Therefore, it can be expressed as below at local distances for body waves,

$$G(\Delta, h) = \frac{1}{\sqrt{\Delta^2 + h^2}} = \frac{1}{r} \quad (5.14)$$

where Δ denotes the epicentral distance (m) from station to earthquake and h denotes the hypocentral distance (m).

$R_{\theta\phi}$ indicates the correction for the radiation pattern for P and S waves. This value has been admitted as 0.4 for P waves by Wyss and Brune (1968), while it has been used as 0.63 for S waves by Boore and Boatwright (1984).

In Equation (5.13), density of the region, denoted by ρ , was assumed as 2.6 g/cm³. Also, the seismic moment, M_0 is defined in Nm that is equal to kg. (m²/sec²) unit when Ω_0 is in meter.sec unit, v is expressed in m/sec and ρ is kg/m³.

$$M_w = \frac{2}{3} \log M_0 - 10.73 \quad (5.15)$$

The source radius (R) values were estimated using the corner frequencies acquired from the calculated spectra.

$$R = \frac{kv_s}{f_c} \quad (5.16)$$

In Equation (5.16) given above;

r = source radius

V_s = shear wave

f_c = corner frequency

To sum up, the process of the calculation of slip follows the estimation source size from the Brune's circular crack model by determining the corner frequencies and computing the slip values from their relation to the rupture area.

In Equation (5.16), k value depends on the type of the spectra used. For a dynamic circular crack using constant rupture velocity, Madariaga (1976) determined k=0.32 for P waves and k=0.21 for S waves for a rupture velocity V_r=0.9.V_s (Wang and Day, 2017). In this study, in the calculation for the slip, k value was taken 0.21 for S- waves for a rupture velocity of V_r=0.9V_s.

As also specified in Section 5.4, the source slip area of each repeater, to check whether they overlap with each other or not, can be estimated using the link between the seismic moment and the source radius.

$$\Delta U = M_0 / \pi \mu R^2 \quad (5.17)$$

Here, the source slip can be estimated using Equation (5.17), where the shear modulus (μ) is taken as 35 Gpa. The corner frequency values that are indicated as 13 Hz from the spectra were used to calculate the slip.

5.7.1. Slip Rate Estimates from Nearly Repeating Events

Figures 5.20 and 5.24 show the waveforms of the repeating event waveforms detected at SLVM station between 2008-2018 for the Cluster 1 and 3, respectively. Two clusters (Cluster1 and Cluster 3) have the largest magnitude repeating events, therefore also detected at SLVT station, ~46 km far from the epicenter of the events (Figure 5.22 and 5.26). The data continuity of the SLVT station after 2018 allows to track the repeaters from these two clusters. It is worth noting that number of repeating events detected at SLVT station was significantly decreased after 2018 (Figure 5.22 and 5.26) and only two repeating events during 2020 are detected for two clusters. During 2019, no repeating event is detected at any cluster. Whether this is due to the detection threshold of SLVT station is unclear.

Figure 5.21 shows the analysis of the Cluster 1, which is the most complete event set detected in this study as it contains largest magnitude events. The signal quality is good for all 3 components. The maximum magnitude is 2.7 but 7 events with magnitudes 2.5 or larger are detected between 2008-2018 from SLVM station (Figure 5.21). Similar observations are displayed for the same cluster using SLVT station in Figure 5.23. On the top panel of Figure 5.21 and 5.23, the daily and cumulative seismicity along the MMF is displayed. The large magnitude earthquakes on the cumulative plots with aftershock decays can be clearly recognized on these plots. No correlation was found between the occurrence of seismic activity in the Marmara Sea and the timing of the repeating events. Although the repeating events are sometimes associated with short-term repeating events and regular seismic activity, no triggering activity is observed due to the earthquake activity in the area. The cumulative slip obtained from the waveforms recorded at SLVT stations between 2008-2020 is smaller than the slip obtained from SLVM station (Figure 5.25). This is possibly a result of the undetected repeaters at SLVT station compared to the detections at SLVM station.

Figures 5.25 and 5.27 show the analysis of the Cluster 3 from SLVM and SLVT stations, respectively. Cumulative slips over the observation period are lower than the cumulative geodetic slip. The number of detected repeating events from SLVT station significantly decrease after 2018.

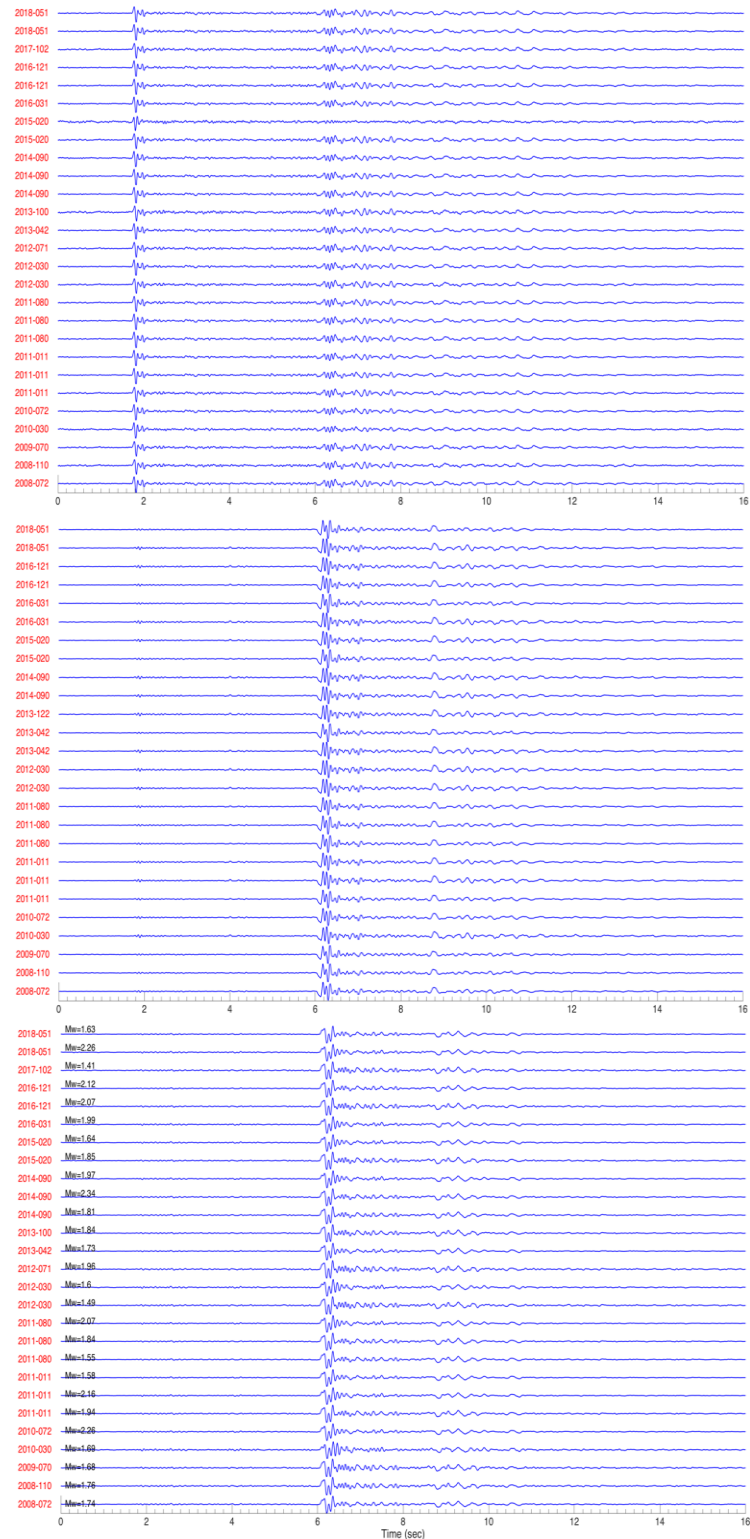


Figure 5.20. The repeating waveforms detected in Cluster 1 from the SLVM station between 2008-2018: vertical (top), N-S (middle) and E-W (bottom) components. Traces are normalized by the maximum value of each trace. The numbers on the left of the traces (red labels) shows the recording date of the event. The numbers on the traces of the E-W components shows the moment magnitudes of each event.

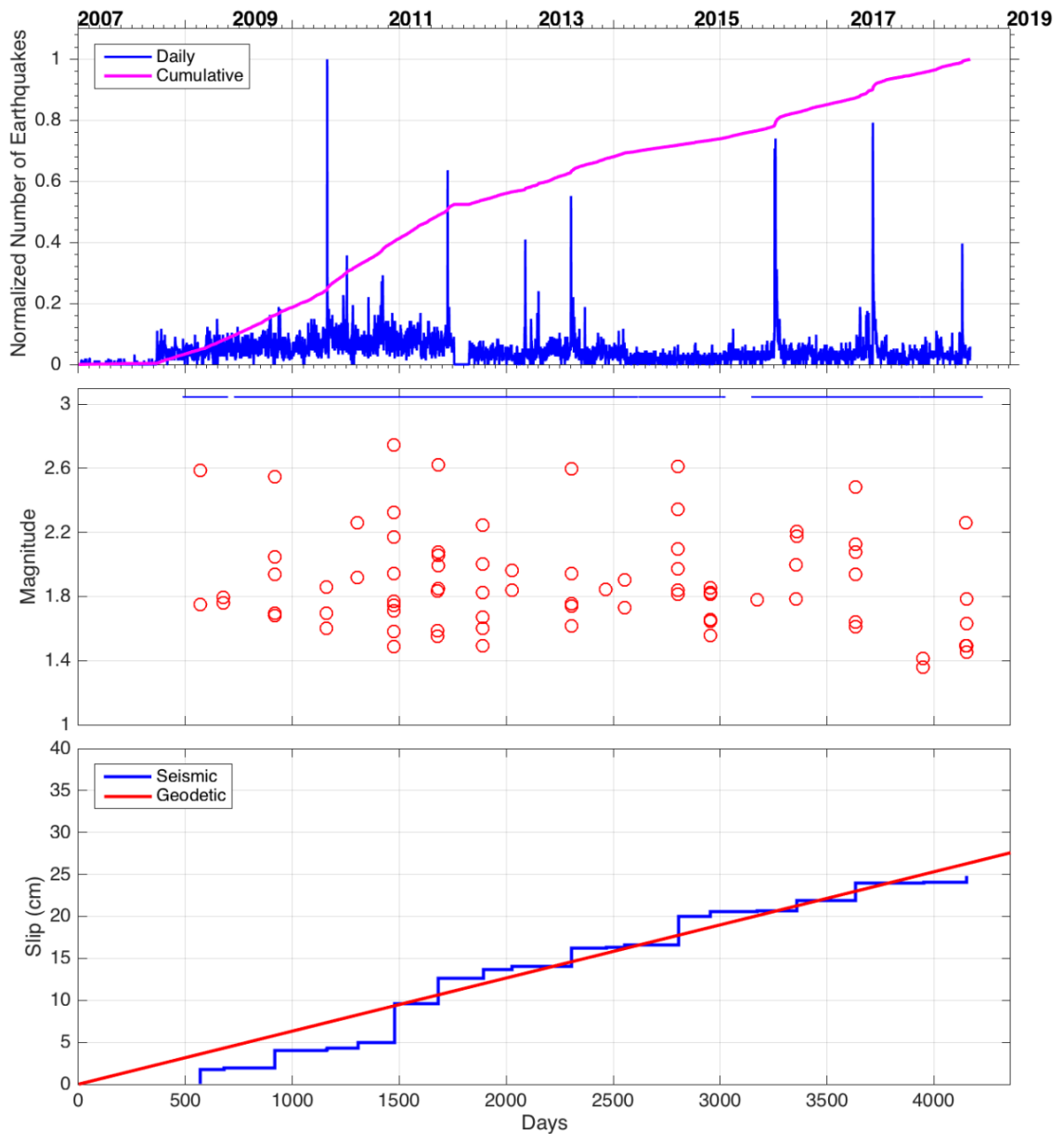


Figure 5.21. The analysis of E-W component of repeating events of Cluster 1 detected at SLVM stations shown in Figure 5.20. Top: Cumulative and daily seismic activity. Middle: The magnitudes of the repeating events in time. The data continuity of the SLVM station is shown on the top of the middle frame (blue). Bottom: Cumulative slip computed from the repeating events shown in the middle panel (blue) and the cumulative geodetic slip computed with a rate of 23 mm/year (red).

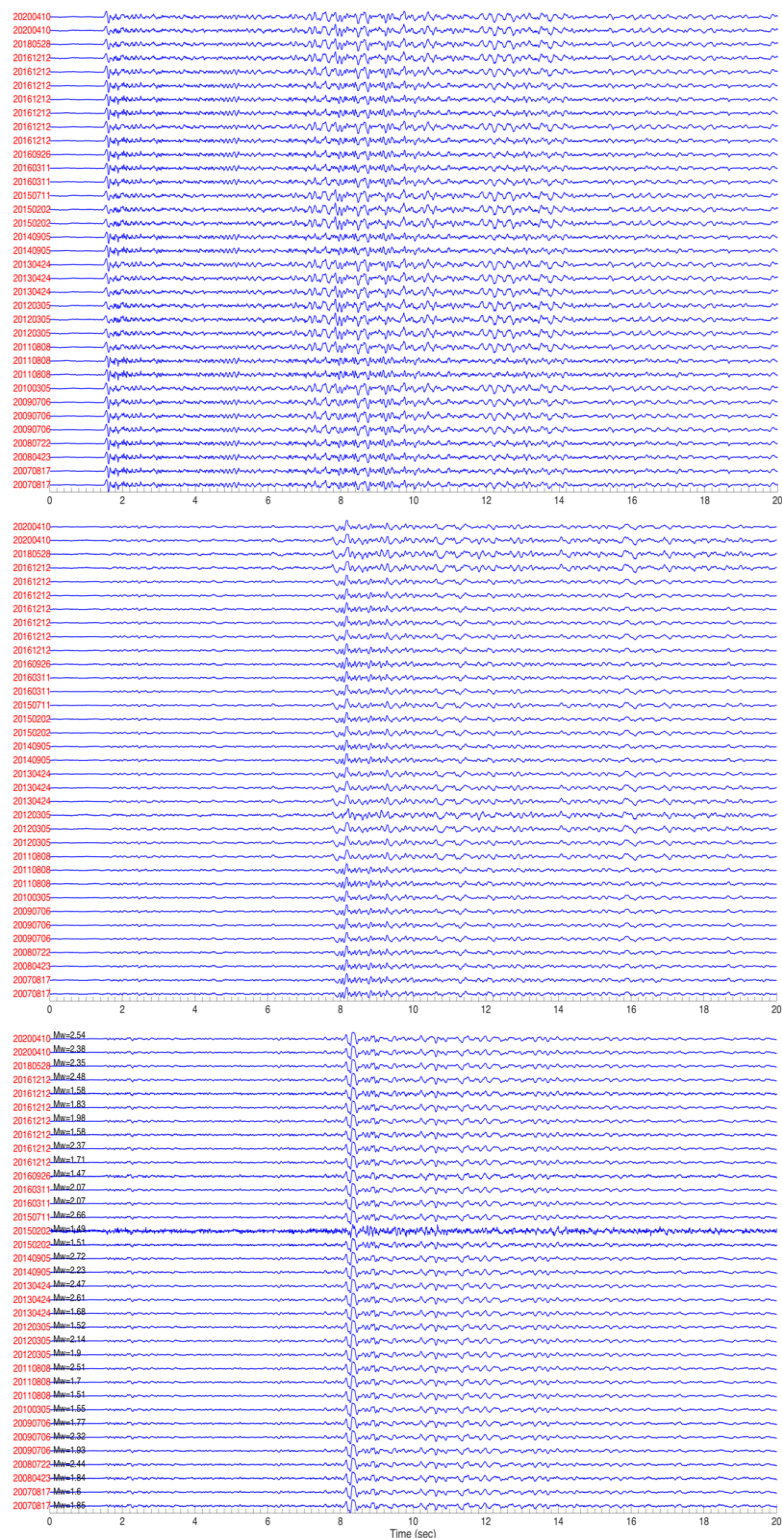


Figure 5.22. The repeating waveforms detected in Cluster 1 from the SLVT station between 2008-2020: vertical (top), N-S (middle) and E-W (bottom) components. Traces are normalized by the maximum value of each trace. The numbers on the left of the traces (red labels) shows the recording date of the event. The numbers on the traces of the E-W components shows the moment magnitudes of each event.

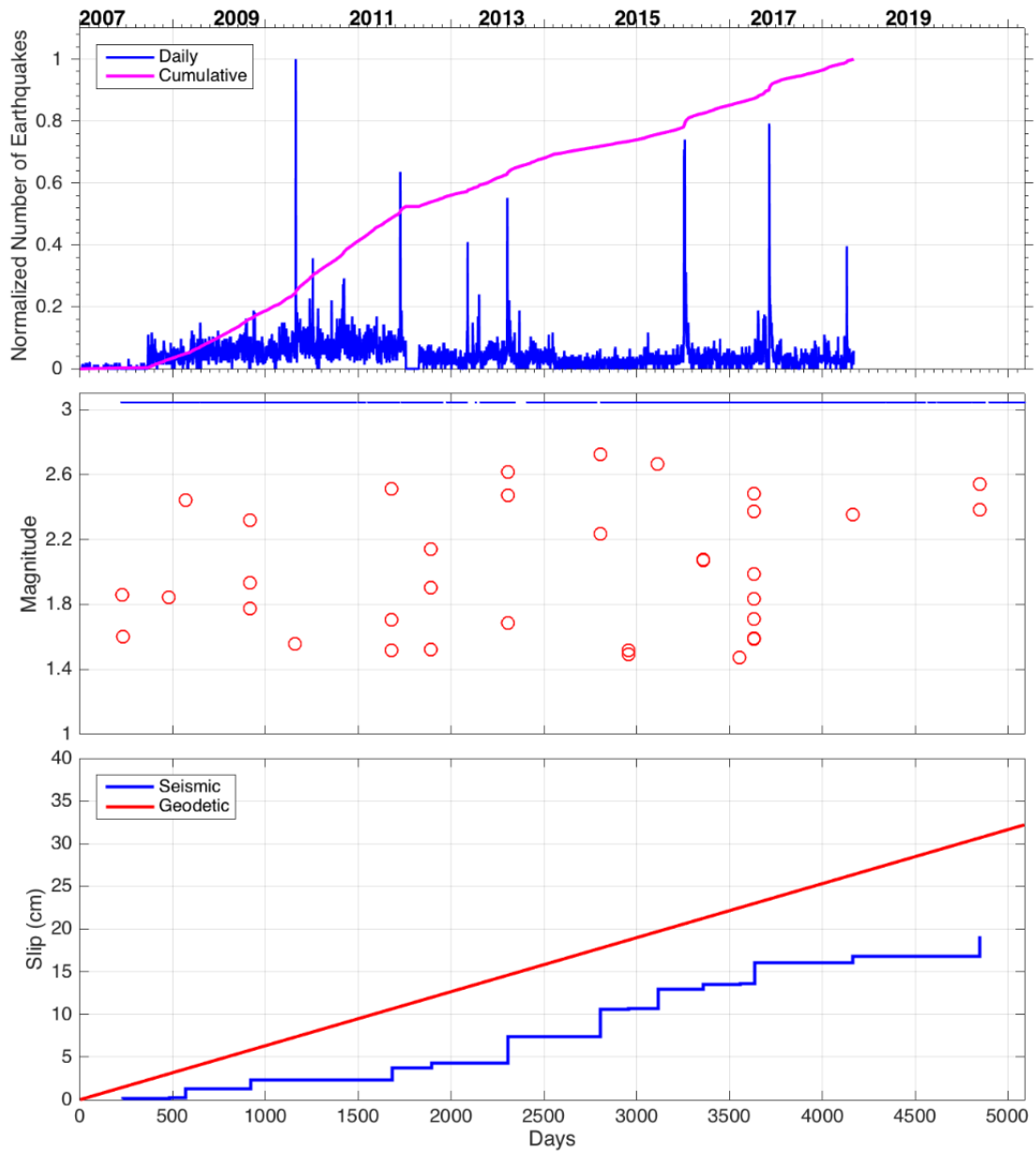


Figure 5.23. The analysis of E-W component of repeating events of Cluster 1 detected at SLVT stations shown in Figure 5.22. Top: Cumulative and daily seismic activity. Middle: The magnitudes of the repeating events in time. The data continuity of the SLVT station is shown on the top of the middle frame (blue). Bottom: Cumulative slip computed from the repeating events shown in the middle panel (blue) and the cumulative geodetic slip computed with a rate of 23 mm/year (red).



Figure 5.24. The repeating waveforms detected in Cluster 3 from the SLVM station between 2008-2018: vertical (top), N-S (middle) and E-W (bottom) components. Traces are normalized by the maximum value of each trace. The numbers on the left of the traces (red labels) shows the recording date of the event. The numbers on the traces of the E-W components shows the moment magnitudes of each event.

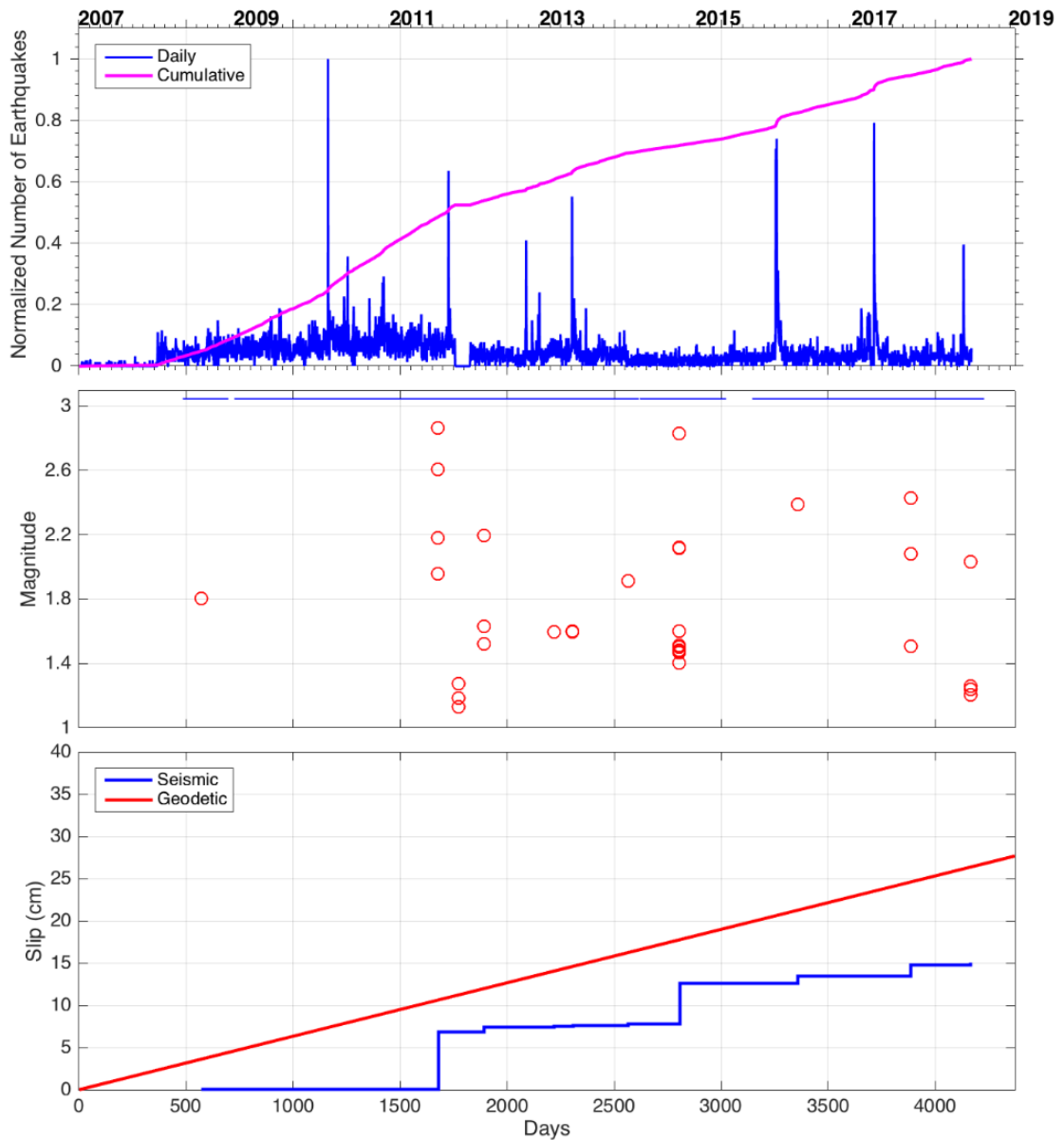


Figure 5.25. The analysis of E-W component of repeating events of Cluster 3 detected at SLVM stations shown in Figure 5.24. Top: Cumulative and daily seismic activity. Middle: The magnitudes of the repeating events in time. The data continuity of the SLVM station is shown on the top of the middle frame (blue). Bottom: Cumulative slip computed from the repeating events shown in the middle panel (blue) and the cumulative geodetic slip computed with a rate of 23 mm/year (red).



Figure 5.26. The repeating waveforms detected in Cluster 3 from the SLVT station between 2008-2020: vertical (top), N-S (middle) and E-W (bottom) components. Traces are normalized by the maximum value of each trace. The numbers on the left of the traces (red labels) shows the recording date of the event. The numbers on the traces of the E-W components shows the moment magnitudes of each event.

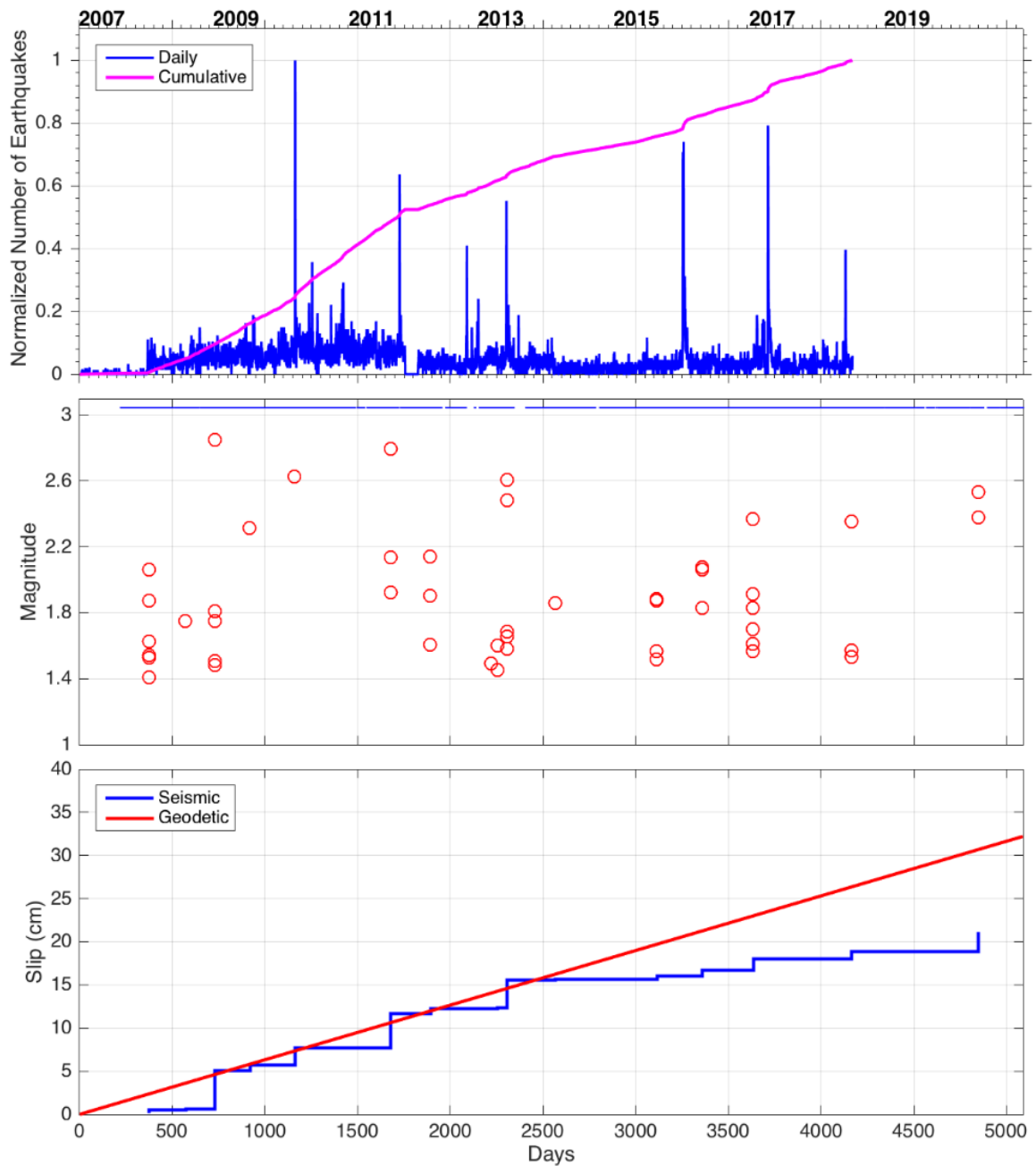


Figure 5.27. The analysis of E-W component of repeating events of Cluster 3 detected at SLVT stations shown in Figure 5.26. Top: Cumulative and daily seismic activity. Middle: The magnitudes of the repeating events in time. The data continuity of the SLVT station is shown on the top of the middle frame (blue). Bottom: Cumulative slip computed from the repeating events shown in the middle panel (blue) and the cumulative geodetic slip computed with a rate of 23 mm/year (red).

5.8. Comparison of the Results with the other studies on Repeating Earthquakes in the Marmara Sea

In this study, 9 repeater clusters were found in the Central Basin using the continuous data recorded at SLVM and SLVT stations between time period from 2008 to 2020 using the template matching method. The same template events are used as Schmittbuhl et al. (2016) so that the repeating events found in this study can be considered as the continuation of the results by Schmittbuhl et al. (2016). The precise estimates of the locations of the repeating events using only OBS data improves kinematic constraints on the geometry of the creeping segment of the MMF. The continuity of the repeating events for 13 years clearly indicates continuous unloading of the same zone through time and is evidence that the Central Marmara region has fully or partially creeping behavior at depth.

The results from the extensometer data given in Yamamoto et al. (2017) and (2019) suggests a partial creeping close to the location of the repeaters found in this work with a slip observed of about 8-11 mm/yr and 10.7 ± 4.7 mm/year, respectively.

The standard approach for the confirmation of the earthquakes to be repeaters is recurrence intervals. As also discussed in Section 4, the repeating events usually follow a standard pattern in terms of their recurrence intervals of time. However, the repeaters that were acquired during the study does not confirm a certain pattern, which was also seen in Konca et al. (2021). The repeaters showing high similarity concerning their waveforms with variable magnitudes and recurrence time intervals have been referred as “near-repeating events” by Shaddox et al. (2021) as also mentioned in the Chapter 4. The repeating earthquake pattern obtained in the thesis seems more compatible with this new terminology: “near-repeating events”. These events were interpreted as the signature of the aseismic transient slip, which may show faulting complexity during aseismic slip, as Shaddox et al., (2021) pointed out. On the other hand, Lengline and Marsan (2009) highlighted that partial rupture of the same earthquakes or the separate asperities close to each other caused short-term repeaters, near Parkfield and the locations of these events are actually not firmly clustered. On the other hand, the repeating events that were named as “near-repeaters” may have resulted from the complex structure of the faults that affect the asperities on the fault zone producing these events.

A study carried out by Bohnhoff et al. (2017) reported 2 repeater pairs in the Central Basin and Western High Cluster. The repeater events found in that study have a magnitude of about 2.8 and a recurrence period of up to 38 months. The magnitudes of the events are larger than $M=2.2$.

Recently, Uchida et al. (2019) claimed to observe the repeaters in the Marmara Sea based on hypocenter locations or the similarity of waveforms. The study indicated that there are repeating earthquakes grouped in 9 sequences with magnitudes changing from 2.3 to 3.2. The 7 sequences of these events were located in the Central Basin on the MMFZ.

The other two sequences given by Uchida et al. (2019) were located in the west and the east of the (close to the boundary of the rupture caused by 1999 İzmit and Düzce earthquakes. The recurrence interval for these events was reported to range between 12-72 months for a 8.2 year period. The total cumulative slip was calculated as 3.6 cm/year for all clusters.

Figure 5.28 shows the locations of the 7 repeating clusters detected in the Marmara Sea. Uchida et al. (2019) used event waveform catalog of Kandilli Observatory and the stations used in their work are quite far from the clusters. They only used the data between 2005 and 2013 and the detection magnitude limit of the event waveform catalog is relatively high. From these clusters, 5 of them are located within the Central Basin. The 5 clusters in the Central Basin displayed in Figure 5.28 are the same clusters as detected by Schmittbuhl et al. (2016) and this study. However, the locations of these clusters in Figure 5.28 are significantly different from this study. In this study, these clusters' locations are highly accurate from the OBS data between 2014-2016 as the repeating events in these clusters are also determined during this time period. Therefore, it is clear that the repeater clusters displayed in Figure 5.28 do not spread into such large area but locally more concentrated. The slip rate estimated using the repeaters by Uchida et al. (2019) is ~ 3.6 cm/yr which is not sensible relative to the geodetic rate (~ 2.5 cm/yr).

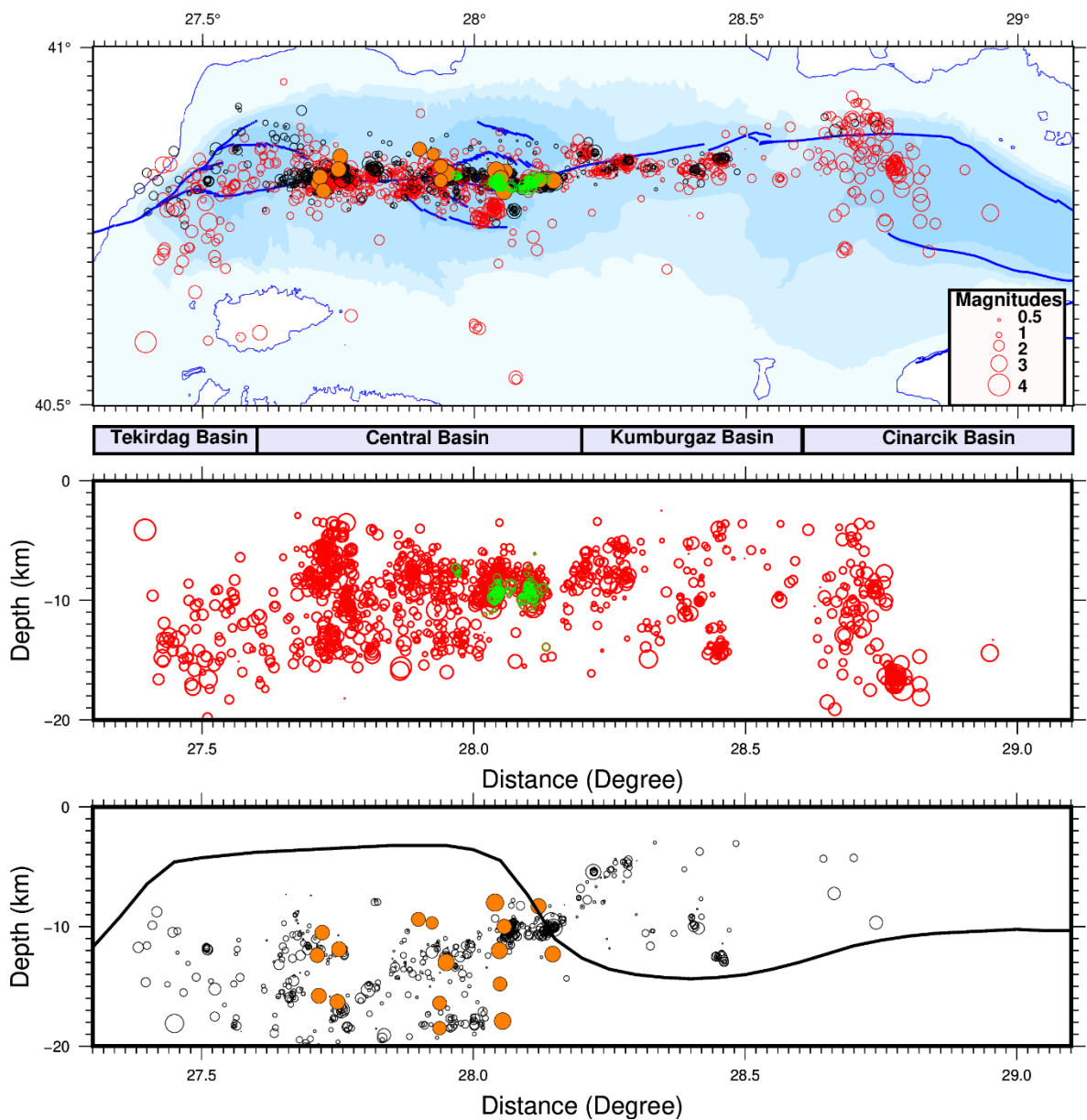


Figure 5.28. The comparison of the microearthquake locations of the current study and Yamamoto et al. (2017). The red circles denote the locations from the present study. The black circles indicate the results of Yamamoto et al. (2017). Green circles show the repeaters obtained in this study. Orange dots denote the repeater found in Uchida et al. (2019). The black line denotes the locking depth given by Schmittbuhl et al. (2015). Top: The horizontal distribution of the earthquake locations. Middle: The depth section obtained in the thesis. Bottom: The depth section depicting the depth results from Yamamoto et al. (2017) with the hypocentral locations of the repeaters from Uchida et al. (2019).

Table 5.2. The methods for the slip estimations of recent studies in the Marmara Region

Studies on Repeating Events in Marmara Sea	Method Used for Search of Repeaters	Time window	Magnitude Range	Recurrence Interval	Range of Frequency	Slip estimate formula
This Study	Template matching at a target station-CC ≥ 0.9	0.7 sec	0,2 - 3.3	Semi-periodic and aperiodic; 5 minutes (for short-term) and ~ 9 months (long-term)	1-15 Hz	Analysis of spectrum based on crack model
Uchida et al. (2019)	Hypocenter calculation	40 sec	2,3 - 3,2	12-72 months	2-10 Hz	Nadeau and Johnson (1998)
Bonhoff et al. (2017)	Hypocenter calculation	240 sec	2,8	12 - 38 months	3-23 Hz	Assuming slip value based on crack model from magnitude of repeaters
Schmittbuhl et al. (2016)	Template matching at a target station - CC ≥ 0.9	15 sec	1.3-1.8	7.6 months	1-10 Hz	Analysis of spectrum based on crack model

Table 5.2 presents a comparison for the slip estimation methods from recent studies. The Figure 5.28 given above shows the location of the repeaters found by the current study and Uchida et al. (2019).

6. DISCUSSION

6.1. Interpretation of Microseismicity in the Marmara Sea

The unbroken segment of the NAF in the Marmara Sea has been investigated since 1999 İzmit earthquake using various systems and methodologies (Armijo et al., 2005; Parsons et al., 2000; Ergintav et al., 2014; Hubert and Ferrari et al., 2000; Schmittbuhl et al., 2015; Klein et al., 2017) and this section has been monitored, especially, since 2002 by local seismic networks (Barış et al., 2002; Ito et al., 2002). The segment expected to rupture holds ~120km of length, potentially generating an earthquake of Mw 7.0-7.4. The precise estimate of the magnitude depends on the extent of the 1912 Mürefte earthquake (Aksoy et al., 2010) in the westernmost part of the MMF as well as on the seismotectonic attributes of the fault. Two of these important attributes are seismogenic zone's thickness and the creeping sections' lengths. As the fault's unbroken segment is totally under the Sea of Marmara, the seismological observations are key to determine the geometrical and kinematic parameters.

This study provides more accurate estimation of the seismogenic zone and the geometry of the active segments of the MMF based on the data from highly dense networks of Ocean Bottom Seismometers. Furthermore, the monitoring of the seismic repeaters with more precise locations and focal mechanism solutions are extended to the end of 2020 following the work of Schmittbuhl et al. (2016).

The relocation results of the micro-events of this study indicates a diffuse seismicity starting at 7-8 km depth and reaching 18 km in the Tekirdağ Basin. The low seismicity rate in this section at depths shallower than 7-8 km can be an indication of a locked fault. This area of the MMF down to the 10 km has also been defined as aseismic by Wollin et al. (2018) from onshore seismic data. Also, Yamamoto et al. (2020) attributed this low seismicity zone, extending to about 11 km below the surface, as a region that carries a potential of producing an earthquake. The slip deficit rates given in Özbey et al. (2021), on the other hand, is about 12 mm/yr for this region from surface to 10 km, showing a partially locked zone. To the east, at the Western High, the seismicity starts at shallower

depths, which is defined as a zone of transition to Central Basin, the seismic activity is highly localized. Yamamoto et al., (2019) found 10 ± 4.7 mm/yr slip rate around 27.7° E from the extensometer observation and interpreted this area as partial creeping zone to a depth of ~ 8 km. The Central Basin has an intense seismic activity compared to the other segments of MMF. The relocation results highlight seismic activity emerging at the shallow depths, starting at 3 km. Recently, the modelling results of Özbey et al., (2021) also indicate creep to the west of 28.2° E whereas locked areas are present in the eastern sections with different locking depths, based on GPS velocities merged with the seafloor geodetic observations. Ergintav et al., (2014) pointed out the presence of the aseismic creep based on low slip deficit rate in the Central Basin, which is in accordance with the results of this study. Furthermore, the areas with intense seismicity rate correlates with the results of the 3-D modelling of the Yılmaz et al., (2022) in the Marmara Sea by utilizing the GPS observations, depicting the existence of the creeping zone in the Western High and the Central Basin. Here, the high seismicity rates in the creeping zones and the low seismicity rates in the high coupling areas are backed up by the findings of the GPS studies such as Ergintav et al., (2014) and Özbey et al., (2021). The results for the Kumburgaz and the western part of Çınarcık Basin display different behavior from other segments of MMF in terms of the seismic activity rates. Between the 28.2° - 28.6° E the seismicity is concentrated between 5-18 km depth, with decreasing seismicity rate to the east. Offshore geodetic measurements of baseline changes together with the observations of sparse seismicity showed that this segment (28.0° - 29.0°) is locked at least down to 3 km (Lange et al., 2019), which agrees with the sparse seismicity of this study. This section is also proposed to be locked down to 10 km by Özbey et al., (2021), which is defined as İstanbul-Silivri Fault segment.

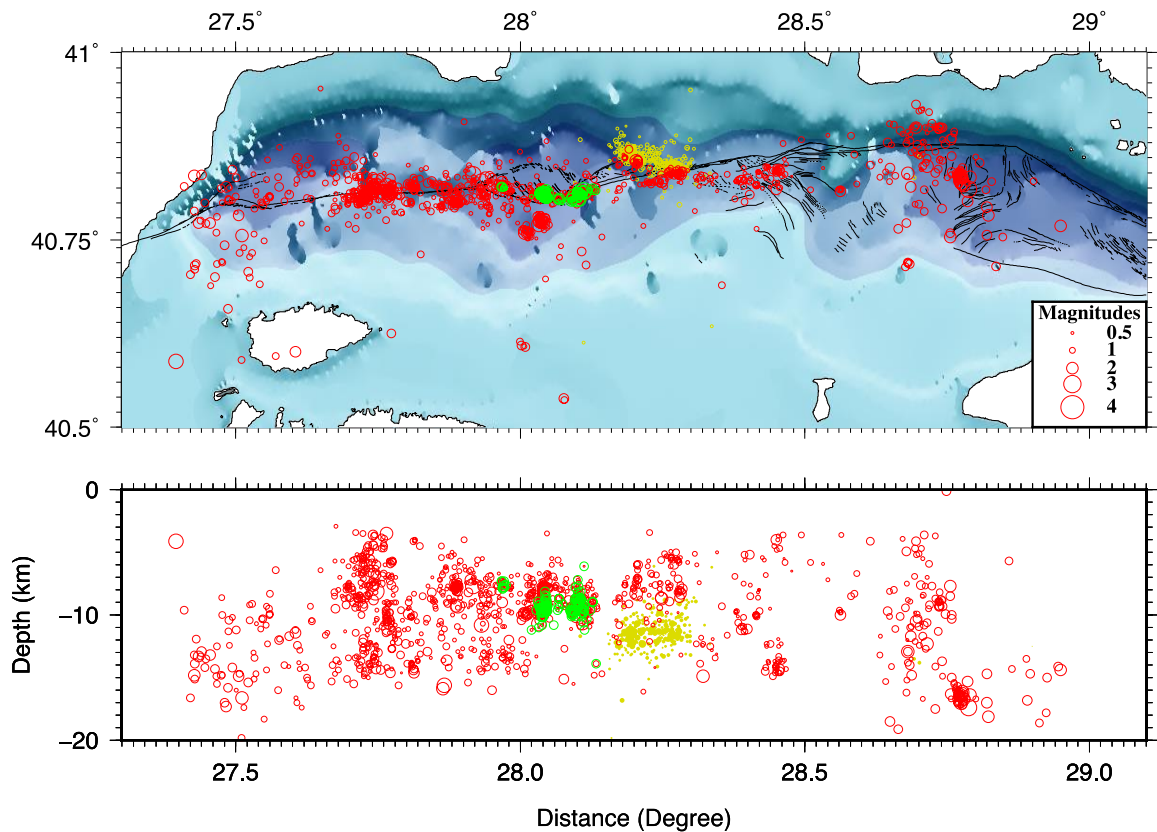


Figure 6.1. The seismicity map (top) and depth (bottom) sections from this study (red circles). The yellow circles show the aftershock locations of 2019 Mw5.8 Silivri earthquake (Karabulut et al., 2020).

The most interesting seismic activity on the MMF since the 1999 Izmit earthquake occurred on 26 September 2019 with Mw5.8 Silivri earthquake. The earthquake occurred at the transition between the Central Basin and Kumburgaz Basin and on the northern branch of the MMF. The seismic activity on the ruptured fault was not detected prior to the earthquake from the regional catalog. However, the seismicity detected from the OBS array of this study clearly detected seismic activity on the ruptured fault (Figure 6.1). It is worthwhile to point out that the depth of the seismic activity during the OBS campaign takes place at depths shallower than the activity during 2019. Therefore, it is clear that the OBS based earthquake location illuminates the fault activity which cannot be detected from the land-based observations.

6.2. Near-repeating Events in the Marmara Sea

The identification of the creeping segments along the MMF is critical to determine rupture extends of a fault rupture and the lack of near field observations due to the Marmara Sea highlights the importance of seismological observations related to the seismic events indicating creeping sections of the fault. The detailed search of seismic repeaters in the Marmara Sea indicated that the Central Basin is currently the only place which hosts these observations. The repeating events of 9 clusters detected in this area by Schmittbuhl et al., (2016) between 2008-2015 is extended in this study to the end of 2020. The locations and the focal mechanisms of these clusters are improved with the availability of the OBS data.

The seismic repeaters, as observed in different tectonic settings (Nadeau and Johnson; 1998), Duverger et al., 2018; Chen et al., 2008; Dominguez et al., 2016; Uchida et al., 2003), with their constant recurrence times and similar magnitudes, provide an accurate computation of slip rate of a creeping fault. However, nearly repeating events do not have such simplicity. The seismic events which are related to the creep can be attributed to the near repeating events that are not periodic, have variable magnitudes and closely located (100-500 m), as introduced by Shaddock et al. (2021). The near-repeating earthquakes tend to occur in the areas of aseismic slip and of transition zone between seismic and aseismic slip, where the seismicity rate is high (Chalumeau et al., 2021). So, the transition zone between creep and locked areas can be associated with the near repeaters, as well as the slip transients in the Marmara Sea. Hence, the presence of the near-repeaters in the Central segment in Marmara Sea is an indicator of an aseismic slip.

Both long term and short term nearly repeating events are observed in the Central Basin of the Marmara Sea. The observed short-term near-repeating events can be interpreted that the whole asperity may not be broken; or the near repeaters may also be result of the failure of the small different asperities which are close to each other, as proposed by Lengline and Marsan (2009) in the Parkfield section of the San Andreas Fault. On the other hand, the long-term near-repeating earthquakes (Cluster 1 and 2) shows semi-periodic intervals. The slip rate computed from the Cluster 1 is found to be close to the geodetic rate. However, the slip rates estimated from the other clusters are lower than

geodetic rates. It is likely that closely located asperities responsible for each repeating event cluster in the creeping zone slip with different rates. As the whole region containing the asperities should slip with the geodetic rate, the clusters with lower slip rates should be compensated by short-term repeating events or regular seismic events. This might explain why the regular seismic events occur at the same locations as the repeating events. The high seismicity rates in the Marmara Sea may also affect the shapes of the recurrence intervals as well as their magnitudes of the near-repeating events, which has also been discussed in Lengline and Marsan (2009) for the Parkfield case. This may be possible for the distinct asperities in the same fault zones, that are so close to each other but with different sizes. On the other hand, an asperity, that overlaps with another one, will change the recurrence period and also the magnitude in the neighborhood once it is ruptured. This situation may result in shortening the intervals and reducing the magnitudes (Lengline and Marsan, 2009; Chalumeau et al., 2021).

In addition, after a large event, the recurrence intervals and the occurrences of the repeaters may be affected, which is also observed after 2019 Silivri earthquake in the Marmara Sea. In this study, the repeating events were not detected in 2019 at SLVT station, which is a result that should be taken into account. On 26 September 2019, a moderate event, $M_w=5.8$ earthquake has been occurred in the east of the repeaters, in Silivri (Karabulut et al., 2020) (Figure 6.1). A similar situation has been observed in 2011 Tohoku earthquake in subduction zone in Japan. Before this event, there have been many repeating events the areas of creeping, that slipping fast during the interseismic period. After 2011 Tohoku earthquake, the number of earthquakes decreases within the asperities in afterslip area. The same case has also been observed in repeaters after the 2016 Ecuadorian $M_w=7.8$ Earthquake aftershocks with M_6 and $M_{6.2}$ (Chalumeau et al., 2021). It is possible that the 2019 earthquake changed the characteristics of the repeater sequences since no repeaters has been detected in 2019. The changes in the characteristics and the occurrences of the near-repeating events may result from a possible slow-slip or static stress changes around the rupture area of the 2019 Silivri earthquake. The evolution of the near-repeating sequences in terms of temporal and spatial change can be investigated by a further study.

The asperities that produce near-repeating events in the Marmara Sea are also likely to interact with each other, showing a complex heterogenous fault structure. The proximity and the temporal evolution of the repeater activity resulted from different clusters can be seen in Figure 6.2 and 6.3. These sequences are also accompanied by the regular events. These interactions can be ruled by the static stress changes resulted from coseismic slip and postseismic creep, as in the case of San Fransisco and Los Angeles repeating events in Parkfield, California, that resulted from different asperities which are spaced in a 70 km zone (Lui and Lapusta, 2016). These events may be relevant to foreshock sequences or the rupture of an asperity leading to repeaters or a migrating postseismic slip from a nearby repeaters. Basically, this may be an implication that the seismicity and the repeater activity with aftershocks and delayed triggering in environment where the faults at least partially creep.

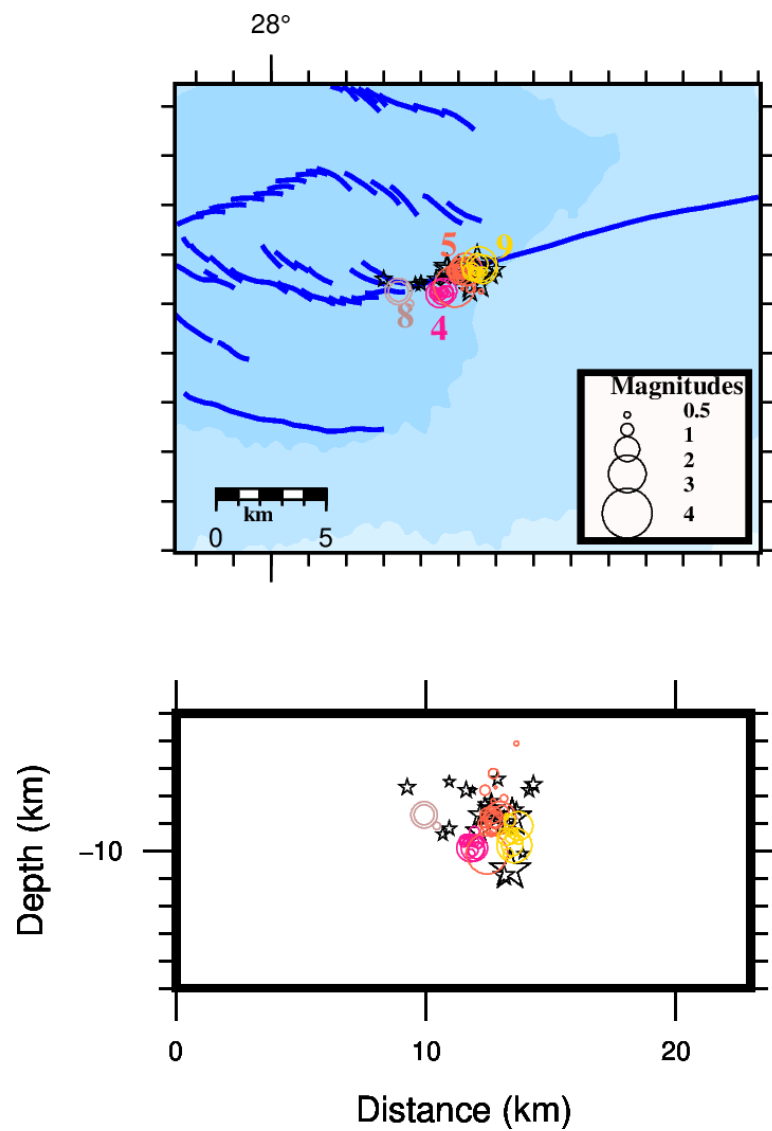


Figure 6.2. The repeater activity between 21.11.2014 and 23.11.2014. Each cluster is shown circles by different color and their cluster numbers are given. Stars denote the regular events occurred in the area. (a) Map view of the locations of the near-repeating clusters. (b) The depth distribution of near-repeater clusters.

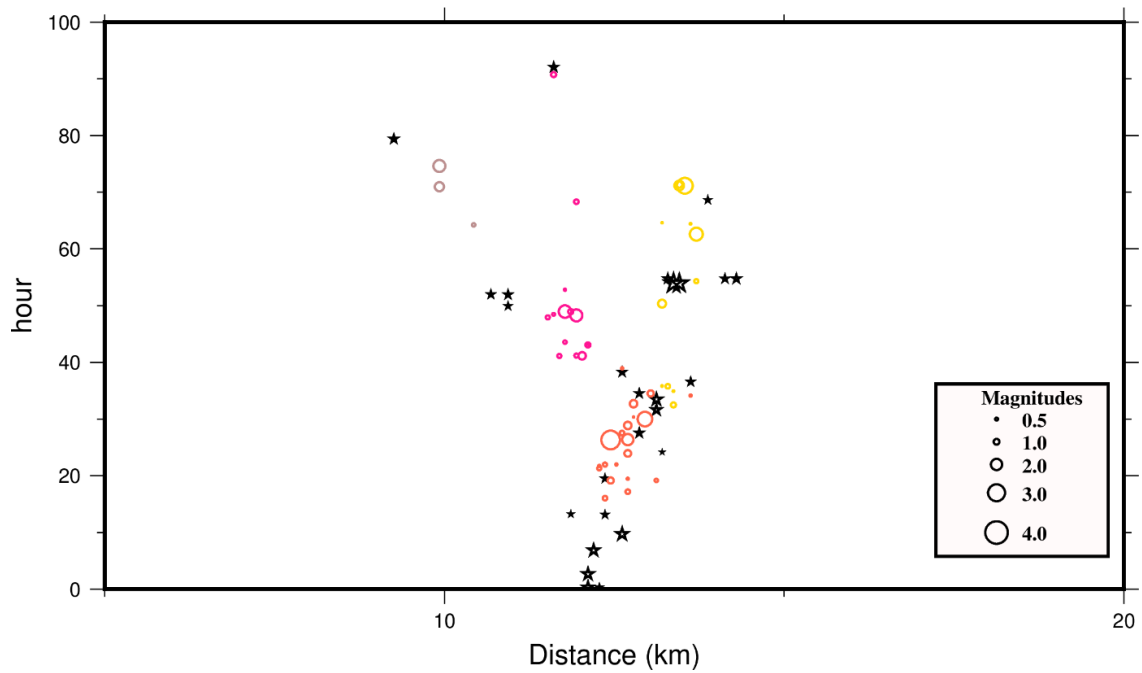


Figure 6.3. The temporal change of the repeater activity between 21.11.2014 and 23.11.2014. Orange, pink, light brown and yellow denote Cluster 5, 4, 8, 9, respectively.

Stars denote the regular events occurred in the area.

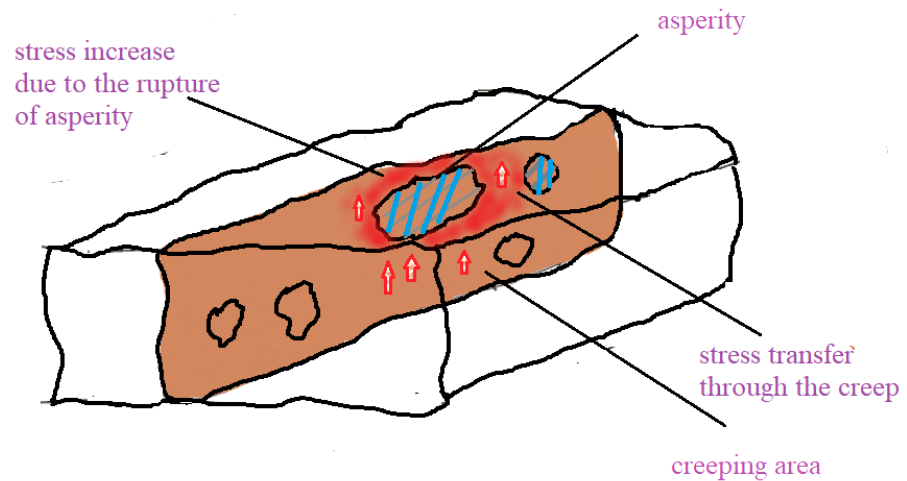


Figure 6.4. Schematic demonstration of the interaction of the asperities in a creeping fault zone. The ruptured asperities in interaction are denoted by blue strips. The arrows represent creeping motions. The red area shows stress increase due to the rupture of the asperity.

In Figure 6.4, a schematic depiction can be seen to explain a possible repeating event interaction scenario that may be valid for the creeping area in the Central Basin. The stress is transferred through the creep, leading to temporal clustering. The seismicity and the repeater activity are controlled by the interaction between the asperities, which will affect the earthquake occurrence in short-time scales.

7. CONCLUSIONS

The objective of this thesis has been to contribute to the knowledge on the behavior of the fault segments in the Sea of Marmara. The interpretation for the regions with low seismicity as locked and the regions with high seismicity rates as creeping portions of the fault zone has been used to show heterogeneous fault structure of the MMF (Yılmaz et al., 2022, Schmittbuhl et al., 2015, Yamamoto et al., 2017, 2020). However, the geometry of the active fault segments and the depth distribution of the seismogenic zone of the Main Marmara Fault has been difficult to accurately determine due to limited near field observations to the fault.

In this study, high precision locations of the microseismicity are obtained beneath the Marmara Sea across the Main Marmara fault using the data from the OBS between the time period starting from September 2014 to April 2016. The results indicate that the diffuse seismic activity rate in Tekirdağ Basin from 7-8 km to 18 km, and especially in Central Basin with a depth range of about 12 km from 3 km to 15 km (Figure 3.10). The abundance of the earthquakes in this fault segment is interpreted to be creeping zone consistent with the studies on GPS observations (Ergintav et al., 2014; Özbey et al., 2021). The seismic slip rate estimated by Schmittbuhl et al. (2016) also showed a high value (0.35 mm/y), which has been interpreted as “deep creep” behavior following the argument of Wdonwski (2009) suggesting that the high level of seismicity signs the creep. The micro events in the Kumburgaz region are starting at 5 km and extends to 19 km. The west of the Çınarcık Basin demonstrates a seismic activity between 3 and 18 km (Figure 3.10). The decreasing seismicity rate in Kumburgaz Basin is considered to be the indication of a locked fault.

A detailed search for the repeating events has been performed from 2008 to 2021 by template matching method using the continuous data from SLVM and SLVT stations. In this part, the detected earthquakes that are closely spaced or partially overlapped, having highly correlated waveforms, were attributed to the near-repeating earthquakes. As a result, 9 near-repeating sequences have been identified in the Central Basin. The improved locations of the repeating earthquakes and focal mechanisms solutions with accurate

seismicity distribution, points out heterogeneities of the fault zone with asperities loaded by the surrounding aseismic slip. The focal mechanisms of the near-repeating clusters conform with the strike-slip mechanism on the MMF, except the near-repeater Cluster 5 which shows normal faulting. The analyses from the near-repeating earthquakes allowed to estimate slip rate for each repeating event cluster. The estimated cumulative slip of each repeating event cluster shows variability relative to the tectonic rate. It appears that the slip rates from some of the repeaters are close to the geodetic rate while others have relatively lower rates. The clusters with lower slip rates are accommodated with short term multiplets or regular microseismic activity. The repeating earthquake activity has decelerated from the end of 2018. It appears that a change on the stress state at the transition from Central Basin to Kumburgaz occurred before-during-after 2019 which Mw=5.8 Silivri earthquake happened. It is unclear if this behavior is temporary or new generation of repeating events will be created.

REFERENCES

- Abercrombie, R., 1995, "Earthquake Source Scaling Relationships from -1 to 5 ML Using Seismograms Recorded at 2.5-Km Depth", *Journal of Geophysical Research*, 100(B12), 24,015–24,036.
- Allmann B.P., P. M. Shearer, 2007 "Spatial and Temporal Stress Drop Variations in Small Earthquakes Near Parkfield, California", *Journal of Geophysical Research*, 112, B04305.
- Allmann, B. P, and P. M. Shearer, 2009, "Global Variations of Stress Drop for Moderate to Large Earthquakes", *Journal of Geophysical Research*, 114, B01310.
- Ambraseys, N.N., and C.F. Finkel, 1987, "The Saros-Marmara Earthquake of 9 August 1912", *Earthquake Engineering and Structural Dynamics*, 15, 189–211.
- Ambraseys N.N., 1988, "Engineering Seismology", *Earthquake Engineering and Structural Dynamics*, 17,1–105.
- Ambraseys N.N., 1989, "Temporary Seismic Quiescence: SE Turkey", *Geophysical Journal International*, 96, 311-331.
- Ambraseys NN and C.F. Finkel, 1991, "Long-term seismicity of Istanbul and of the Marmara Sea region", *Terra Nova*, 3(5):527–539.
- Ambraseys, N.N., and C.F. Finkel, 1995, *The Seismicity of Turkey and Adjacent areas. A Historical Review, 1500-1800*, Eren Yayıncılık, Istanbul.
- Ambraseys, N.N., J.A. Jackson, 1998, "Faulting Associated with Historical and Recent Earthquakes in the Eastern Mediterranean Region." *Geophysical Journal International*, 133, 390-406.

- Ambraseys, N.N. and J.A. Jackson, 2000, "Seismicity of Sea of Marmara (Turkey) since 1500", *Geophysical Journal International*, 141, F1-F6.
- Ambraseys, N.N, 2001, "The Earthquake of 1509 in the Sea of Marmara, Turkey", *Bulletin of the Seismological Society of America*, 91(6), 1397-1416.
- Ambraseys, N.N., 2002, "The Seismic Activity of the Marmara Sea Region over the Last 2000 years, *Bulletin of the Seismological Society of America*, 92, 1–18.
- Ambraseys, N.N, 2009, *Earthquakes in the Mediterranean and Middle East: A Multidisciplinary Study of Seismicity up to 1900*, Cambridge University Press, Imperial College, London.
- Armijo, R., B. Meyer, S. Navarro, G. King, A. Barka, 2002, "Asymmetric Slip Partitioning in the Sea of Marmara Pull-Apart: A Clue to Propagation Processes of the North Anatolian Fault", *Terra Nova*, 14, 80–86.
- Armijo, R., N. Pondard, B. Meyer, G. Uçarkuş, B.M.d. Lepinay, J. Malavieille, S. Dominguez, M. A. Gustcher, S. Schmidt, C. Beck, N. Çağatay, Z. Çakır, C. İmren, K. Eriş, B. Natalin, S. Özalaybey, L. Tolun, I. Lefevre, L. Seeber, L. Gasperini, C. Rangin, O. Emre and K. Sarıkavak, 2005, " Submarine Fault Scarps in the Sea of Marmara Pull-Apart (North Anatolian Fault): Implications for Seismic Hazard in İstanbul", *Geochemistry Geophysics Geosystems*, V.6, Q06009.
- Ariyoshi K, T. Matsuzawa, J.P. Puerto, R. Nakata, T. Hori, Y. Kaneda, A. Hasegawa, 2012, "Migration Process of very Low-Frequency Events Based on A Chain-Reaction Model and Its Application to the Detection of Preseismic Slip for Megathrust Earthquakes", *Earth Planets Space*, 64(8), 693–702.
- Anderlini, L., E. Serpelloni, and M. E. Belardinelli, 2016, "Creep and Locking of A Low-Angle Normal Fault: Insights from the Altotiberina Fault in the Northern Apennines (Italy)", *Geophysical Research Letters*, 43, 4321–4329.

- Aksoy, M.E., M. Meghraoui, M. Vallée, Z. Çakır, 2010, "Rupture Characteristics of the A.D. 1912 Mürefte (Ganos) Earthquake Segment of the North Anatolian Fault (western Turkey)", *Geological Society of America*, Vol.38, pp.37-57.
- Akyüz, H.S., R. Hartleb, A. Barka, E. Altunel, G. Sunal, B. Meyer and R. Armijo, 2002, "Surface Rupture and Slip Distribution of the 12 November 1999 Düzce Earthquake (M 7.1), North Anatolian Fault, Bolu, Turkey", *Bulletin of the Seismological Society of America*, 92, 61–66.
- Aktuğ, B., A. Kılıçoğlu, O. Lenk and M.A. Gürdal, 2009, "Establishment of Regional Reference Frames for Quantifying Active Deformation Areas in Anatolia", *Studia Geophysica et Geodaetica*, 53, 169-183.
- Allen, R. 1982, "Automatic Phase Pickers: Their Present Use and Future Prospects.", *Bull. Seismol. Soc. Am.*, 72, 225–242.
- Altınok, Y., B. Alpar, N. Ozer, and H. Aykurt, 2011, Revision of The Tsunami Catalogue Affecting Turkish Coasts and Surrounding Regions, *Natural Hazards and Earth System Science*, 11, 273–291.
- Barka A.A., K. Kadinsky-Cade, 1988, "Strike-slip fault geometry in Turkey and its influence on earthquake activity", *Tectonics*, 7, 663–684.
- Bariş, S., A. Ito, S.B. Üçer, Y. Honkura, N. Kafadar, T. Komut, A.M. Işıkara, 2002, "Microearthquake Activity Before the Izmit Earthquake In The Eastern Marmara Region, Turkey (1 January 1993–17August 1999)", *Bulletin of the Seismological Society of America*, 92, 394–405.
- Bakun, W.H., and A.G. Lindh, 1985, "The Parkfield, California Earthquake Prediction Experiment", *Science*, 229, 619-624.

- Bakun, W.H., and T.V. McEvilly, 1979, “Are Foreshocks Distinctive? Evidence from the 1966 Parkfield and the 1975 Oroville, California Sequences”, *Bulletin of the Seismological Society of America*, 69, 1027-1038.
- Bakun, W. H., G. C. King, and R. S. Cockerham ,1986, *Seismic Slip, Aseismic Slip, And The Mechanics Of Repeating Earthquakes On The Calaveras Fault, California*, In *Earthquake Source Mechanics*, edited by S. Das, J. Boatwright, and C. H. Scholz, American Geophysical Union, 195–207, Washington, D. C.
- Batsi, E., A. Lomax, J.B.Tary, F. Klingelhoefer, V. Riboulot, S. Murphy, S. Monna, N. Özel, D. Kalafat, H. Saritas, G. Cifçi, N. Çagatay, L. Gasperini, L. Géli, 2018, “An Alternative View of the Microseismicity along the Western Main Marmara Fault”, *Bulletin of the Seismological Society of America*, 108 (5A).
- Barka, A., 1996, “Slip Distribution along the North Anatolian Fault Associated with the Large Earthquakes of the Period 1939 to 1967”, *Bulletin of the Seismological Society of America*, 86,1238–1254.
- Barka, A., 1999, “The 17 August, 1999, Izmit Earthquake”, *Science*, 285, 1858–1859.
- Bayrakci, G., M. Laigle, A. Bécel, A. Hirn, T. Taymaz, S. Yolsal-Çevikbilen and team, SEISMARMARA, 2013, “3-D Sediment-Basement Tomography of the Northern Marmara Trough By A Dense Obs Network at the Nodes of A Grid of Controlled Source Profiles along the North Anatolian Fault”, *Geophysical Journal International*, 194, 1335–1357.
- Başarır Baştürk, N., N.M. Özel, Y. Altınok, and T.Y. Duman, 2017, *Türkiye ve Yakın Çevresi için Geliştirilmiş Tarihsel Dönem (MÖ 2000 - MS 1900) Deprem Katalogu*, MTA Özel Yayınlar Serisi, 35, 249 s. Ankara.
- Başarır Baştürk, N., N.M. Özel, Ö. Necmioğlu, 2016b, “A Compilation of the Historical Earthquakes Database for Marmara Region from 2000 B.C. to 1900 A.D. in frame

of Marsite and Mardim Projects”, *European Geoscience Union, Austria*,17-22, April, 2016, Vienna.

Başarır Baştürk, N., N.M. Özel, M. Caciagli, M.,2016a, “Seismic parameters re-determined from historical seismograms of 1935-Erdek–Marmara Island and 1963-Çınarcık Earthquakes”, *Earth Planet and Space*, 68, 158.

Başarır N., 2011, *Reassessment of the Seismic Parameters from Historical Seismograms of 1912 Mürefte-Şarköy, 1935 Erdek-Marmara Island and 1963 Çınarcık Earthquakes*, M.S. Thesis, Boğaziçi University.

Becel, A., M. Laigle, B., De Voogd, A. Hirn, T. Taymaz, S. Yolsal-Cevikbilen and H. Shimamura, 2010, “North Marmara Trough Architecture of Basin Infill, Basement and Faults, from Psdm Reflection and Obs Refraction Seismics”, *Tectonophysics*, 490, 1–14

Behrmann, J., J. Yang, and the CoZone Working Group, 2006, *Convergent Plate Boundaries and Collison Zones*, Continental Scientific Drilling, 289-335, Kiel, Germany.

Berberian M. and S. Arshadi, 1976, “On the Evidence of the Youngest Activity of the North Tabriz Fault and the Seismicity of Tabriz City”. *Geological Survey of Iran*, 39, 397-418.

Beeler, N.M., D.L. Lockner, S.H. Hickman, 2001, “A Simple Stick-Slip and Creep-Slip Model for Repeating Earthquakes and Its Implication for Microearthquakes at Parkfield”, *Bulletin of the Seismological Society of America*, 91, 1797–1804.

Bentz, S., 2020, *Earthquake Nucleation Processes Across Different Scales and Settings*, Phd Dissertation, Berlin,

- Blanpied, M. L., D. A. Lockner and J. D. Byerlee, 1995, “Frictional Slip of Granite at Hydrothermal Conditions”, *Journal of Geophysical Research*, 100(B7), 13,045–13,064.
- Bouchon, M., H. Karabulut, M. Aktar, S. Ozalaybey, J. Schmittbuhl, and M. Bouin, 2011, “Extended Nucleation of the 1999 *M_w* 7.6 Izmit Earthquake”, *Science*, 331, 877–880.
- Bouchon, M., V. Durand, D. Marsan, H. Karabulut, and J. Schmittbuhl, 2013, “The Long Precursory Phase of Most Large Interplate Earthquakes”, *Nature Geoscience*, 6(4), 299–302.
- Boore, D. M. and J. Boatwright, 1984, “Average Body-Wave Radiation Coefficients”, *Bulletin of the Seismological Society of America*, 74, 5, 1615-1621.
- Bonhoff, M., F. Bulut, G. Dresen, P.E. Mallin, T. Eken, M.Aktar, 2013, “An earthquake gap south of İstanbul”, *Nature Communication*, 4, 1999.
- Bohnhoff, M., C. Wollin, D. Domigall, L. Küperkoch, P. Martínez-Garzón, G. Kwiatek, G.Dresen, P.E. Malin., 2017, “Repeating Marmara Sea Earthquakes: Indication for Fault Creep”, *Geophysical Journal International*, 210, 1, 332-339.
- Bourouis, S., and P. Bernard ,2007, “Evidence for Coupled Seismic and Aseismic Fault Slip During Water Injection in the Geothermal Site Of Soultz (France), and Implications for Seismogenic Transients”, *Geophysical Journal International*, 169(2), 723–732.
- Brune, J., 1970, “Tectonic Stress and the Spectra of Seismic Shear Waves from Earthquakes”, *Journal of Geophysical Research*, 75, 4997-5009.
- Can, B., 2019, *Source Properties of Micro-earthquakes in Eastern Marmara and their Connection to the Structure of the Çınarcık Basin*, Phd Dissertation, Boğaziçi University, İstanbul.

- Chalumeau, C., H. Agurto-Detzel, L. Barros, P. Charvis, A. Galve, 2021, “Repeating Earthquakes at the Edge of the Afterslip of the 2016 Ecuadorian MW 7.8 Pedernales Earthquake”, *Journal of Geophysical Research: Solid Earth*, 126 (5).
- Çakır, Z., J-B. De Chabalier, R. Armijo, B. Meyer, A. Barka, and G. Peltzer, 2003, “Coseismic and early postseismic slip Associated with the 1999 Izmit Earthquake (Turkey), From Sar Interferometry and Tectonic Field Observations”, *Geophysical Journal International*, 155, 93-110.
- Çakır, Z., S. Ergintay, H. Ozener, U. Dogan, A. M. Akoglu, M. Meghraoui and R. Reilinger, 2012, “Onset of Aseismic Creep on Major Strike-Slip Faults”, *Geology*, 40, 1115–1118.
- Chen K.H., M.N. Robert and R.J. Rau, 2007, “Towards A Universal Rule on The Recurrence Interval Scaling of Repeating Earthquakes?”, *Geophysical Research Letters*, 34, L16308.
- Chen, K. H., R.M. Nadeau, and R.J. Rau, 2008, “Characteristic Repeating Earthquakes in An Arc-Continent Collision Boundary Zone: The Chihshang Fault of Eastern Taiwan”, *Earth and Planetary Science Letters*, 276(3–4), 262–272.
- Chen, T, N. and Lapusta, 2009, “Scaling of Small Repeating Earthquakes Explained by Interaction of Seismic and Aseismic Slip in A Rate and State Fault Model”, *Journal of Geophysical Research*, 11, B01311.
- Chen, K. H., and R. Bürgmann ,2017, “Creeping Faults: Good News, Bad News?”, *Reviews of Geophysics*, 55, 282–286.
- Chen, K. H., R. Bürgmann and R.. M. Nadeau, 2013, “Do Earthquakes Talk to Each Other? Triggering and Interaction of Repeating Sequences at Parkfield”, *Journal of Geophysical Research*, 118:165–182.

- Cole, A.T. and W.L. Ellsworth, 1995, “Earthquake Clustering and the Long-Term Evolution of Seismicity Near Parkfield, California”, *Seismological Research Letters*, 66 (2), 28.
- Dieterich, J. H., 1978, “Time-Dependent Friction and The Mechanics of Stick-Slip”, *Pure and Applied Geophysics*, 116(4–5), 790–806.
- Duverger, C., S., Lambotte, P. Bernard, H. Lyon-Caen, A. Deschamps and A. Necessian, 2018, “Dynamics of Microseismicity and Its Relationship with the Active Structures in the Western Corinth Rift (Greece)”. *Geophysical Journal International*, 215(1), 196–221.
- Duman T.Y., T. Çan , Ö. Emre, F.T. Kadiroğlu , N. Başarır Baştürk, T. Kılıç , S. Arslan, S. Özalp , R.F. Kartal , D. Kalafat, F. Karakaya, T. Eroğlu Azak , N.M. Özel , S. Ergintav, S. Akkar , Y. Altınok, S. Tekin, A. Cingöz, A.İ. Kurt, 2016, “Seismotectonic Database of Turkey”, *Bulletin of Earthquake Engineering*, 16, 3277-3316.
- Duman T.Y., T. Çan, Ö. Emre, F.T. Kadiroğlu , N. Başarır Baştürk, T. Kılıç , S. Arslan, S. Özalp , R.F. Kartal , D. Kalafat, F. Karakaya, T. Eroğlu Azak, N.M. Özel , S. Ergintav, S. Akkar , Y. Altınok, S. Tekin, A. Cingöz, A.İ. Kurt, 2016, *Türkiye Sismotektonik Haritası*, (Ed.T.Y. Duman), Maden Tetkik ve Arama Genel Müdürlüğü, Özel Yayınlar Serisi, 34, 11-56. Ankara. Türkiye.
- Dominguez, L. A., T. Taira and M.A. Santoyo, 2016, “Spatiotemporal Variations of Characteristic Repeating Earthquake Sequences along the Middle America Trench in Mexico”, *Journal of Geophysical Research: Solid Earth*, 121(12), 8855–8870.
- Dieterich, J. H., 1978, “Time-Dependent Friction and the Mechanics of Stick-Slip”, *Pure and Applied Geophysics*, 116(4–5), 790–806.
- Eaton, D. W., M. Van der Baan, B. Birkelo and J.-B. Tary, 2014, “Scaling Relations and Spectral Characteristics of Tensile Microseisms: Evidence for Opening/Closing

- Cracks during Hydraulic Fracturing”, *Geophysical Journal International*, 196, 1844-1857.
- Eshelby, J.D., 1957, “The Determination of the Elastic Field of an Ellipsoidal Inclusion and Related Problems”, *Proceedings of the Royal Society A*, 241, 376-396.
- Ergintav, S., R. Reilinger, R. Çakmak, M. Floyd, Z. Cakir, U. Doğan, R. King, S. McClusky and H. Ozener ,2014, “Istanbul’s Earthquake Hot Spots: Geodetic Constraints on Strain Accumulation along Faults in the Marmara Seismic Gap”, *Geophysical Research Letters*, 41, 5783–5788.
- Ergin, K., U. Güçlü, Z. Uz, 1967, *Türkiye ve Civarinin Deprem Kataloğu (M.S. 11-1964)*, Arz Fiziği Enstitüsü Yayınları, 24, 169, İTÜ, Maden Fakültesi, İstanbul.
- Ergin K, U., Güçlü, G. Aksoy, 1971, *Türkiye ve Civarinin Deprem Kataloğu (1965-1970)*, Arz Fiziği Enstitüsü Yayınları, 24, 169, İTÜ, Maden Fakültesi, İstanbul.
- Emre, O., T. Duman, S. Özalp, H. Elmac, S. Olgun and F. Saroğlu, 2013, *1/1.125.000 Olcekli Turkiye Diri Fay Haritasi*, Maden Tetkik ve Arama Genel Müdürlüğü Özel Yayınlar Serisi, Ankara, Türkiye.
- Ellsworth, W.L., 1995, *Characteristic Earthquake and Long-Term Earthquake Forecasts: Implications of Central California Seismicity*, In: Cheng FY, Sheu MS (eds) *Urban Disaster Mitigation: The Role of Science and Technology*, Elsevier, Oxford.
- Filikçi B., K.K. Eriş, N. Çağatay, A. Sabuncu, A. Polonia, 2017, Late Glacial to Holocene Water Level and Climate Changes in the Gulf of Gemlik, Sea of Marmara: Evidence From Multi-Proxy Data, *Geo-marine Letters*, 37, 501-513.
- Funning, G. J., R. Burgmann, A. Ferretti, F. Novali, and A. Fumagalli, 2007, “Creep on The Rodgers Creek Fault, Northern San Francisco Bay Area From A 10 Year Ps-Insar Dataset”, *Geophysical Research Letters*, 34, L19306.

- Gao, D., H. Kao, B. Wang, 2021, “Misconception of Waveform Similarity in the Identification of Repeating Earthquakes”, *Geophysical Research Letters*, 48, 13, e2021GL092815.
- Geller R., and C. Mueller, 1980, “Four Similar Earthquakes in Central California”, *Geophysical Research Letters*, 7,821–824.
- Güçlü, U., G. Altınbaş, H. Eyidoğan H., 1986, *A Catalogue of Turkey and Surrounding Area (1971-1975)*, Technical Report, İstanbul Technical University, Faculty of Mines no 30, İstanbul.
- Godano, M., P. Bernard and P. Dublanchet, 2015, “Bayesian Inversion of Seismic Spectral Ratio for Source Scaling. Application to a Persistent Multiplet in the Western Corinth Rift”, *Journal of Geophysical Research*, 120, no. 11, 7683–7712.
- Han, L., J. Wong and J. C. Bancroft, 2009, Time Picking and Random Noise Reduction on Microseismic Data, *CREWES Research Report*, 21.
- Hanks T.C., H. Kanamori, 1979, “A Moment Magnitude Scale”, *Journal of Geophysical Research*, 84, 2348–2350.
- Harris, R. A., 2017, “Large Earthquakes and Creeping Faults”, *Reviews Geophysics*, 55, 169–198.
- Hergert, T., O. Heidbach, A. Bécel and M. Laigle, M., 2011, “Geomechanical Model of the Marmara Sea Region-I. 3-D Contemporary Kinematics”, *Geophysical Journal International*, 185(3), 1073–1089.
- Hilley, G. E., R. Bürgmann, A. Ferretti, F. Novali, and F. Rocca, 2004, “Dynamics of Slow-moving Landslides from Permanent Scatterer Analysis”, *Science*, 304, 1952–1955.

- Hubert-Ferrari A., A. Barka, E. Jacques, S. Nalbant, B. Meyer, R. Armijo, P. Tapponnier, G. King, 2000, “Seismic Hazard in the Marmara Sea Region Following the 17 August 1999 İzmit Earthquake”, *Nature*, 404, 269–273.
- Lange, D., H. Kopp, 2019, “Seafloor Observation in the Sea of Marmara: Acoustic Direct Path-Ranging, Pressure, And Temperature Data”, *Pangaea*, .
- Lin, F., 2018, *Digital Signal Processing for Micro-Seismic Event Detection on Embedded Platforms*, MS Thesis, Computer Engineering and Networks Laboratory Swiss Federal Institute of Technology (ETH) Zurich.
- Lui, S. K. Y. and N. Lapusta, 2016, “Repeating Microearthquake Sequences Interact Predominantly Through Postseismic slip”, *Nature communications*, 7, 13020.
- Hancilar, U. 2012, “Identification of Elements at Risk for A Credible Tsunami Event for Istanbul”, *Natural Hazards and Earth System Science*, 12(107–119).
- Hreinsdóttir, S. and R. A. Bennett, 2009, “Active Aseismic Creep on the Alto Tiberina Low-Angle Normal Fault, Italy”, *Geology*, 27(8), 683–686.
- Hayward T.W., M.G.Bostock, 2017, “Slip Behavior of the Queen Charlotte Plate Boundary Before and After The 2012, Mw 7.8 Haida Gwaii Earthquake: Evidence from Repeating Earthquakes”, *Journal of Geophysical Research: Solid Earth*, 122, 8990– 9011.
- Ito, A., B. Ücer, S. Barıs , A. Nakamura, Y. Honkura, T. Kono, S. Hori, A. Hasegawa, R. Pektas, and A. M. Işıkara, 2002, “Aftershock Activity of the 1999, İzmit, Turkey, Earthquake Revealed from Microearthquake Observations”, *Bulletin of Seismological Society of America*, 92, 418–427.
- Guidoboni. E., A. Comastri and G. Triana, 1994, “*Catalogue of Ancient Earthquakes in the Mediterranean Area up to the 10th Century*”, Istituto Nazionale di Geofisica, p. 504, Rome.

- Guidoboni, E. and A. Comastri, 2005, *Catalogue of Earthquakes and Tsunamis in the Mediterranean Area from the 11th to the 15th Century*, INGV-SGA. Bologna, 2005.
- Hamaguchi, H. and A. Hasegawa, 1975, “Recurrent Occurrence of The Earthquakes with Similar Wave Forms and Its Related Problems”, *Zisin*, 28,153–169.
- Igarashi, T., T. Matsuzawa, N. Umino, A. Hasegawa, 2001, “Spatial Distribution of Focal Mechanisms for Interplate and Intraplate Earthquakes Associated with the Subducting Pacific Plate Beneath the Northeastern Japan Arc: A Triple-Plated Deep Seismic Zone”, *Journal of Geophysical Research* 106, 2177–2191.
- Igarashi, T., T. Matsuzawa, A. Hasegawa, 2003, “Repeating Earthquakes and Interplate Aseismic Slip in the Northeastern Japan Subduction Zone”, *Journal of Geophysical Research*, 108.
- Igarashi, T., 2010, “Spatial Changes of Inter-Plate Coupling Inferred from Sequences of Small Repeating Earthquakes in Japan”, *Geophysical Research Letters*, 37, L20304.
- Jolivet, R., C. Lasserre, M.-P. Doin, G. Peltzer, J.-P. Avouac, J. Sun and R. Dailu, 2013, “Spatio-temporal Evolution of Aseismic Slip Along the Haiyuan Fault, China: Implications for Fault Frictional Properties”, *Earth and Planetary Science Letters*.
- Karabulut, H., J. Schmittbuhl, S. Özalaybey, O. Lengliné, A. M Kömeç, V. Durand, M. Bouchon, G. Daniel, M.P. Bouin, 2011, “Evolution of the Seismicity in the Eastern Marmara Sea A Decade Before and After The 17 August 1999 Izmit Earthquake”, *Tectonophysics*, 510, 17–27.
- Karabulut, H., S.E. Guvercin, F. Eskikoy, A. O. Konca and S. Ergintav, 2020, “The Moderate Size 2019 September Mw 5.8 Silivri Earthquake Unveils the Complexity

- of the Main Marmara Fault Shear Zone”, *Geophysical Journal International*, 2020, 224, 377–388.
- Kato, A., K. Obara, T. Igarashi, H. Tsuruoka, S. Nakagawa, and N. Hirata, 2012, “Propagation of Slow Slip Leading up to the 2011 M_w 9.0 Tohoku-Oki Earthquake”, *Science*, 335(6069), 705–708.
- Kato, A., and S. Nakagawa, 2014, “Multiple Slow-Slip Events During A Foreshock Sequence of the 2014 Iquique, Chile M_w 8.1 Earthquake”, *Geophysical Research Letters*, 41, 5420–5427.
- Keilis-Borok, V. I., 1960, “Investigation of The Mechanism of Earthquakes (English translation)”, *Soviet Research in Geophysics*, 4,29.
- Klein, E., Z. Duputel, F. Masson, H. Yavasoglu and P. Agram, 2017, “Aseismic Slip and Seismogenic Coupling in the Marmara Sea: What Can We Learn from Onland Geodesy?”, *Geophysical Research Letters* 44, 2017GL072777.
- Kissling, E., W. Ellsworth, D. Eberhart-Phillips and U. Kradolfer, 1994, “Initial Reference Models in Local Earthquake Tomography”, *Journal of Geophysical Research*, 99, 19,635–19,646.
- Konca, A. Ö., H. Karabulut, S.E. Güvercin, F. Eskiköy, S. Özarpacı, A. Özdemir et al., 2021, “From Interseismic Deformation with Near-Repeating Earthquakes to Co-Seismic Rupture: A Unified View of the 2020 M_w 6.8 Sivrice (Elaziğ) Eastern Turkey Earthquake”. *Journal of Geophysical Research: Solid Earth*, 126, e2021JB021830.
- Korkusuz Öztürk, Y., N.M. Özel, A.D. Özbakir, 2015, “States of Local Stresses in the Sea of Marmara Through the Analysis of Large Numbers of Small Earthquakes”, *Tectonophysics*, 665, 37-57.

- Korkusuz Öztürk, Y., 2019, *Dynamic Earthquake Rupture Simulations in the Sea of Marmara*, Phd Dissertation, Boğaziçi University, İstanbul.
- Laigle, M., A. Becel, B. De Voogd, A. Hirn, T. Taymaz et al., 2008, “A First Deep Seismic Survey in the Sea of Marmara: Deep Basins and Whole Crust Architecture and Evolution”, *Earth Planetary Science Letters*, 270, 168-179.
- Langbein, J. J., J. R. Murray, and H. A. Snyder, 2006, “Coseismic and Initial Postseismic Deformation from the 2004 Parkfield, California, Earthquake, Observed by Global Positioning System, Electronic Distance Meter, Creepmeters, and Borehole Strainmeters”, *Bulletin of Seismological Society of America*, 96(4B), S304–S320.
- Le Pichon, X., A.M.C. Sengör, E. Demirbag, C. Rangin, C. Imren, R. Armijo, N. Gorur, N. Cagatay, B.M. De Lepinay, B. Meyer, R. Saatçılar, B. Tok, 2001, “The Active Main Marmara Fault”, *Earth and Planetary Sciences Letters*, 192(4), 595–616.
- Le Pichon, X., N. Chamot-Rooke, C. Rangin, A.M.C. Sengör, 2003, “The North Anatolian Fault in the Sea of Marmara”, *Journal of Geophysical Research: Solid Earth*, 108, B4.
- Lengline, O. and D. Marsan, 2009, “Inferring the Coseismic and Postseismic Stress Changes Caused by the 2004 $M_w = 6$ Parkfield Earthquake from Variations of Recurrence Times of Microearthquakes”, *Journal of Geophysical Research*, 114, B10303.
- Lengline, O., L. Lamourette, L. Vivin, N. Cuenot and J. Schmittbuhl, 2014, “Fluid-induced Earthquakes with Variable Stress Drop”, *Journal of Geophysical Research: Solid Earth*, 119, 8900–8913.
- Lienert, B. R. E., E. Berg and L.N. Frazer, 1986, “Hypocenter: An Earthquake Location Method Using Centered, Scaled, and Adaptively Least Squares”, *Bulletin of Seismological Society of America*, 76:771–783.

- Li, C., Z. Peng, D. Yao, H. Guo, Z. Zhan, and H. Zhang, 2018, “Abundant Aftershock Sequence of the 2015 Mw 7.5 Hindu Kush Intermediate-Depth Earthquake”, *Geophysical Journal International*, 213(2), 1121–1134.
- Lienert, B. R. E. and J. Havskov, 1995, “A Computer Program for Locating Earthquakes Both Locally and Globally”, *Seismological Research Letters*, 66:26–36.
- Madariaga, R., 1976, “Dynamics of An Expanding Circular Fault”, *Bulletin of Seismological Society of America*, 66(3), 639–666.
- Meade, B. J., B. H. Hager, S. C. McClusky, R. E. Reilinger, S. Ergintav, L. Onur, A. Barka, and H. Özener, 2002, “Estimates of Seismic Potential in the Marmara Sea Region from Block Models of Secular Deformation Constrained by Global Positioning System Measurements”, *Bulletin of the Seismological Society of America*, 92, 208–215.
- Meng, L., H. Huang, R. Burgmann, J. P. Ampuero, and A. Strader, 2015, “Dual Megathrust Slip Behaviors of the 2014 Iquique Earthquake Sequence”, *Earth and Planetary Sciences Letters*, 411, 177–187.
- Mihailović, J., 1927, *Grandes Le Catastrophes Seismiques la me de Marmara*, Institute Seismologique de l'Universite de Belgrad, 1927.
- McEvelly T.V., Casaday K.B., 1967, “The Earthquake Sequence of September, 1965 Near Antioch, California”, *Bulletin of the Seismological Society of America*, 57, 113–124.
- McClusky, S., S. Balassanian, A. Barka, C. Demir, S. Ergintav, I. Georgiev, O. Gurkan, M. Hamburger, K. Hurst, H. Kahle, K. Kastens, G. Kekelidze, R. King, V. Kotzev, O. Lenk, S. Mahmoud, A. Mishin, M. Nadriya, A. Ouzounis, D. Paradissis, Y. Peter, M. Prilepin, R. Reilinger, I. Şanlı, H. Seeger, A. Tealeb, M.N. Toksöz, G. Veis, 2000, “Global Positioning System Constraints on Plate Kinematics and

- Dynamics in the Eastern Mediterranean and Caucasus”, *Journal of Geophysical Research*, 105, 5695–5719.
- Moore, D. E., and D. A. Lockner, 2013, “Chemical Controls on Fault Behavior: Weakening of Serpentine Sheared Against Quartz-Bearing Rocks and Its Significance for Fault Creep in the San Andreas System”, *Journal of Geophysical Research: Solid Earth*, 118, 1–13.
- Moore, D. E. and M. J. Rymer, 2007, “Talc-bearing Serpentine and the Creeping Section of the San Andreas Fault”, *Nature*, 448, 795–797.
- Murru, M., A. Akinci, G. Falcone, S. Pucci, R. Console and T. Parsons, $M \geq 7$ Earthquake Rupture Forecast and Time-Dependent Probability for the Sea of Marmara Region, Turkey, *Journal of Geophysical Research: Solid Earth*, 121, 2679–2707, 2016.
- Nadeau R.M., T.V. McEvelly, 2004, “Periodic Pulsing of Characteristic Microearthquakes on the San Andreas Fault”, *Science*, 303, 220–222.
- Nadeau, R., M. Antolik, P. A. Johnson, W. Foxall and T. V. McEvelly, 1994, “Seismological Studies at Parkfield III: Microearthquake Clusters in the Study of Fault-Zone Dynamics”, *Bulletin of the Seismological Society of America*, 84, 247–263.
- Nadeau, R., W. Foxall and T. McEvelly, 1995, “Clustering and Periodic Recurrence of Microearthquakes on the San Andreas Fault at Parkfield”, California, *Science*, 267(5197), 503–507.
- Nadeau, R. M., and L. R. Johnson, 1998, Seismological Studies at Parkfield VI: Moment Release Rates and Estimates of Source Parameters for Small Repeating Earthquakes, *Bulletin of the Seismological Society of America*, 88, 790 – 814.
- Nadeau RM, T.V. McEvelly, 1999, “Fault Slip Rates at Depth from Recurrence Intervals of Repeating Microearthquakes”, *Science*, 285, 718–721.

- Omori, F., 1905, “Horizontal Pendulum Observations of Earthquakes in Tokyo: Similarity of the Seismic Motion Originating at Neighbouring Centres”, *Publication of the Earthquake Investigation Committee in Foreign Language*, 21, 9–102.
- Oglesby, D.D., P.M. Mai, K. Atakan, S. Pucci, 2008, “Dynamic Models of Earthquakes on the North Anatolian Fault Zone Under the Sea of Marmara: Effect of Hypocenter Location”, *Geophysical Journal. International*, 35, L18302.
- Okay, A. I., A. Kaşlılar-Özcan, C. İmren, A. Boztepe-Güney, E. Demirbağ and İ. Kuşçu, 2000, “Active Faults and Evolving Strike-Slip Basin in the Marmara Sea, Northwest Turkey: A Multichannel Seismic Reflection Study”, *Tectonophysics*, 189-218.
- Öztürk. Y and G. Örgülü, 2018, “Akaike Bilgi Kriteri Yöntemi ile P ve S Dalgası Varış Zamanlarının Kestirimi”, *İstanbul Yer Bilimleri Dergisi*, 29,1, 45-53.
- Ozel, N.M., O. Necmioglu, A.C. Yalciner, D. Kalafat, M. Erdik, 2011, “Tsunami Hazard in the Eastern Mediterranean and Its Connected Seas: Toward A Tsunami Warning Center in Turkey”, *Soil Dynamics and Earthquake Engineering*, 31:598–610.
- Özbey, V., M. S. Özeren, P. Henry, E. Klein, G. Galgana, H. Karabulut, L.Dietrich, R. Mccaffrey, 2021, “Kinematics of the Marmara Region: A Fusion of Continuum and Block Models”, *Mediterranean Geoscience Reviews*, 3, 57-78.
- Papazachos B.C. and C. Papazachou, 2003, *The Earthquakes of Greece*, Ziti Publications, 286 pp. (in Greek), Thessaloniki, Greece.
- Papazachos, B., C.H. Papaioannou, C. Papazachos and A. Savvaidis, 1997, *Atlas of Isoleismal Maps for Strong Shallow Earthquakes in Greece and Surrounding Area (426 B.C.-1995)*, Technical Report, University of Thessaloniki, Geophysical Laboratory, Publication 4, 13p.,176 maps, Thessaloniki.

- Parsons, T., S. Toda, R. Stein, A. Barka, J. Dieterich, 2000, “Heightened of Large Earthquakes Near Istanbul: An Interaction-Based Probability Calculation”, *Science*, 288, 661–665.
- Parsons, T., 2004, “Recalculated Probability of $M \geq 7$ Earthquakes Beneath the Sea of Marmara, Turkey”, *Journal of Geophysical Research*, 109, B05304.
- Parke, J.R. et al., 2000, “Active faults in the Sea of Marmara, Western Turkey, Imaged by Seismic Reflection Profiles”, *Terra Nova*, in press.
- Peng, Z. And P. Zhao, 2009, Migration of Early Aftershocks Following the 2004 Parkfield Earthquake, *Nature Geoscience* ,2(12), 877-881.
- Perol, T., M. Gharbi and M. Denolle, 2018, “Convolutional Neural Network for Earthquake Detection and Location”, *Science Advances*, 4, e1700578.
- Perfettini, H., J. Schmittbuhl, J. R. Rice and M. Cocco, 2001, “Frictional Response Induced by Time-Dependent Fluctuations of the Normal Loading”, *Journal of Geophysical Research*, 106(B7), 13,455–13,472.
- Perfettini, H. and J.-P. Avouac, 2004, “Postseismic Relaxation Driven by Brittle Creep: A Possible Mechanism to Reconcile Geodetic Measurements and the Decay Rate of Aftershocks, Application to the Chi-Chi Earthquake, Taiwan”, *Journal of Geophysical Research*, 109, B02304.
- Perfettini, H., J. Schmittbuhl and A. Cochard, 2003, “Shear and Normal Load Perturbations on a Two-dimensional Continuous Fault: 1. Static Triggering”, *Journal of Geophysical Research*, 108(B9), 2408.
- Pondard, N., R. Armijo, G.C. King, B. Meyer and F. Flerit, 2007, “Fault Interactions in the Sea of Marmara Pull-Apart (North Anatolian Fault): Earthquake Clustering and Propagating Earthquake Sequences”, *Geophysical Journal International*, 171(3), 1185-1197.

- Poupinet G, W.L. Ellsworth, J. Frechet, 1984, "Monitoring Velocity Variations in the Crust Using Earthquake Doublets: An Application to the Calaveras Fault, California", *Journal of Geophysical Research*, 89, 5719–5731.
- Pınar N, E. Lahn, 1952, *Annotated Catalogue of Earthquakes of Turkey*, Ankara, Turkey: Ministry of Public Works Directorate of Construction and Urban Affairs Publication (in Turkish), 1952.
- Reilinger, R.E., Ergintav, S., Burgmann, R., McClusky, S., Lenk, O., Barka, A., Gürkan, O., Hearn, L., Feigl, K.L., Çakmak, R., Aktuğ, B., Özener, H., Toksöz, M.N., 2000, "Coseismic and Postseismic Fault Slip for the 17 August 1999, M = 7.5, Izmit, Turkey Earthquake", *Science*, 289, 1519– 1524.
- Reilinger, R.E. et al., 2002, "Coseismic and Postseismic Fault Slip for the 17 August 1999, M = 7.5, Izmit, Turkey Earthquake", *Science*, 289, 1519– 1524.
- Reilinger, R., S. McClusky, and P. Vernant, et al., 2006, "GPS Constraints on Continental Deformation in the Africa-Arabia-Eurasia Continental Collision Zone and Implications for the Dynamics of Plate Interactions", *Journal of Geophysical Research*, 111, B5.
- Sakic, P., H. Piété, V. Ballu, J-Y. Royer, H. Kopp, D. Lange, F. Petersen, M.S. Özeren, S. Ergintav, L. Geli, P. Henry, A. Deschamps, 2016, "No Significant Steady State 23 Surface Creep along the North Anatolian Fault Offshore İstanbul: Results Of 6 Months of Seafloor Acoustic Ranging", *Geophysical Research Letters*, 43, 6817–6825.
- Savage J.C. and M. Lisowski, 1993, "Inferred Depth of Creep on the Hayward Fault, Central California", *Journal of Geophysical Research*, 98, 787-793.
- Sbeinati et al., 2005, "The Historical Earthquakes of Syria: An Analysis of Large and Moderate Earthquakes from 1365 B.C. to 1900 A.D.", *Annals of Geophysics*, 48, 3.

- Schmittbuhl, J., H. Karabulut, O. Lengliné, and M. Bouchon, 2015, “Seismicity Distribution and Locking Depth along the Main Marmara Fault, Turkey”, *Geochemistry Geophysics Geosystems*, 17, 954-965.
- Schmittbuhl, J., H. Karabulut, O. Lengline, and M. Bouchon, 2016, “Long-lasting Seismic Repeaters in the Central Basin of the Main Marmara Fault”, *Geophysical Research Letters*, 43, 9527–9534.
- Stabile, T., C. Satriano, A. Orefice, G. Festa and A. Zollo, 2012, “Anatomy of A Microearthquake Sequence on An Active Normal Fault”, *Scientific Reports*, 2, 410.
- Stein, R.S., A.A., Barka, J.H. Dieterich, 1997, Progressive Failure on the North Anatolian Fault Since 1939 by Earthquake Stress Triggering, *Geophysical Journal International*, 128, 594–604.
- Soysal, H., S. Sipahioğlu, D. Kolçak, Y. Altınok, 1981, “Türkiye ve Çevresinin Tarihsel Deprem Kataloğu, M.Ö. 2100 – M.S. 1900”, TÜBİTAK Proje No: TBAG 341, 87s., İstanbul.
- Suleiman, A.S., P. Albini, P. Migliavacca, 2004, “A Short Introduction to Historical Earthquakes in Libya”, *Annals of Geophysics*, 47, 2/3, 545-554.
- Schaff, D. P., G. C. Beroza and B. E. Shaw, 1998, “Postseismic Response of Repeating Aftershocks”, *Geophysical Research Letters*, 25(24), 4549–4552.
- Shelly, D. R., D. P. Hill, F. Massin, J. Farrell, R. B. Smith, T. Taira, 2013, “A Fluid-Driven Earthquake Swarm on The Margin of The Yellowstone Caldera”, *Journal of Geophysical Research*, 118, 4872–4886.
- Shelly, D. R, G. C. Beroza, S. Ide, 2007, “Non-volcanic Tremor and Low-Frequency Earthquake Swarms”, *Nature*, 446, 305–307.

- Smith, A., F. Oktay, T. Taymaz, J. Jackson, H. Basaran, B. Alpar, M. Simsek and S. Kara, 1995, “High Resolution Seismic Profiling in The Sea Of Marmara–NW Turkey: Late Quaternary Sedimentation and Seal-Level Changes”, *Geological Society of America Bulletin*, 197, 923–936.
- Shaddox, H. R., S.Y. Schwartz and N.M. Bartlow, 2021, “Afterslip and Spontaneous Aseismic Slip on the Anza Segment of the San Jacinto Fault Zone, Southern California”, *Journal of Geophysical Research: Solid Earth*, 126, e2020JB020460.
- Shaddox, H. R., S.Y. Schwartz, 2019, “Subducted Seamount Diverts Shallow Slow Slip to the Forearc of the Northern Hikurangi Subduction Zone, New Zealand”, *Geology*, 47(5), 415–418.
- Shebalin, N.V. and R.E. Tatevossian, 1997, *Catalogue of Large Historical Earthquakes of the Caucasus. In: giardini, d. and Balassian, s. (eds), Historical and Prehistorical Earthquakes in the Caucasus*, NATO ASI Series Partnership Sub-series 2, Environment, Kluwer Academic Publishers, 28, 201–232, Dordrecht, The Netherlands.
- Shebalin N.V., V. Karnik V., D. Hadzievski, (eds), 1974, *Catalogue of Earthquakes of the Balkan Region*, I, UNDP-UNESCO Survey of the Seismicity of the Balkan Region, 600 pp, Skopje,
- Stucchi, M., A. Rovida, A.A., Gomez Capera, P. Alexandre, T. Camelbeeck, M.B. Demircioglu, P. Gasperini, V. Kouskouna, R.M.V. Musson, M. Radulian, K. Sesetyan, S. Vilanova, D. Baumont, H. Bungum, D. Fäh, W. Lenhardt, K. Makropoulos, J.M. Martinez Solares, O. Scotti, M. Živčić, P. Albini, J. Batllo, C. Papaioannou, R. Tatevossian, M. Locati, C. Meletti, D. Viganò, and D. Giardini, 2013, “The SHARE European Earthquake Catalogue(SHEEC) 1000–1899”, *Journal of Seismology*, 17, 523–544.
- Scholz, C. H., 1998, “Earthquakes and Friction Laws”, *Nature*, 391, 37–42.

- Tan, O., M.C.Z., Tapirdamaz and A.Yörük, 2008, “The Earthquake Catalogues For Turkey”, *Turkish Journal of Earth Science*, 17, 405–418.
- Talebi, S. and T. Boone, 1998, “Source Parameters of Injection-Induced Microseismicity”, *Pure and Applied Geophysics*, 153, 113–130.
- Taira, T.A., R. Bürgmann, R.M. Nadeau, D.S. Dreger, 2014, “Variability of fault slip behavior along the San Andreas Fault in the San Juan Bautista Region”, *Journal of Geophysical Research: Solid Earth*.
- Taymaz, T., J.A. Jackson, D. McKenzie, 1991, “Active Tectonics of the North and Central Aegean Sea”. *Geophysical Journal International*, 106, 433 – 490.
- Toksöz, M.N., A.F. Shakal, J. Michael, 1979, “Space-time Migration of Earthquakes Along the North Anatolian Fault Zone and Seismic Gaps”, *Pure and Applied Geophysics*, 117, 1258–1270.
- Templeton, D. C., R. Nadeau, R. Burgmann, 2007, “Behavior of Repeating Earthquake Sequences in Central California and the Implications for Subsurface Fault Creep”, *Bulletin of the Seismological Society of America*, 98(1), 52-65.
- Templeton, D. C., R.M. Nadeau and R. Bürgmann, 2008, “Behavior of Repeating Earthquake Sequences in Central California and the Implications for Subsurface Fault Creep”, *Bulletin of the Seismological Society of America*, 98(1), 52–65.
- Uchida, N., T. Matsuzawa, A. Hasegawa, and T. Igarashi, 2003, “Interplate Quasistatic Slip Off Sanriku, NE Japan, Estimated from Repeating Earthquakes”, *Geophysical Research Letters*, 30.
- Uchida, N., A. Hasegawa, T. Matsuzawa, T. Igarashi, 2004, “Pre- and Post-Seismic Slip on The Plate Boundary Off Sanriku, Ne Japan Associated with Three Interplate Earthquakes as Estimated from Small Repeating Earthquake Data”, *Tectonophysics*, 385,1–15.

- Uchida, N., T. Matsuzawa, A. Hasegawa and T. Igarashi, 2005, “Recurrence Intervals of Characteristic $M4.8 \pm 0.1$ Earthquakes Off Kamaishi, NE Japan—Comparison with Creep Rate Estimated from Small Repeating Earthquake Data”, *Earth and Planetary Science Letters*, 233, 155–165.
- Uchida, N., K. Shimamura, T. Matsuzawa and T. Okada, 2015, “Postseismic Response of Repeating Earthquakes Around the 2011 Tohoku-Oki Earthquake: Moment Increases Due to the Fast Loading Rate”, *Journal of Geophysical Research*, 120.
- Uchida, N., T. Inuma, R.M. Nadeau, R. Bürgmann R. Hino, 2016, “Periodic Slow Slip Triggers Megathrust Zone Earthquakes in Northeastern Japan”, *Science*, 351, 488–492.
- Uchida, N., D. Kalafat, A. Pınar, Y.Yamamoto, 2019, "Repeating Earthquakes and Interplate Coupling Along the Western Part of the North Anatolian Fault", *Tectonophysics*, 769, 228185.
- Uchida, N., 2019, “Detection of Repeating Earthquakes and Their Application in Characterizing Slow Fault Slip”, *Progress in Earth and Planetary Science*, 6, 40.
- Uchida, N., R. Bürgmann, 2019, “Repeating Earthquakes”, *Annual Review of Earth and Planetary Sciences*, 47, in press.
- Uçarkuş, G., Z. Çakır and R. Armijo, 2011, “Western Termination of The Mw 7.4, 1999 İzmit Earthquake Rupture: Implications for the Expected Large Earthquake in the Sea of Marmara”, *Turkish Journal of Earth Sciences*, 20, 379–394.
- Wang, Y. and S. M. Day, 2017, “Seismic Source Spectral Properties of Crack-Like and Pulse-Like Modes of Dynamic Rupture”, *Journal of Geophysical Research: Solid Earth*, 122, 6657–6684.

- Waldhauser, F., D.P. Schaff, 2008, "Large-Scale Relocation of Two Decades of Northern California Seismicity Using Cross-Correlation and Double-Difference Methods", *Journal of Geophysical Research: Solid Earth*, 113: B08311.
- Wdowinski, S., 2009, "Deep Creep as a Cause for the Excess Seismicity Along the San Jacinto Fault", *Nature Geoscience*, 2(12), 882–885.
- Wei, M., D. Sandwell and Y. Fialko, 2009, "A Silent Mw 4.7 Slip Event of October 2006 on the Superstition Hills Fault, Southern California", *Journal of Geophysical Research*, 114.
- Wollin, C., Bohnhoff, M., Martínez-Garzón, P., Küperkoch, L. and Raub, C., 2018, "A Unified Earthquake Catalogue for the Sea of Marmara Region, Turkey, Based on Automatized Phase Picking and Travel-Time Inversion: Seismotectonic Implications", *Tectonophysics*, 747-748, 416–444.
- Wong, H., E. Lüdmann, T. Ulug, and E. Özel, 1995, "The Sea of Marmara: A Boundary Sea in an Escape Tectonic Regime", *Tectonophysics*, 244, 231–250.
- Wyss, M., J. Brune, 1968, "Seismic Moment, Stress and Source Dimensions for Earthquakes in the California-Nevada Region", *Journal of Geophysical Research*, 73, 24-42.
- Williams, J. R., J.C. Hawthorne and O. Lengliné, 2019, "The Long Recurrence Intervals of Small Repeating Earthquakes May Be Due to the Slow Slip Rates of Small Fault Strands", *Geophysical Research Letters*, 46(22), 12823–12832.
- Yamamoto, Y., N. Takahashi, A. Pinar, D. Kalafat, S. Citak, M. Comoglu, R. Polat, Y. Kaneda, 2017, "Geometry and Segmentation of the North Anatolian Fault Beneath the Marmara Sea, Turkey, Deduced from Long-Term Ocean Bottom Seismographic Observations", *Journal of Geophysical Research*.

- Yamamoto, R., M. Kido, Y. Ohta, N. Takahashi, Y. Yamamoto, A. Pinar et al., 2019, “Seafloor Geodesy Revealed Partial Creep of the North Anatolian Fault Submerged in the Sea of Marmara”, *Geophysical Research Letters*, 46, 1268–1275.
- Yamamoto, Y., D. Kalafat, A. Pinar, N. Takahashi, Z. Coskun, R. Polat, Y. Kaneda, H. Ozener., 2020, “Fault Geometry Beneath the Western and Central Marmara Sea, Turkey, Based on Ocean Bottom Seismographic Observations: Implications for Future Large Earthquakes”, *Tectonophysics*, 791, 228568.
- Yao, D., J.I. Walter, X. Meng, T.E. Hobbs, Z. Peng, A.V. Newman et al., 2017, “Detailed Spatiotemporal Evolution of Microseismicity and Repeating Earthquakes Following the 2012 Mw 7.6 Nicoya Earthquake”, *Journal of Geophysical Research: Solid Earth*, 122(1), 524–542. 2016JB013632.
- Yoon, C. E., O. O’Reilly, K. J. Bergen, and G. C. Beroza, 2015, “Earthquake Detection Through Computationally Efficient Similarity Search”, *Science Advances*, 1, e1501057.
- Yılmaz, Z., A.Ö. Konca, S. Ergintav, 2022, “The Effect of the 3-D Structure on Strain Accumulation and the Interseismic Behavior Along the North Anatolian Fault in the Sea of Marmara”, *Journal of Geophysical Research: Solid Earth*, 127, 3.
- Yu, W.C., T.R.A. Song and P.G. Silver, 2013, “Repeating Aftershocks of the Great 2004 Sumatra and 2005 Nias Earthquakes”, *Journal of Asian Earth Sciences*, 67–68(68), 153–170.
- Zerbst, L., 2020, *Identification of Repeating Events within the Aftershock Sequence of the MW = 8.0 1995 Antofagasta Earthquake, Chile*, Bachelor Thesis, Karlsruhe Institute of Technology, Germany.
- Zollo, A., A. Orefice and V. Convertito, 2014, “Source Parameter Scaling and Radiation Efficiency of Microearthquakes Along the Irpinia Fault Zone in Southern Apennines, Italy”, *Journal of Geophysical Research: Solid Earth*, 119, 3256–3275.

<https://earthquake.usgs.gov/learn/parkfield/hist.php/>, accessed on October 20, 2021.

http://www.conservation.ca.gov/cgs/geologic_hazards/earthquakes/Pages/09282004_eq_info.aspx/, accessed on April 9, 2017.

<http://funnel.sfsu.edu/creep/WhatsCreepPage.html/>, accessed on May 10, 2022.